Simulation Studies of Refrigerant Fluids(Dissertation_全文)

AUTHOR(S):

Yamamoto, Ryoichi

SIMULATION STUDIES OF REFRIGERANT FLUIDS

Ryoichi YAMAMOTO

1995

Preface

The present thesis is a summary of my studies carried at Division of Molecular Engineering, Graduate School of Engineering, Kyoto University from April 1992 to August 1994. In this thesis, I describe a series of simulation studies on static and dynamic properties of refrigerant fluids.

This thesis consists of two parts. Part I describes studies on thermodynamic properties of fluoro propane fluids by means of Monte Carlo simulation using realistic potential models. Since fluoro propane is expected to be used as alternative refrigerants in place of chloro fluoro carbons which are completely limited to use in near future, it is important to estimate, even roughly, thermodynamic properties of fluoro propane by molecular simulations.

Almost all refrigerators use the enthalpy difference between gas and liquid phases of refrigerants in order to achieve effective heat transfer; the refrigerant fluids undergo vapor-liquid phase separation in refrigerators. Thus, it is also of interest to investigate physical properties of refrigerant fluids during phase separation. However, there are few simulation studies which concern phase separations even for simple model fluids. In Part II of the thesis, I describe studies on phase separations of the Lennard-Jones model fluids by means of molecular dynamics simulation.

Refrigerant fluids have long been investigated by physical chemists from macroscopic (thermodynamic or hydrodynamic) viewpoints. I wish the present work could contribute to understanding of basic properties of refrigerant fluids from a microscopic (molecular-based) point of view.

Rokko, Kobe

September 1995 Ryoichi Yamamoto

Contents

General Introduction

In the course of the present studies, I concern equilibrium and non-equilibrium properties of refrigerant fluids by means of molecular simulations, i.e., Monte Carlo and molecular dynamics simulations. This thesis consists of two parts. Part I (Chapters 1 and 2) concerns the thermodynamic properties of fluoro propane fluids which are promising alternative refrigerants in place of the certain chloro fluoro carbons. Part II (Chapters 3 to 6) concerns equilibrium and non-equilibrium properties of simple model fluids in a vapor-liquid coexistence region.

I. Simulation Studies of Fluoro Propane Fluids

The industrial production and the commercial use of the certain chloro fluoro carbons (CFCs) are to be limited completely in near future according to the Montreal protocol. The necessity has therefore increased to find the environmentally safe refrigerants with a low contribution to the ozone depletion and the global warming effect. Hydro fluoro carbons (HFCs) are promising alternative refrigerants because they have similar thermodynamic properties to CFCs with no ozone depletion potential. Some fluoro ethanes have already been used for such a purpose; for example, HFC-134a (CH_2FCF_3) is used commercially in place of CFC-12 (CCl_2F_2). Furthermore, some fluoro propanes are also expected to be used. Although a lot of experimental reports have appeared on the thermo-physical properties of HFCs [1, 2], there are few theoretical studies based on a microscopic (molecular based) consideration. A main purpose of Part I of the thesis is to characterize the thermodynamic (macroscopic) properties of fluoro propane fluid in terms of the molecular based (microscopic) properties.

Part I of the thesis consists of Chapters 1 and 2. Chapter 1 describes the physical reasons to explain a contradiction mentioned below by modeling the intermolecular pair potentials for two fluoro propanes. A main purpose of Chapter 2 is to develop a simple and reliable potential model usable in simulation studies for a series of fluoro propanes.

It is known for fluoro alkanes that the monomer properties seem to contradict the fluid thermodynamic properties as follows: when an isomer has a fully fluorinated terminal carbon (-CF_3), its boiling point is lower than that of the other isomers without -CF_3. One can see a typical example in a pair of isomer, $CH_3CF_2CF_3$ (HFC-245cb, CB) and $CH_2FCF_2CHF_2$ (HFC-245ca, CA) [2]. Since CB molecule has two terminal groups CF_3 and CH_3 on the opposite sides, its dipole moment is clearly larger than that of CA; thus CB is expected to have larger intermolecular attractive interaction than CA. The experimental thermodynamic properties, however, suggest the other way around. For example, CA has a nearly 40 K higher normal boiling point (T_b) than CB. These data indicate that CA has larger attractive interaction than CB. Thus, I investigate physical reasons to explain this contradiction by modeling the intermolecular potentials for the isomers CA and CB.

As is mentioned above, fluoro propanes are also expected to be used as alternative refrigerants. Many kinds of fluoro propanes are synthesized and tested routinely at present to choose good candidates among them. It is however supposed that quite long time and a great deal of effort are needed to accomplish such a routine work for all HFCs, since there are a large number of compounds and isomers. If we can estimate the thermodynamic properties directly from their molecular properties (chemical formula, molecular structures, pair potentials, etc...) without any experimental data, it is possible to save a large amount of effort and time for finding appropriate CFC alternatives. Although some empirical or semi-empirical methods have already been proposed to estimate the thermodynamic properties of fluids from the molecular properties on the basis of molecular kinetic theory, such methods are good only for some simple fluids composed of monatomic or diatomic nonpolar molecules. Concerning HFCs, one can easily suppose that such estimations are difficult because these molecules have a large polarization and asymmetric shape. Computer simulations are expected to be a powerful tool to estimate the macroscopic (thermodynamic) properties even for fluids composed of complicated molecules. The advantage of computer simulation is that one can calculate any desired macroscopic properties directly from the microscopic (inter- and intra-molecular) properties. We expect that we can estimate, even roughly, the thermodynamic properties of HFCs by molecular simulation using simple and transferable potential models. Such simple potential models have already been proposed for hydrocarbons, alcohols and water using the site-site interaction form [3]. However, no potential model usable in systematic computer simulation studies has been proposed for HFCs so far, except for the potential model which we have proposed for CA and CB. The procedure which we adopted to construct the pair potential models for CB and CA is simple and transferable to other fluoro propanes in general. One can construct the pair potential models and perform systematic molecular simulations by use of the procedure. This model also shows fairly good agreements with the quantum-chemical-calculation results. Monte Carlo simulations are performed for four kinds of fluoro propane: HFC-245ca, HFC-245cb, HFC-236fa ($CF_3CH_2CF_3$, FA) and C_3F_8, and also for propane. These results are described in Chapter 2.

II. Simulation Studies on Phase Equilibria and Phase Separation of Simple Model Fluids

Part II of the thesis consists of Chapters 3 to 6. Chapters 3 and 4 concern the underlying physical reasons behind the van der Waals like loop (small-size loop) by means of molecular dynamics simulations. In Chapter 3, I consider the relationship between average domain size of the system undergoing vapor-liquid phase separation and the magnitude of the small-size loop. In Chapter 4, I consider the relationship between the magnitude of surface free energy of the vapor-liquid interface and the depth of the small-size loop. Chapters 5 and 6 describe studies of vapor-liquid phase separation by means of molecular dynamics simulations. The asymptotic growth law of the vapor-liquid phase separation for the two- and three-dimensional one-component Lennard-Jones fluids is discussed in Chapter 5. In Chapter 6, the relationship between statistical properties of the domain structure during phase separation and the system temperature is discussed.

It is widely known that there is a serious problem when one deals with phase equilibrating phenomena by means of molecular simulations. A van der Waals like loop always appears in both typical molecular dynamics and Monte Carlo computer simulations for a small system. The van der Waals (vdW) equation of states [4] is a widely known phenomenological equation which can predict the vapor-liquid phase transition. The vdW equation is based on the mean-field approximation which takes into account the free space available to each molecule and the excess pressure due to the attractive interaction between molecules with an assumption that the correction depends only on the mean fluid density. In a real system, different phases with different densities can coexist in two phase region. Hence, the vdW equation is by no means valid in a coexistence region. This is the reason why the vdW equation predicts a strange behavior on PV isotherm, the vdW loop, in a two phase coexistence region.

Many efforts have been done to construct the phase diagrams of model fluids such as Lennard-Jones (LJ) fluid by molecular simulations [5, 6, 7, 8]. Interestingly, a van der Waals like loop appears in both typical molecular dynamics and Monte Carlo computer simulations for a small system, even though no mean-field like assumption is made in the simulation. It has been suggested that the apparent "loop" is owing to the finite-size effect in the simulation. In molecular simulations, small unit cells, typically composed of several hundred of particles, are used due to computational restrictions. Although the periodic boundary conditions (PBC) are used to eliminate the finite size effect of the system, the system essentially does not allow density fluctuations whose wave lengths are larger than the unit cell size. These constraints are considered to be the origin of the vdW loop observed in molecular simulations. A simple question arises here: "Does the vdW loop completely vanish in an infinitely large scale molecular simulation?" In simulation studies, the vdW loop has firstly been observed in a pioneering work done by Alder and Wainwright [9] on the liquid-solid phase transition in a hard-disk (two-dimensional hard-core) system. Nowadays, it is generally believed that the magnitude of the vdW loop will become weaker with increasing system size and will completely vanish in an infinitely large scale simulation in which surface effects can be negligible. Although such a tendency of the vdW loop has been predicted by a theoretical analysis based on the thermodynamics [10],

it has never been confirmed directly through a molecular simulation. Thus, molecular dynamics simulations are performed using a large system composed of 55 296 particles to confirm whether the vdW loop tends to vanish as expectedly by such a large-scale simulation.

The underlying physical reasons behind the small-size loop are explored the surface free energy cost in the course of the domain formations during phase separation. It plays a central role for the explanation of the apparent small-size loop in the computer simulation. Therefore, one can expect that the loop effect should be reduced in a phase-coexisting state where the surface free energy (or surface tension) is somewhat small, and for which small system size simulation may be sufficient for the calculation of an accurate equation of states. Next, I demonstrate this point by using two different simulations with a modified Lennard-Jones model. Finally, a figure is given. This figure is useful for choosing a sensible, if not the minimum, system size for a computer simulation in order to accomplish a reasonably accurate equation of states without large loop effect.

Dynamical aspects of phase separations are not very well understood. Many experimental, theoretical, and numerical approaches have been applied to this problem [11]. Lifshitz and Slyozov have theoretically analyzed the dynamics of aggregation of solute from supersaturated dilute solutions using a scaling concept [12]. They found that the late-time behavior of the growth law of the solute domain scales as $l(t) \sim t^{\frac{1}{3}}$, where $l(t)$ is the characteristic length of the domain size. This relation is known as the Lifshitz–Slyozov rule and agrees well with x-ray scattering experiments on spinodal decomposition.

Numerical studies have also been done for phase separation problems by using Monte Carlo (MC) simulations for kinetic Ising models. Two types of kinetic Ising model are studied. One is the Glauber model in which the order parameter is not conserved, and the other is the Kawasaki model in which the order parameter is conserved. The former model is considered to be a good model for magnets, and the latter is good for metal alloys. The MC studies for these models are summarized in Refs. 11 and 13. It has been found that both the Glauber and the Kawasaki models show power law growth of domain size as $l(t) \sim t^a$, and the growth exponent a is found to be $\frac{1}{2}$ for the Glauber model and $\frac{1}{3}$ for the Kawasaki model. The growth law for the Kawasaki model agrees with the Lifshitz-Slyozov

rule. A different type of numerical studies has been applied to phase separation problems based on either of the following two phenomenological equations, i.e., the time-dependent Ginzburg-Landau (TDGL) equation which is the case for nonconserved order parameter,

$$\frac{\partial\psi(\mathbf{r},t)}{\partial t} = -L\frac{\delta H[\psi(\mathbf{r},t)]}{\delta\psi(\mathbf{r},t)}, \tag{1}$$

or the Cahn-Hilliard-Cook (CHC) equation which is the case for conserved order parameter,

$$\frac{\partial\psi(\mathbf{r},t)}{\partial t} = L\nabla^2\frac{\delta H[\psi(\mathbf{r},t)]}{\delta\psi(\mathbf{r},t)}, \tag{2}$$

where $\psi(\mathbf{r},t)$ is the order parameter of the system at point $\mathbf{r}$ and at time t, L is a phenomenological parameter, and $H[\psi(\mathbf{r},t)]$ is the coarse-grained free-energy functional given by

$$H[\psi(\mathbf{r},t)] = \int d\mathbf{r}\left[\frac{1}{2}(\nabla\psi)^2 - \frac{\tau}{2}\psi^2 + \frac{g}{4}\psi^4\right], \tag{3}$$

with temperature-dependent phenomenological parameters τ and g which are positive. The late-time growth behavior of phase separations has been discussed by solving these equations numerically. Oono and Puri have proposed an efficient computational method to solve TDGL and CHC equations using discrete space and time [14]. This numerical method is called the cell dynamical system (CDS). Using CDS, it is found that the average domain size $l(t)$ shows a power law growth as $l(t) \sim t^a$ in the late stage, and the exponent a is found to be $\frac{1}{2}$ for the TDGL equation and $\frac{1}{3}$ for the CHC equation. These results coincide with the Monte Carlo results for the Glauber and the Kawasaki models. Thus, it is believable that the growth exponent is $\frac{1}{2}$ for the case of nonconserved order parameter and $\frac{1}{3}$ for the case of conserved order parameter.

Recent progress of computers makes it possible to study phase separation phenomena by molecular dynamics (MD) simulation. The advantage of MD simulation is that both static and dynamic correlations and hydrodynamic effects are all taken into consideration. The hydrodynamic effects are known to be important in the late stages of the phase separation dynamics of fluid systems such as fluid binary mixtures and polymer melts [15, 16, 17, 18, 19, 20]. Velasco and Toxvaerd [21] have carried out MD simulations for two-dimensional binary fluid mixtures and found that the growth exponent is $\frac{1}{2}$ in the early stage, and that a crossover to a higher exponent takes place in the late stage.

Ma *et al.* [22] have also performed MD simulations for three-dimensional binary fluid mixtures and found that the growth exponent is 0.55. Both the MD results show that the growth exponent is clearly larger than $\frac{1}{3}$, which is predicted by MC studies or the CHC equation which ignore the hydrodynamic effects. For the case of a one-component fluid, the characteristic time scale relevant to the vapor-liquid phase separation is too short to observe experimentally. Koch *et al.* [23] have studied the dynamics of vapor-liquid phase separation in a two-dimensional one-component fluid by MD simulations using a 5041-particle system. They have found that the characteristic length scale of the system grows in proportion to $t^{\frac{1}{2}}$ for the isothermal simulation and in proportion to $t^{\frac{1}{3}}$ for the adiabatic simulation. They have analyzed their simulation results by a similar way to Lifshitz and Slyozov and concluded that the growth exponent of $\frac{1}{2}$ obtained from their isothermal simulations is independent of the system dimensionality [23, 24].

In this study, I investigate more accurately the dynamics of vapor-liquid phase separation in two- and three-dimensional fluids via MD simulations with a 50 000-particle system for two dimensions and with a 78 732-particle system for three dimensions. The main purpose of the present work is to examine the analysis of Koch *et al.* on the isothermal phase separation, which stated that the growth exponent is $\frac{1}{2}$ and independent of the system dimensionality. First, their isothermal simulation results on a two-dimensional fluid are checked by adopting a much larger system size. Then the growth law dynamics in a three-dimensional fluid are studied by MD simulation. If the present study shows that the growth exponents are $\frac{1}{2}$ in both two- and three-dimensions, it strongly suggests that their analysis is correct. In the adiabatic condition (the exponent is $\frac{1}{3}$ in Koch *et al.*'s simulation), the separation dynamics is supposed to be more complicated than the isothermal case. Since the system temperature increases with time because of the latent heat, the free-energy functional has a time dependency; it corresponds to the case in Eq. (3) that the parameters τ and g are not constant during the separation process. In this study, only the isothermal case is treated.

Phase separation is a typical subject of pattern formation far from equilibrium. The important characteristics of phase separation are the random nature of the domain pattern and its growth [11]. While there are few purely theoretical treatments for such a

nonequilibrium process, many computational studies have been made. As is mentioned above, the growth law of the domain size has been extensively investigated by means of computer simulations in the spinodal region where the uniform phase is unstable. An important finding from MD simulations is that the domain pattern undergoing phase separation shows a fractal nature under certain conditions. Schöbinger *et al.* [25] have performed a constant-temperature Langevin dynamics simulation for the two-dimensional LJ fluid at a reduced temperature $T^* = 0.45$. They found that the capacity dimension of the domain (liquid clusters) is 1.8, being clearly smaller than the Euclidean dimension of 2. Desai and Denton [26] have performed a constant-NVE MD simulation for the two-dimensional LJ fluid at a reduced temperature $T^* \approx 0.5$ and found that the domain has a fractal dimension of 1.7. Such fractal behavior is also predicted analytically by Klein [27] using scaling in an early stage of the spinodal decomposition. In the present study, the relationship between statistical properties of domain structures and system temperatures is studied by means of MD simulation. The asymptotic form factor of the domain pattern undergoing spinodal decomposition is determined for various temperatures using scaling and its temperature dependence is studied. In particular, I analyze the asymptotic tail of the form factor in the large-wave-number limit to determine the domain-wall structure.

References

[1] *Thermophysical Properties of Environmentally Acceptable Fluorocarbons, HFC-134a and HCFC-123*, edited by Japanese Association of Refrigeration, (Tokyo, 1991).

[2] A. L. Beyerlein, D. D. DesMarteau, S. H. Hwang, N. D. Smith, and P. Joyner, in *Proceeding of International CFC and Halon alternatives conference* (Maryland, 1991), p. 396.

[3] W. L. Jorgensen, J. D. Madura, and C. J. Swenson, J. Am. Chem. Soc. **106**, 6638 (1984); W. L. Jorgensen, J. Phys. Chem. **90**, 1276 (1986); W. L. Jorgensen, J. Chandraseklar, J. D. Madura, R. W. Impey, and M. L. Klein, J. Chem. Phys. **76**, 926 (1983).

[4] J. D. van der Waals, *Doctoral Dissertation* (Leiden, 1873).

[5] J. P. Hansen and L. Verlet, Phys. Rev. **184**, 151 (1969).

[6] J. J. Nicolas, K. E. Gubbins, W. B. Streett, and D. J. Tildesley, Mol. Phys. **37**, 1429 (1979).

[7] J. K. Johnson, J. A. Zollweg, and K. E. Gubbins, Mol. Phys. **78**, 591 (1993).

[8] Y. Choi, T. Ree, and F. H. Ree, J. Chem. Phys. **99**, 9917 (1993).

[9] B. J. Alder and T. E. Wainwright, Phys. Rev. **127**, 359 (1962).

[10] J. E. Mayer and W. W. Wood, J. Chem. Phys. **42**, 4268 (1965).

[11] J. D. Gunton, M. San Miguel, and P. S. Sahni, in *Phase Transitions and Critical Phenomena*, edited by C. Domb and J. L. Lebowitz (Academic, New York, 1983), Vol. 8.

[12] I. M. Lifshitz and V. V. Slyozov, J. Phys. Chem. Solids **19**, 35 (1961).

[13] A. Sadiq and K. Binder, J. Stat. Phys. **35**, 517 (1984).

[14] Y. Oono and S. Puri, Phys. Rev. A **38**, 434 (1988); **38**, 1542 (1988).

[15] N. C. Wong and C. Knobler, J. Chem. Phys. **69**, 725 (1976).

[16] E. D. Siggia, Phys. Rev. A **20**, 595 (1979).

[17] T. Koga and K. Kawasaki, Phys. Rev. A **44**, R817 (1991).

[18] S. Puri and B. Dünweg, Phys. Rev. A **45**, R6977 (1992).

[19] J. E. Farrell and O. T. Valls, Phys. Rev. B **40**, 7027 (1989).

[20] J. E. Farrell and O. T. Valls, Phys. Rev. B **42**, 2353 (1990).

[21] E. Velasco and S. Toxvaerd, Phys. Rev. Lett. **71**, 388 (1993).

[22] W-J. Ma, A. Maritan, J. R. Banavar, and J. Koplik, Phys. Rev. A **45**, R5347 (1992).

[23] S. W. Koch, R. C. Desai, and F. F. Abraham, Phys. Rev. A **27**, 2152 (1983).

[24] R. C. Desai, S. W. Koch, and F. F. Abraham, Physica A **118**, 136 (1983).

[25] M. Schöbinger, S. W. Koch, and F. F. Abraham, J. Stat. Phys. **42**, 1071 (1986).

[26] R. C. Desai and A. R. Denton, in *On Growth and Form*, edited by H. E. Stanley and N. Ostrowsky (Martinus Nijhoff, The Hague, 1986).

[27] W. Klein, Phys. Rev. Lett. **65**, 1462 (1990).

Part I.

Simulation Studies of Fluoro Propane Fluids

Chapter 1.

Intermolecular Interaction of Fluoro Propane

Abstract

Intermolecular interaction is studied for an isomer pair of fluoro propane, $CH_3CF_2CF_3$ (HFC-245cb, CB) and $CH_2FCF_2CHF_2$ (HFC-245ca, CA). CB has a larger dipole moment than CA. This may suggest that CB has larger intermolecular attractive interaction than CA; the reverse is, however, found from the experimental data: normal boiling point, critical temperature, and heat of vaporization. Systematic *ab initio* calculations have been done for both CB dimer and CA dimer, and confirmed that the former has smaller attractive interaction than the latter. On the basis of these calculations, a pair potential model has been constructed for the two isomers. This model has 11 Lennard-Jones and Coulomb interaction sites in a molecule, and can explain why CB dimer has smaller attractive interaction than CA dimer. One can easily extend it also to a series of fluoro propanes, and perform systematic molecular simulations.

I. Introduction

Since the Montreal protocol, settled in 1987, limits the industrial production of certain chloro fluoro carbons (CFCs), the necessity has increased to search the environmentally safe refrigerants with a low contribution to the ozone depletion and the global warming. Hydro fluoro carbons (HFCs) are expected as a promising alternative refrigerant to CFCs; some fluoro ethanes have already been used for such a purpose, and some fluoro propanes are synthesized and tested experimentally. Although a lot of experimental reports have appeared on the thermo-physical properties of HFCs [1, 2], there are few theoretical studies based on a microscopic consideration. Our main purpose is to study the thermodynamic (macroscopic) properties of fluoro propane fluid in connection with their molecular-based (microscopic) properties. Thermodynamic properties are governed by the intermolecular interaction. Reliable pair potential models are to be constructed for certain fluoro propanes in order to start such a microscopic investigation, since there is no reliable model for them at this moment.

Table I. The dipole moment and thermodynamic properties of CB and CA.

Formula	dipole moment† (Debye)	T_b (K)	T_c (K)	ΔH_{vap} ($kJ \cdot mol^{-1}$)
$CH_3CF_2CF_3$ (CB)	2.2363	254.85	381.65	23.65
$CH_2FCF_2CHF_2$ (CA)	1.7315	298.11	451.55	29.05

† evaluated from our *ab initio* calculation (6-31G*/MP2)

It is widely known for fluoro alkanes that the monomer properties seem to contradict the fluid thermodynamic properties: *when an isomer has a fully fluorinated terminal carbon (CF_3), its boiling point is lower than that of any other isomers without CF_3.* One can find a typical example in the case of a pair of isomer, $CH_3CF_2CF_3$ (HFC-245cb, CB) and $CH_2FCF_2CHF_2$ (HFC-245ca, CA) [2]. In Table I some of their physical properties are summarized with the dipole moment values evaluated from our *ab initio* calculation. Since CB molecule has CF_3 group, its dipole moment is larger than that of CA; thus CB is

expected to have larger intermolecular attractive interaction than CA. The experimental thermodynamic properties, however, suggest that CA has larger attractive interaction than CB; for example, CA has a nearly 40 K higher normal boiling point (T_b) than CB. In this chapter, the physical reason to explain this contradiction is mainly discussed. Furthermore, a reliable potential model is constructed for a series of fluoro propane by extracting the intrinsic factor of the intermolecular interaction which is dominant both in CA and CB dimers.

II. Quantum-Chemical Calculations

Systematic quantum-chemical calculations have been carried out to estimate the magnitude of the intermolecular interaction for both CB and CA dimers using GAUSSIAN 90 program [4]. Throughout the calculations, the 3-21G basis set was used, and the electron correlation effects were introduced by the second order of Møller-Plesset (MP2) perturbation theory.

There are some rotational isomers of CA. The structure of each rotational isomer was optimized by the energy gradient method. Then, the ratio of Boltzmann factor was calculated and found to be about 9:1 at 300 K between the most stable rotational isomer and the second one; only the most stable rotational isomer of CA is treated in this work. On the other hand, CB has no rotational isomer. In further calculations, the optimized molecular structures are used as a rigid body.

Dimer calculations have been done for 29 (CB) and 30 (CA) kinds of dimer configuration at several intermolecular distances; eight representative configurations are depicted in Fig. 1 (a) to (d) for CB, and (e) to (h) for CA. These configurations are called CA1 to CA4 and CB1 to CB4, respectively, as is shown in Fig. 1.

The *ab initio* results for CB1 to CB4 are shown in Fig. 2 (a) to (d) with dashed lines and open circles; those for CA1 to CA4 are shown in Fig. 3 (a) to (d). One can see the attractive interaction exists in CB2 to CB4 and CA2 to CA4. From these figures, the following observations are made:

1. The attractive interaction is characterized by the intermolecular electrostatic inter-

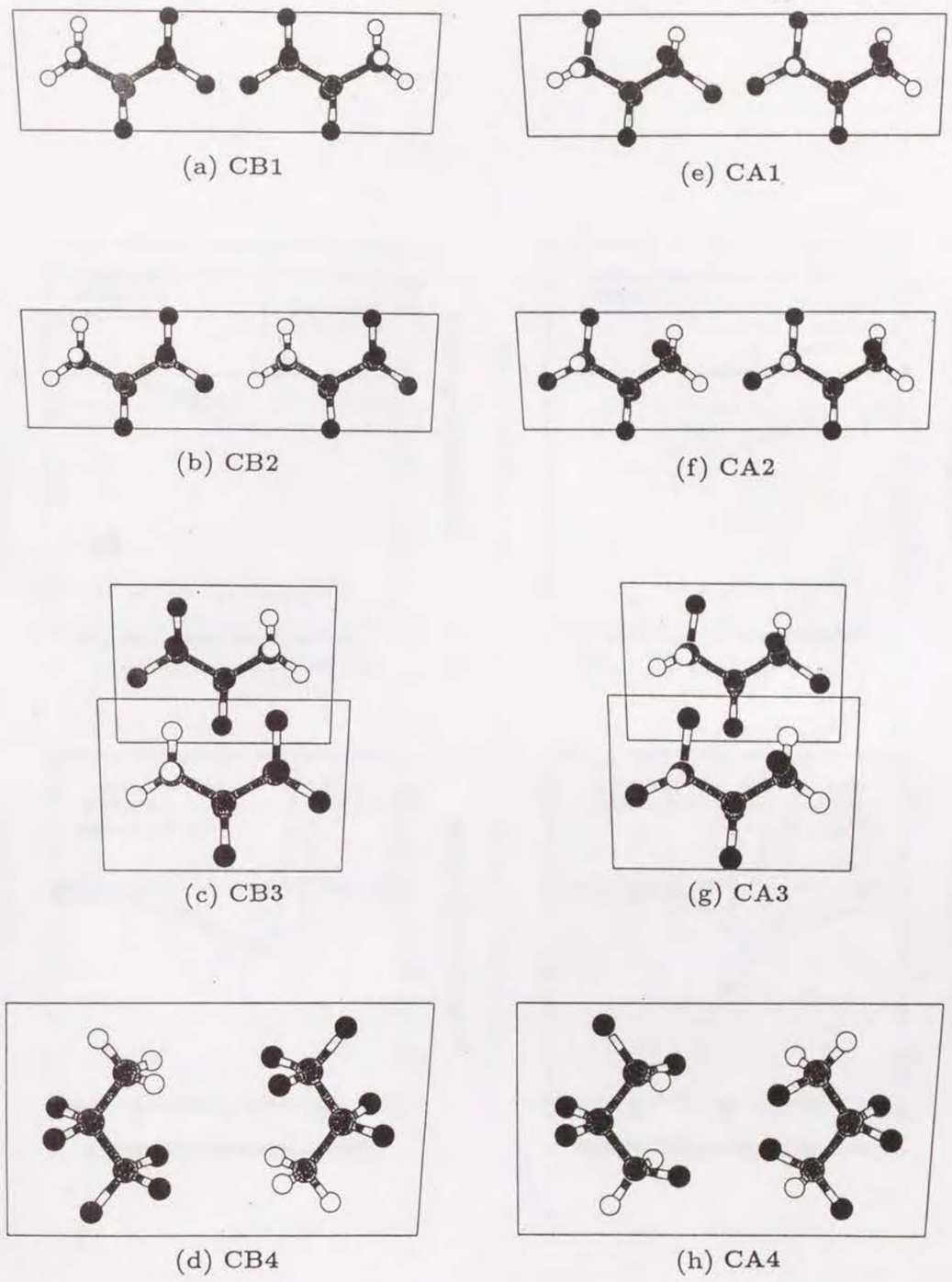

Fig. 1. The dimer configurations: (a) CB1, (b) CB2, (c) CB3, (d) CB4, (e) CA1, (f) CA2, (g) CA3, and (h) CA4. White, black, and gray spheres refer to H, F, and C, respectively.

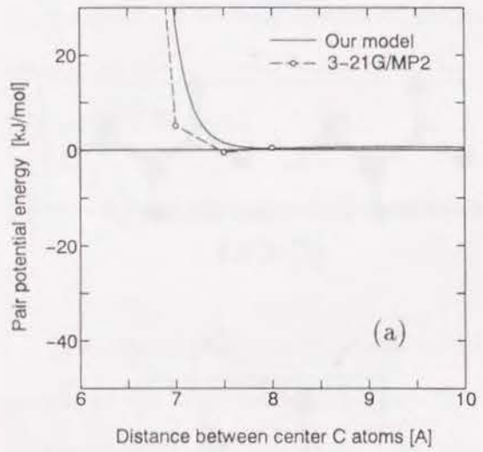

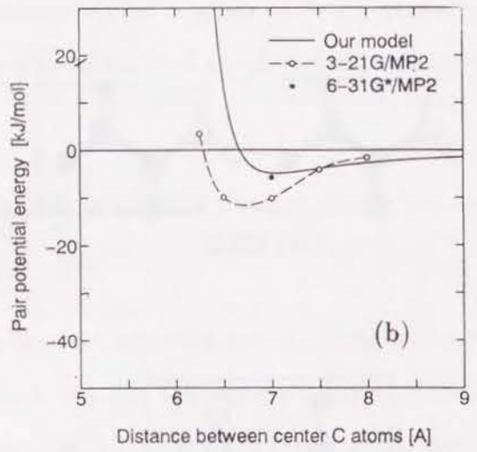

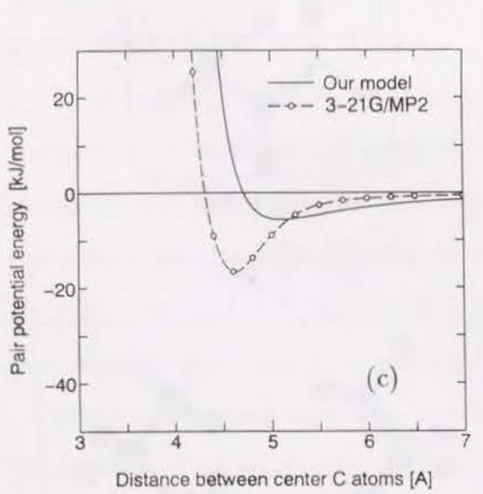

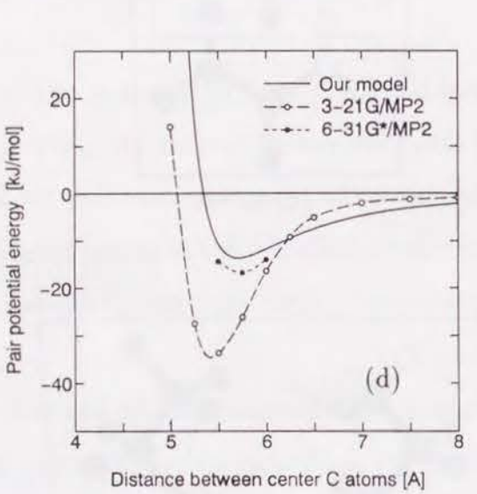

Fig. 2. Comparisons of intermolecular potential curves of CB dimer: (a) CB1, (b) CB2, (c) CB3, and (d) CB4. The solid lines are our model. The dashed lines with open circles are 3-21G/MP2 data; the dotted lines with filled circles are 6-31G*/MP2 data.

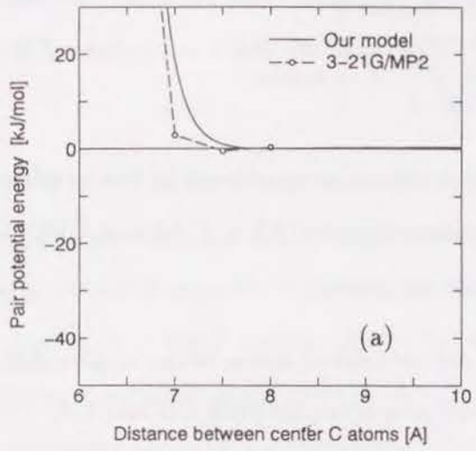

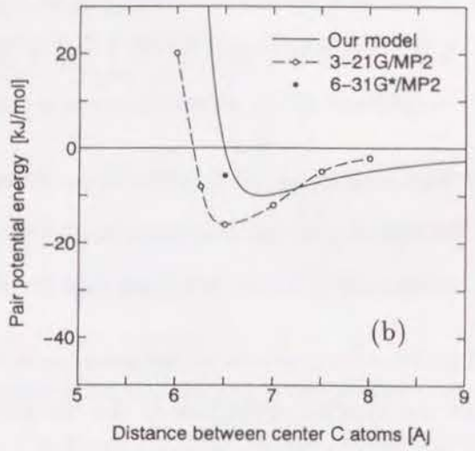

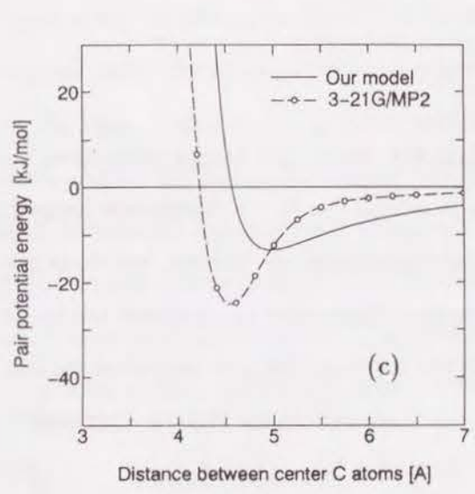

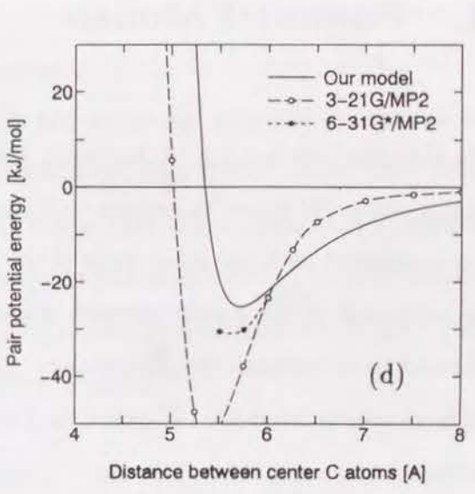

Fig. 3. Comparisons of intermolecular potential curves of CA dimer: (a) CA1, (b) CA2, (c) CA3, and (d) CA4. The solid lines are our model. The dashed lines with open circles are 3-21G/MP2 data; the dotted lines with filled circles are 6-31G*/MP2 data.

action between H and F. If there exists the hydrogen bond like interaction such as C–H···F–C, the potential curve shows large attractive interaction (H···F bond). If the H···F bond cannot be formed, the potential curve is repulsive type as seen in CA1 and CB1.

2. There is a noticeable difference in the potential minimum value between CA2 and CB2, for which one H···F bond is formed. *Note that the order is reverse of the magnitude of the dipole moment given in Table I.*

3. The magnitude of the attractive interaction is almost proportional to the number of the H···F bond as seen from the comparisons among CA2 to CA4 and CB2 to CB4 in which one, two, and four H···F bonds are formed.

The above differences in the potential minima are considered as one of the origins that makes the peculiar difference in the thermodynamic properties between CB and CA.

III. Potential Models

In the previous section, it has been shown that CA dimer has larger attractive interaction than CB dimer in certain configurations in which the H···F bonds are formed; this is consistent with the magnitude of the fluid thermodynamic properties, but does not agree with that of the dipole moment of each monomer. Molecular simulations are to be performed to investigate this discrepancy. For such the purpose, the pair potential models have been constructed for CB and CA. The 11 sites "Lennard-Jones (LJ) + Coulomb " type function is adopted as follows,

$$E_{pair} = \sum_{a}^{11}\sum_{b}^{11}\left[4\epsilon_{ab}\left(\left(\frac{\sigma_{ab}}{r_{ab}}\right)^{12} - \left(\frac{\sigma_{ab}}{r_{ab}}\right)^{6}\right) + \frac{e^2 z_a z_b}{4\pi\varepsilon_0 r_{ab}}\right], \qquad (1)$$

where subscripts a and b refer to the a-th and the b-th sites in the paired molecules, r_{ab}, ε_0, and e are the distance between sites, the dielectric constant of vacuum, and the charge of the electron. The L-J parameters (ϵ_{ab}, σ_{ab}) for each atom (C, H, F) were taken form CHARM package program [3] without any modifications, and the cross terms were determined by the Lorentz–Berthelot combining rule. The partial charges (z_a, z_b)

Table II. Potential parameters common to CB and CA.

atom	σ_{aa} (Å)	ϵ_{aa}/k_B (K)	z_a (e)
H	2.370	21.14	+0.21
F	2.940	39.25	−0.30
C	3.207	45.44	†

† to be determined to give neutral charge for each carbon unit (CH_3, CF_2, CF_3, CH_2F, and CHF_2)

for H and F atoms were evaluated from our Mulliken population analysis on CB and CA monomers with the 6-31G*/MP2 level. The Mulliken population analysis showed that the partial charges for H atoms are almost identical in both CB and CA monomers; the same is true for F atoms. Thus, the common values are used for CB and CA. These parameters are summarized in Table II. The population analysis also shows that a partial charge for each carbon unit (CH_3, CF_2, CF_3, CH_2F, and CHF_2) is almost neutral; thus I put a partial charge on each C atom to give a neutral charge for above-mentioned each carbon unit. For example, we put a partial charge of $-0.63e$ on C atom in CH_3.

In Figs. 2 and 3, our pair potential models are compared with the present *ab initio* data. Although our models show qualitative agreement with the *ab initio* data, systematic differences are observed quantitatively. It seems that these quantitative differences between our models and *ab initio* data are attributed to the insufficient basis set; this was confirmed by the comparison with the results using a more flexible basis set (6-31G*/MP2) at several points, which were also plotted in Figs. 2 and 3.

IV. Analysis of H···F Bond

In this section, our potential models are used to explain the difference between the attractive interaction of CB dimer and that of CA dimer. CB2 and CA2, in which one H···F bond is formed, are considered. The molecular interaction energy can be divided into the several contributions of each site–site interaction by using our potential model. These divisions are summarized in Table III. The energy values used in those divisions

Table III. Factors contributing to the total interaction in CB2 and CA2 configurations. (in kJ·mol^{-1})

	Coulomb							L–J	Total
	opposite terminal carbon unit					Other	Total		
	H–F	H–H F–F	C–C	C–H C–F	Total				
CB	–210.6		–183.9	392.2	–2.3	–1.2	–3.5	–0.0	–3.5
	–210.6			208.3					
CA	–123.8	86.2	–15.1	42.3	–10.4	1.4	–9.0	–0.9	–9.9
	-37.6			27.2					

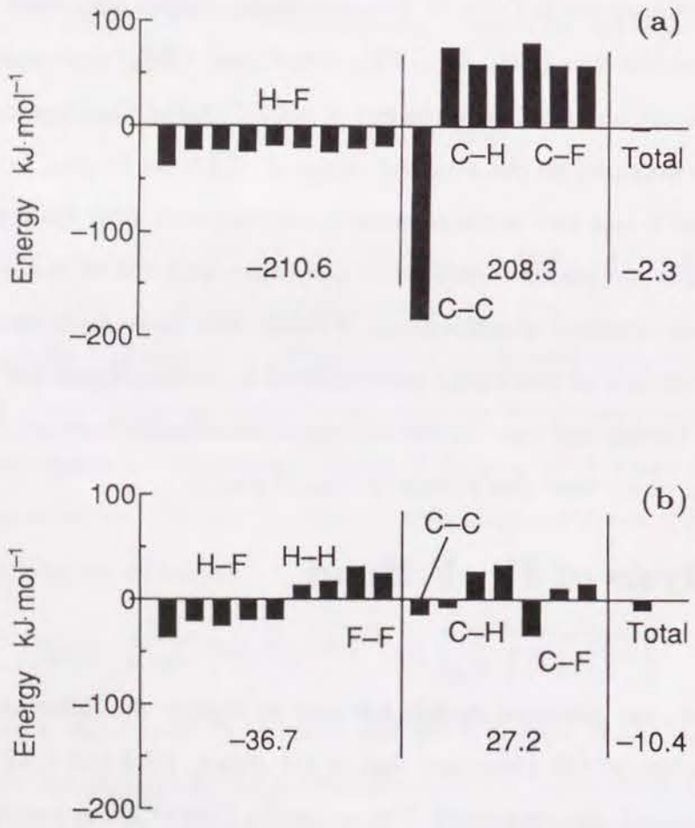

Fig. 4. The site-site contributions of the interaction between opposite terminal carbon units for (a) CB2 and (b) CA2.

are calculated at an intermolecular distance where the potential curve shows a minimum value. This table shows that the difference in the attractive interaction is characterized by the difference in the Coulomb term. In particular, the Coulomb term between the pair of opposite terminal carbon units is the predominant factor; this term consists of 16 site-site components as is shown in Fig. 4 (a) and (b). The difference in the Coulomb term between the pair of opposite terminal carbon units is explained as below.

1. CB2 has nine pairs of H-F interaction; on the other hand, CA2 has five pairs of H-F, two pairs of H-H, and two pairs of F-F interactions.These site–site interactions make CB2 have over 5 times larger attractive interaction (-210.6 kJ·mol^{-1}) than CA2(-37.6 kJ·mol^{-1}).

2. In our model, all carbon units are set to be electro-statically neutral. This leads the each terminal carbon to have notable different partial charge. These values are 0.9 e and -0.63 e in CB2; on the other hand, those are 0.39 e and -0.12 e in CA2. The former pair causes large C-C attractive interaction and, at the same time, extra large C-H and C-F repulsive interactions. The latter pair causes small C-C attractive interaction and small C-H and C-F repulsive interactions. These site–site interactions make CB2 have over 7 times larger repulsive interaction (208.3 kJ·mol^{-1}) than CA2 (27.2 kJ·mol^{-1}).

As is demonstrated above, the difference in the partial charge of the terminal C causes large differences in the magnitude of the repulsive C–H and C–F interactions. On the delicate balance between the attractive H–F interaction and the disturbance to them, CA2 has larger attractive interaction than CB2.

V. Concluding Remarks

Ab initio quantum-chemical calculations and subsequent preparation of intermolecular potential function have been carried out for a pair of isomers, CB and CA. The experimental data suggest that CB has smaller intermolecular attractive interaction than CA in contradiction with the fact that CB has a larger dipole moment than CA.

The *ab initio* calculations showed that the attractive interaction is characterized by the electrostatic intermolecular interaction between H and F. It was also confirmed that the order in the magnitude of the attractive interaction for CB dimer and CA dimer is reverse to that of the dipole moment value. This difference in the attractive interaction can be the reason for the peculiar differences in thermodynamic properties between CB and CA.

To understand the above contents more in detail, molecular simulations are to be performed. For such a purpose, pair potentials have been constructed for CB and CA using atom-atom interaction models. On the basis of our model, the difference is explained as follows. The partial charges located on the C atoms disturb the attractive interaction between H and F. This effect is more significant in CB dimer than in CA dimer because the absolute value of the partial charge on each C atom is larger in CB than in CA. This makes CB dimer has smaller intermolecular interaction than CA dimer.

The procedure adopted to construct the pair potential models for CB and CA is simple and transferable to other fluoro propanes in general. One can construct pair potential models and perform systematic simulation studies in the following manner.

1. Structures of any fluoro propane molecule are optimized by the energy gradient method of quantum-chemical programs.

2. L-J parameters can be taken from Table II.

3. Partial charges for H and F are taken from Table II, and those for C are determined to give a neutral charge for each carbon unit.

4. Pair potential models are constructed by putting these L-J and Coulomb interaction sites on the optimized monomer structures.

5. One can perform molecular simulations and calculate the thermodynamic properties.

Preliminary Monte Carlo (MC) simulations have already been performed using the present potential model for CB and CA. The critical temperatures are calculated and shown in Table IV with experimental values. Although the MC values are higher than the experimental one for both CB and CA, a good agreement is observed for the ratio (T_c

Table IV. Comparison of the critical temperature between experimental and MC results.

	CB K	CA K	Ratio (CA / CB)
Experiment	381.65	451.55	1.18
Monte Carlo	446.0	556.2	1.25

for CA / T_c for CB) between MC results and experimental data. Our potential models appear to represent the qualitative difference of the thermodynamic properties between CB and CA. The result of extensive MC studies is described in Chapter 2.

References

[1] Thermophysical Properties of Environmentally Acceptable Fluorocarbons, HFC-134a and HCFC-123, edited by Japanese Association of Refrigeration, (Tokyo, 1991).

[2] A. L. Beyerlein, D. D. DesMarteau, S. H. Hwang, N. D. Smith, and P. Joyner, in *Proceeding of International CFC and Halon alternatives conference* (Maryland, 1991), p. 396.

[3] B. R. Brooks, R. E. Bruccoleri, B. D. Olafson ,D. J. States, S. Swaminathan and M. Karplus, J. Comput. Chem. **4**, 187 (1983).

[4] M. J. Frisch, M. Head-Gordon, G. W. Trucks, J. B. Foresman, H. B. Schlegel, K. Raghavachari, M. Robb, J. S. Binkley, C. Gonzalez, D. J. Defrees, D. J. Fox, R. A. Whiteside, R. Seeger, C. F. Melius, J. Baker, R. L. Martin, L. R. Kahn, J. J. P. Stewart, S. Topiol, and J. A. Pople, *Gaussian 90, Revision J*, (Gaussian, Inc., Pittsburgh PA, 1990).

Chapter 2.

Monte Carlo Simulation of Fluoro Propane

Abstract

Monte Carlo (MC) simulations have been performed for propane and four fluoro propanes: HFC-245ca, HFC-245cb, HFC-236fa and C_3F_8, using a transferable potential model which agrees well with quantum chemical calculations. Although the present MC results on the thermodynamic properties show qualitative agreements with the experimental data, the quantitative agreements are not satisfactory. An empirical scaling factor is therefore introduced into the potential function to improve agreements of the MC results with the experiments. It is found that the agreements are clearly improved by using the scaling factor. The carbon-carbon pair distribution functions are calculated for propane and compared with experimental x-ray scattering data. The agreements between the simulations and the experiments are good.

I. Introduction

It has been decided that the industrial production and the commercial use of the certain chloro fluoro carbons (CFCs) will be completely limited in 21st century. The necessity has therefore increased to find the environmentally safe refrigerants with a low contribution to the ozone depletion and the global warming. Hydro fluoro carbons (HFCs) are promising alternative refrigerants because they have similar thermodynamic properties to CFCs with no ozone depletion potential. Some fluoro ethanes have already been used for such a purpose; for example, HFC-134a (CH_2FCF_3) is used commercially in place of CFC-12 (CCl_2F_2). Furthermore, some fluoro propanes are synthesized and tested at present. It is however supposed that long time and many efforts are needed to synthesize and test all of HFCs routinely since there are many such compounds and isomers. If we can estimate the thermodynamic properties directly from their molecular properties (structures, interaction, etc...) without any experimental data, we can save effort and time for finding appropriate CFC alternatives.

Although some empirical or semi-empirical methods have already been proposed to estimate the thermodynamic properties of fluids from the molecular properties, such methods are good only for some simple fluids composed of monatomic or diatomic nonpolar molecules. Concerning the HFCs, one can easily suppose that the large polarization of those molecules makes such an empirical estimation difficult. Computer simulations are expected to be a powerful tool to estimate the macroscopic (thermodynamic) properties of fluids composed of complicated molecules. The advantage of computer simulation is that one can calculate any desired macroscopic properties directly from the microscopic (inter- and intra-molecular) properties. I expect that we can estimate, even roughly, the thermodynamic properties of HFCs by molecular simulation using simple and transferable potential models. Such simple potential models have already been proposed for hydrocarbons [1], alcohols [2] and water [3] using site-site interaction model. However, no potential model usable in a systematic computer simulation study has been proposed for HFCs as far as I know. Recently, we proposed [4] a pair potential model for an isomer pair of

fluoro propanes, HFC-245ca ($CH_2FCF_2CHF_2$, CA) and HFC-245cb ($CH_3CF_2CF_3$, CB). This model was confirmed to show fairly good agreements with our quantum chemical calculations.

The main purpose of the present study is to perform molecular simulations for some fluoro propanes using the procedure which we adopted to construct the potential model for CA and CB and to develop a simple and reliable potential model which is usable in simulation study for a series of fluoro propane. Our final aim is to develop a general procedure to construct potential models good for a series of HFCs in order to estimate the thermodynamic properties of HFCs efficiently by simulation with less experimental data.

II. Methodology

A. Simulation details

Monte Carlo (MC) simulations have been done for four fluoro propanes: HFC-245ca, HFC-245cb, HFC-236fa ($CF_3CH_2CF_3$, FA) and C_3F_8. I have done MC simulations also for propane as a reference fluid. 216 molecule systems are used implementing the periodic boundary conditions in all the present simulations. Initial configurations are generated randomly, then equilibration runs are done. After the equilibration of the system was confirmed, the internal energy and the pressure are monitored and averaged over 5000 or 10000 MC steps. The simulations are done in the canonical (NVT constant) ensemble. The intermolecular potential energy E_{ij} between molecules i and j is truncated if r_{ij} is larger than r_c, where r_{ij} is the distance between centers of mass of the molecules i and j, r_c is a potential cutoff radius. $r_{cut} = 13$Å is adopted in this work. The long range corrections from LJ term are included into the potential energy and the pressure. Those are given by

$$U_{LRC} = \sum_{a}^{11}\sum_{b}^{11} \frac{8}{9}\pi\epsilon_{ab}\rho\sigma_{ab}^3 \left[\left(\frac{\sigma_{ab}}{r_{cut}}\right)^9 - 3\left(\frac{\sigma_{ab}}{r_{cut}}\right)^3\right], \quad (1)$$

$$P_{LRC} = \sum_{a}^{11}\sum_{b}^{11} \frac{32}{9}\pi\epsilon_{ab}\rho^2\sigma_{ab}^3 \left[\left(\frac{\sigma_{ab}}{r_{cut}}\right)^9 - \frac{3}{2}\left(\frac{\sigma_{ab}}{r_{cut}}\right)^3\right], \quad (2)$$

where the subscripts a and b refer to the a-th site in the molecule i and the b-th site in the molecule j. ϵ_{ab} and σ_{ab} are the LJ parameters between the site a and b, ρ is the number density. The long range corrections from coulomb term are ignored assuming that there exists no orientational order beyond the cutoff radius in the liquid state in this work. Further descriptions on MC simulations are available in the literature [5].

B. Potential model (Model I)

The united-atom (UA) model, which treats methyl or methylene group as a single interaction site, is usually used to simulate hydrocarbons. Many simulation studies support that UA model is a good assumption to simulate a series of hydrocarbons. However, UA model is supposed not good enough to simulate fluoro propanes because the intermolecular electrostatic interaction between H and F is important in fluoro propane fluids. We have proposed a simple intermolecular potential model for CA and CB [4]. This potential model has 11 Lennard–Jones (12:6) interaction site and 11 fractional charges explicitly on all atoms. The pair potential energy between two molecules i and j is given by

$$E_{ij} = \sum_{a}^{11}\sum_{b}^{11}\left[4\epsilon_{ab}\left\{\left(\frac{\sigma_{ab}}{r_{ab}}\right)^{12} - \left(\frac{\sigma_{ab}}{r_{ab}}\right)^{6}\right\} + \frac{e^2 z_a z_b}{4\pi\varepsilon_0 r_{ab}}\right], \qquad (3)$$

where r_{ab}, ε_0, and e are the distance between site a and b, the dielectric constant of vacuum, and the electric charge of the electron, respectively. The LJ parameters for like interactions ϵ_{aa} and σ_{aa} were taken form CHARM package program [6] without any modifications. Those for unlike interactions were determined by the Lorentz–Berthelot combining rule. The fractional charges z_a on H and F were determined from our Mulliken population analysis on CB and CA monomers using the 6-31G* basis set. The electron correlation effects were introduced by the second order of Møller-Plesset (MP2) perturbation theory. The population analysis on CA and CB has shown that each carbon unit (CH_3, CF_2, CF_3, CH_2F, and CHF_2) is electro-statically almost neutral; thus the fractional charge on each C atom is determined to give a neutral charge on above-mentioned each the carbon unit. For example, I put –0.63e on C atom in CH_3 unit. The potential parameters are summarized in Table I. The lowest energy molecular structures have been determined by the energy gradient method in Gaussian 90 quantum chemical package program [7]. The

Table I. Potential parameters used in this work.

atom	σ_{aa} (Å)	ϵ_{aa}/k_B (K)	z_a (e)
H	2.370	21.14	+0.21
F	2.940	39.25	–0.30
C	3.207	45.44	[a]

[a]to be determined to give a neutral charge for each carbon unit (CH_3, CF_2, CF_3, CH_2F and CHF_2)

structure optimizations have been performed using the 3-21G/MP2 level. Pair potential curves derived from this model are shown together with the *ab initio* data for CA and CB in Fig. 1 (a) and (b), respectively. One can see that the pair potential curves for CA and CB from this potential model show good agreements with the *ab initio* data.

The procedure which we adopted to construct the intermolecular potentials for CB and CA is simple and transferable to any other fluoro propanes. One can construct the intermolecular potentials and perform molecular simulations for other fluoro propanes in the following manner.

1. One can determine the lowest energy structures of any desired molecules using the energy gradient method in *ab initio* quantum-chemical programs such as Gaussian program.
2. The LJ parameters for C, H and F are taken from Table I.
3. The fractional charges on H and F are taken from Table I, and those on C are determined by the rule which give a neutral charge on each carbon unit.
4. The intermolecular potentials are constructed by putting those LJ and coulomb interaction site on each atom of the optimized molecules.
5. One can perform molecular simulations and calculate desired properties.

The molecules are treated as a rigid body. In this study, this procedure is extended to propane and other two fluoro propanes; FA and C_3F_8. This model is called Model I in this thesis.

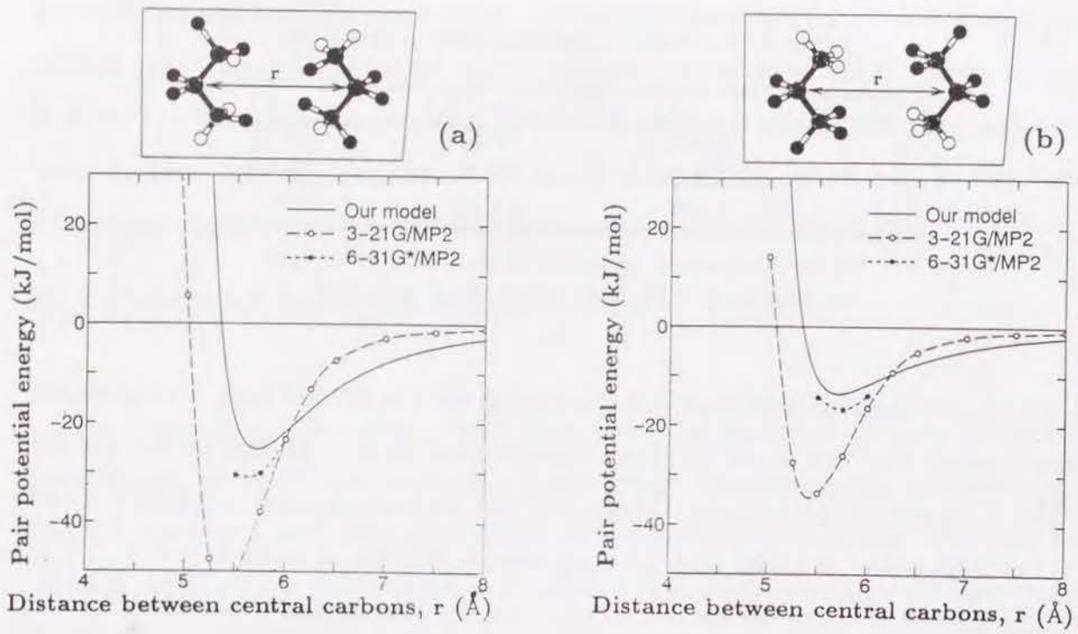

Fig. 1. Comparisons of intermolecular potential curves between our model (Model I) and *ab initio* data: (a) HFC-245ca and (b) HFC-245cb. The solid lines are our model; the dashed lines with open circles are 3-21G/MP2 data; the dotted lines with filled circles are 6-31G*/MP2 data.

III. Thermodynamic Properties

A. Internal energy

I have performed MC simulations for propane, CA, CB and FA using Model I. The configurational internal energy U has been calculated at the experimentally obtained saturated liquid densities and normal boiling temperatures. Table 2 shows a comparison of U from the present MC simulations and the experimental data. The experimental values of U for propane are taken from Ref. 8, in which U is calculated from the experimental data on the second virial coefficients $B(T)$, the saturation pressures P_{sat} and the latent heat of vaporization ΔH_{vap} given by

$$U \simeq -\Delta H_{vap} + P_{sat}(V_g - V_l) + \frac{RT}{V_g}[T\frac{dB(T)}{dT} - B(T)], \tag{4}$$

Table II. Comparison of experiments and simulation results using Model I on the configurational internal energy U.

		Propane		HFC-245ca	HFC-245cb	HFC-236fa
	T (K)	95	230	298	255	272
	ρ (mol/l)	17.0	13.2	10.0	9.4	9.5
Exp.	U (kJ/mol)	-23.60	-17.01	-26.57	-21.51	-23.36
MC	U (kJ/mol)	-29.1	-20.5	-39.8	-27.0	-37.8

where V_g and V_l are the saturated liquid and vapor molar volumes, R is the gas constant. Since no accurate equation of state is available for fluoro propanes, U for fluoro propanes are roughly obtained from the experimental data [9] only on ΔH_{vap} by

$$U \simeq -\Delta H_{vap} + RT. \tag{5}$$

Although agreements between the MC and the experimental results are qualitatively good, quantitative agreements are not satisfactory. This is attributed to that Model I overestimates the intermolecular potential energy for all fluids treated in this study.

B. Equation of state

I have done MC simulations at several temperatures and densities to construct equations of state for five fluids: propane, CA, CB, FA and C_3F_8, using Model I. All the simulation results are plotted in Fig. 2 (a) to (e). Those data are fitted into 8-constant Benedict-Webb-Rubin (BWR) equation of state, which is given by

$$\begin{aligned} P &= RT\rho + (B_0RT - A_0 - C_0/T^2)\rho^2 + (bRT - a)\rho^3 \\ &\quad + \alpha a\rho^6 + (c\rho^3/T^2)(1 + \gamma\rho^2)\exp(-\gamma\rho^2), \end{aligned} \tag{6}$$

where $A_0, B_0, C_0, a, b, c, \alpha$ and γ are the fitting constants and determined separately for each fluid. Isotherms calculated from the BWR equations are also shown in Fig. 2 (a) to (e) with solid lines. The critical points are derived from those BWR equations of state. These data are compared with experimental data in Table III. Although the agreements between the experiments and the simulations are rather good qualitatively, the quantitative agreements are not satisfactory. One can see from Table III that the critical

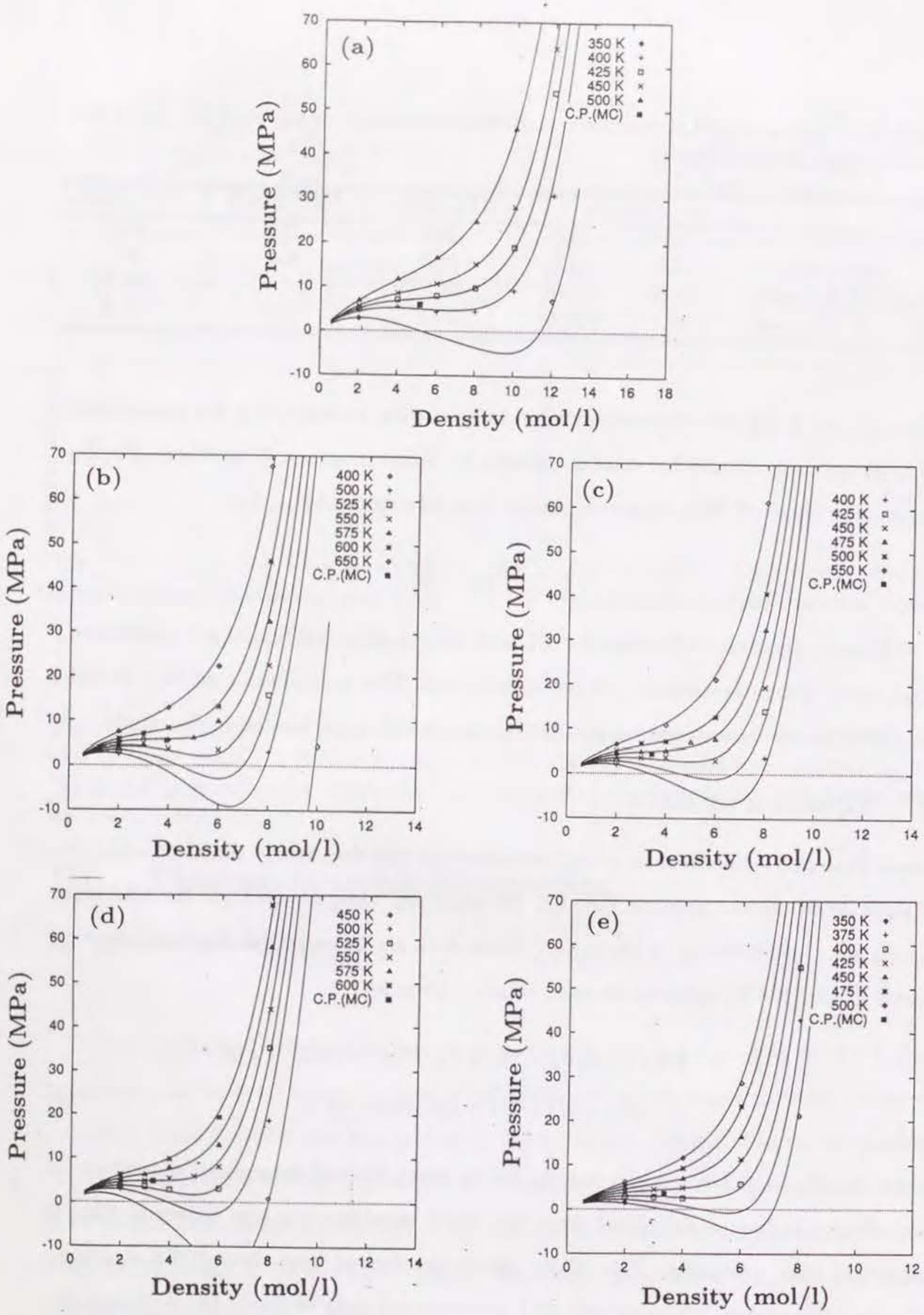

Fig. 2. Isotherms calculated from the MC data using Model I: (a) propane, (b) HFC-245ca, (c) HFC-245cb, (d) HFC-236fa and (e) C_3F_8. The solid lines are isotherms from BWR equations of state which are obtained by least square fittings of the MC data.

Table III. Comparisons of experiments and simulation results using Model I on the critical parameters.

		Propane	HFC-245ca	HFC-245cb	HFC-236fa	C_3F_8
Exp.	T_c (K)	369.82	451.55	381.65	403.75	345.10
	P_c (MPa)	4.250	3.855	3.113	3.177	2.671
	ρ_c (mol/l)	4.92	3.95	3.72	3.66	3.34
MC	T_c (K)	410.2	572.5	464.7	549.4	410.3
	P_c (MPa)	5.92	5.45	4.29	4.73	3.49
	ρ_c (mol/l)	5.16	3.96	3.45	3.36	3.36

temperatures predicted by the simulations are always much higher than the experimental data. It means that Model I tends to overestimate the intermolecular interactions for all these fluids.

C. Modification of Model I (Model II)

As is mentioned in the previous subsections, Model I was found to overestimate the intermolecular potential energy. I therefore modify Model I by introducing an empirical scaling factor into the potential function in order to improve the quantitative agreements of MC results with the experiments as follows,

$$E_{ij} = \lambda \sum_{a}^{11} \sum_{b}^{11} \left[4\epsilon_{ab} \left\{ \left(\frac{\sigma_{ab}}{r_{ab}} \right)^{12} - \left(\frac{\sigma_{ab}}{r_{ab}} \right)^{6} \right\} + \frac{e^2 z_a z_b}{4\pi\varepsilon_0 r_{ab}} \right]. \tag{7}$$

The scaling factor λ is determined by adjusting it until the MC result reproduces the experimental value of U for CB at the saturated liquid density. A plot of U from simulations against the scaling factors is shown in Fig. 3. $\lambda = 0.83$ is adopted and commonly used for a series of fluoro propanes treated in this work. This model is called Model II in this thesis. MC simulations were performed for each fluid using Model II, and U was calculated at the experimental saturated liquid densities. The results are summarized in Table IV. Although disagreements of MC with the experiments are still not small, one can see that the agreements are much improved for all the fluids.

The equations of state for Model II can be constructed by scaling those for Model I,

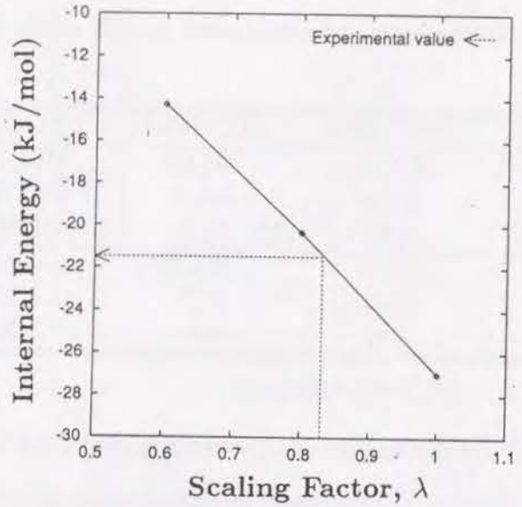

Fig. 3. The empirical scaling factor versus configurational internal energy of HFC-245cb. The scaling factor of 0.83 is adopted in Model II.

Table IV. Simulation results using Model II on the configurational internal energy U.

		Propane		HFC-245ca	HFC-245cb	HFC-236fa
	T (K)	95	230	298	255	272
	ρ (mol/l)	17.0	13.2	10.0	9.4	9.5
MC	U (kJ/mol)	-24.0	-15.9	-31.2	-21.3	-29.9

which have been constructed in the previous subsection, as follows,

$$P = \lambda F(T/\lambda, \rho), \tag{8}$$

where $F(T, \rho)$ is the equations of state for Model I. The critical points for Model II are listed in Table V. We can see from Table V that the quantitative agreements between MC and the experiments are clearly improved by using the scaling factor. Our purpose is developing a simple procedure to construct the potential model which is usable in simulation studies for a series of fluoro propanes. Model II is expected to be a reliable model for this purpose.

Table V. Simulation results using Model II on the critical parameters.

		Propane	HFC-245ca	HFC-245cb	HFC-236fa	C_3F_8
MC	T_c (K)	340.5	475.2	385.7	456.0	340.5
	P_c (MPa)	4.91	4.52	3.56	3.93	2.90
	ρ_c (mol/l)	5.16	3.96	3.45	3.36	3.36

IV. Liquid Structures

A. Propane

Many simulation studies have already been made for liquid hydrocarbons [1, 8, 10, 11, 12, 13]. I have also performed MC simulations for liquid propane using Model II. The intermolecular carbon–carbon pair distribution function was calculated for saturated liquid propane at 95 and 230 K. The results are shown in Fig. 4 (a) and (b) together with the experimental x-ray diffraction data measured at 92 and 228 K [14]. The agreements of MC with the experiments are good. Our MC results reproduce a split in the first peak, which is commonly observed in both experimental and simulation studies for liquid propane. There also exist some disagreements: the left half of the first peaksfrom the simulations are slightly smaller, and the right half of the first peaksfrom the simulations are slightly larger than the experiments, and the both left and right half of the first peaks shift to small r direction. Those minor disagreements might be improved by careful adjustments of the potential parameters using more experimental data, however such a modification is out of our aim.

B. HFC-245

Although HFC-245ca and HFC-245cb are isomers, their thermodynamic properties are notably different; for example, CA has a nearly 40 K higher normal boiling temperature (T_b) than CB. It is reported in Chapter 1 that CA has larger intermolecular attractive interaction than CB in certain dimer configurations in which the hydrogen-bond like interaction between H and F is important (see Fig.1). Thus, it is natural to expect

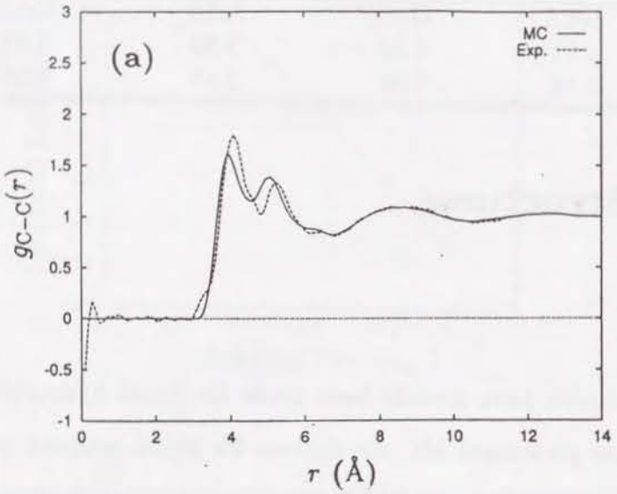

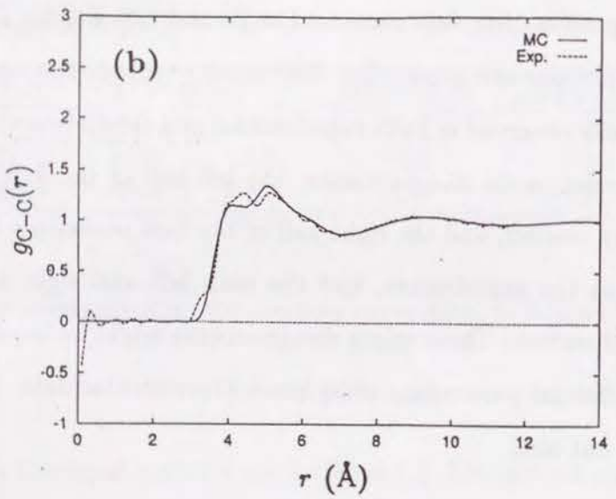

Fig. 4. Comparisons of carbon-carbon pair distribution functions from the present simulations using Model II and those from experiments at 95 K (a) and 230 K (b).

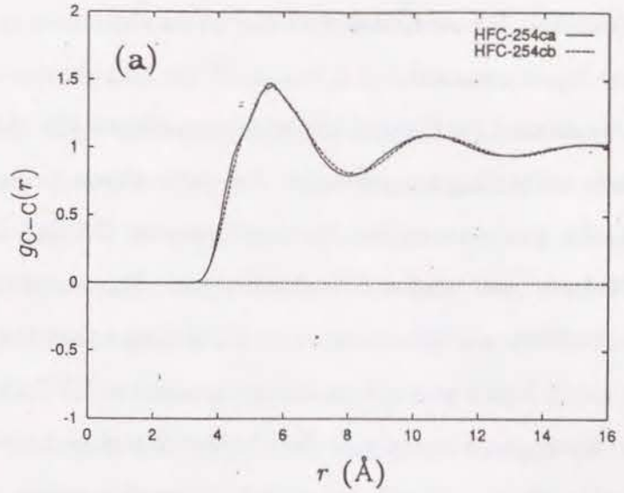

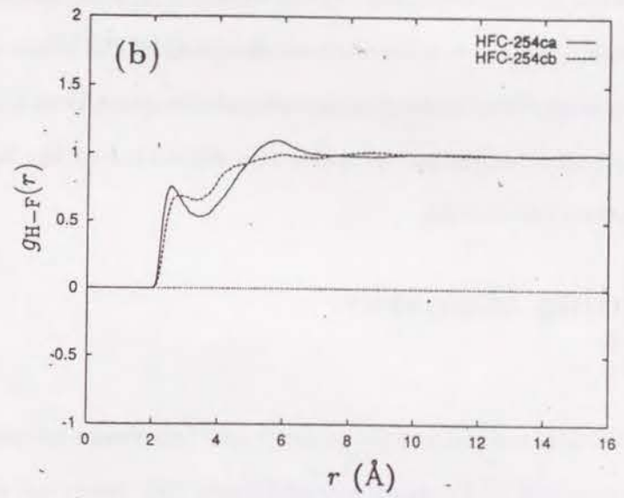

Fig. 5. Comparisons of liquid structures between HFC-245cb and HFC-245ca. Carbon-carbon pair distribution functions from present simulations using Model II are shown in (a), and those of hydrogen-fluorine are shown in (b).

that this is the main reason to explain the difference in their thermodynamic properties. Of course, we cannot discuss the thermodynamic properties of fluids only from data on certain dimer configurations. We need to discuss the liquid structures.

We investigate the liquid structures of CA and CB by MC simulations using Model II. Simulations were performed for CA and CB at the experimentally obtained saturated liquid densities and normal boiling temperatures. Fig. 5 (a) shows a comparison of intermolecular carbon–carbon pair distribution functions between CA and CB. One can see that both CA and CB have quite similar C-C distributions. This suggests that molecular orientations in both the fluids are quite similar. It is also found that the split in the first peak, which is observed in liquid propane, no longer appears in HFC-245. The comparison of intermolecular hydrogen–fluorine pair distribution functions between CA and CB is shown in Fig. 5 (b). We can clearly see a peak in small r region in both CA and CB fluids. This suggests that the hydrogen-bond like interaction between H and F really exists in the liquid state in both the fluids. In the case of CA, the first peak slightly shifts to the small r direction, and the peak is sharper than that of CB. This is attributable to the fact that CA has larger intermolecular attractive interaction than CB. I can say that the difference in their thermodynamic properties is attributed to the difference in their intermolecular attractive interaction.

V. Concluding Remarks

We have performed MC simulations for propane and four fluoro propanes: HFC-245ca, HFC-245cb, HFC-236fa and C_3F_8 using a transferable pair potential model (Model I). From the simulation results on the thermodynamic properties (U and P), it is found that Model I overestimates the intermolecular potential energies. Therefore, I have modified Model I by introducing an empirical scaling factor into the potential function (Model II). Model II reproduces the thermodynamic properties fairly well.

I have calculated the carbon-carbon pair distribution functions for liquid propane at 95 and 230 K using Model II and compared them with the x-ray scattering experiments. The agreements between MC and the experimental data are good. Model II has successfully

reproduced a split in the first peak, which is commonly observed in both experiments and other simulation studies of liquid propane.

Liquid structures of an isomer pair of fluoro propanes, CA and CB, have also been investigated. It is confirmed that both CA and CB have almost identical carbon-carbon pair distributions. The hydrogen-bond like interaction between H and F exists in the liquid state. As is shown in Chapter 1 that the intermolecular attractive interaction of CA is larger than CB in the certain dimer configurations in which the hydrogen-bond like H–F interaction is important. We can conclude that the notably large difference in the thermodynamic properties between CA and CB is attributed to the difference in intermolecular attractive interaction of them.

I emphasize here that our aim is not to perform an accurate molecular simulation for a certain fluid using a complicated potential model. Our final purpose is to perform systematic simulations for a series of HFCs, which have a possibility to use in place of CFCs, in order to estimate the thermodynamic properties of HFCs using less experimental data. We can conclude that Model II is expected to be a reliable potential model for a series of fluoro propanes to perform systematic molecular simulations.

References

[1] W. L. Jorgensen, J. D. Madura, and C. J. Swenson, J. Am. Chem. Soc. **106**, 6638 (1984).

[2] W. L. Jorgensen, J. Phys. Chem. **90**, 1276 (1986).

[3] W. L. Jorgensen, J. Chandraseklar, J. D. Madura, R. W. Impey, and M. L. Klein, J. Chem. Phys. **76**, 926 (1983).

[4] R. Yamamoto, O. Kitao, and K. Nakanishi, Mol. Simulation. **12**, 383 (1994).

[5] M. P. Allen and D. J. Tildesley, *Computer Simulation of Liquids*, (Oxford University, Oxford, 1987).

[6] B. R. Brooks, R. E. Bruccoleri, B. D. Olafson, D. J. State, S. Swaminathan, and M. Karplus, J. Comput. Chem. **4**, 187 (1983).

[7] M. J. Frisch, M. Head-Gordon, G. W. Trucks, J. B. Foresman, H. B. Schlegel, K. Raghavachari, M. Robb, J. S. Binkley, C. Gonzalez, D. J. Defrees, D. J. Fox, R. A. Whiteside, R. Seeger, C. F. Melius, J. Baker, R. L. Martin, L. R. Kahn, J. J. P. Stewart, S. Topiol, and J. A. Pople, *Gaussian 90, Revision J*, (Gaussian Inc., Pittsburgh PA, 1990).

[8] S. Gupta, J. Yang, and N. R. Kestner, J. Chem. Phys. **89**, 3733 (1988).

[9] A. L. Beyerlein, D. D. DesMarteau, S. H. Hwang, N. D. Smith, and P. Joyner, in *Proceeding of International CFC and Halon alternatives conference* (Maryland, 1991), p. 396.

[10] R. Lustig, Mol. Phys. **59**, 173 (1986).

[11] R. Lustig and W. A. Steele, Mol. Phys. **65**, 475 (1988).

[12] S. Toxvaerd, J. Chem. Phys. **91**, 3716 (1989).

[13] S. Toxvaerd, J. Chem. Phys. **93**, 4290 (1990).

[14] H. Habenschuss and A. H. Narten, J. Chem. Phys. **85**, 6022 (1986).

Part II.

Simulation Studies on Phase Equilibria and Phase Separation of Simple Model Fluids

Chapter 3.

Can the "van der Waals loop" vanish?: Effect of domain size

Abstract

The van der Waals (vdW) equation of states predicts a strange mode of behavior, called the vdW loop, for the PV isotherm in the vapor-liquid coexistence region. Similar behavior is commonly observed also for the PV isotherm in the same region in molecular simulations. In this study, molecular dynamics simulations have been performed for a large system composed of 55 296 particles to confirm whether the vdW loop tends to vanish as expected with such a large-scale simulation. The simulation result shows that the magnitude of the vdW loop exhibits a remarkable system-size dependence. The vdW loop of the present 55 296-particle system is found to be much weaker than that of the 256-particle system. The magnitude of the vdW loop has been studied in terms of the characteristic domain size, is found to decrease with the growth of the average domain size.

I. Introduction

The van der Waals (vdW) equation of states [1] is a well known phenomenological equation which can predict the vapor-liquid phase transition, and is given by

$$P = RT\left(\frac{V}{N} - b\right)^{-1} - a\frac{N^2}{V^2} \tag{1}$$

where P, V, T, and N are the pressure, the volume, the temperature, and the number of particles of a system under consideration, respectively. R is the gas constant. The vdW equation is based on the following two ideas: the term $(\frac{V}{N} - b)$ instead of $\frac{V}{N}$ takes into account the free space available to each particle, while the pressure correction, $-a\frac{N^2}{V^2}$, takes into account the excess pressure due to the attractive interaction between particles assuming that the correction depends only on the mean fluid density. Therefore, the vdW equation is a one-phase model for a fluid system, and a uniform density is assumed even in the vapor-liquid coexistence region. In the real system, however, different phases with different densities can coexist in the two phase region. Hence, the vdW equation is not valid in the coexistence region. This is why the vdW equation predicts a strange mode of behavior for the PV isotherm, the 'vdW loop', in the two-phase coexistence region. Although the region $\left(\frac{\partial P}{\partial V}\right)_T \leq 0$ may exist as a meta-stable state in a uniform fluid such as an over heated liquid or an over saturated vapor, the region $\left(\frac{\partial P}{\partial V}\right)_T > 0$ called the spinodal region is mechanically unstable that cannot be observed experimentally.

Many efforts have been made to construct the phase diagrams of model fluid systems, such as Lennard-Jones (LJ) fluid, by molecular simulation method [2, 3, 4, 5]. The vdW like loop is commonly observed for the PV isotherm in the two phase region. One might wonder why such a mechanically unstable loop can be obtained by molecular simulation. In molecular simulation studies, a small unit cell, typically containing several hundred particles, is used due to computational limitations. Although the periodic boundary conditions (PBC) are commonly used to eliminate the finite size effect of the system, the system essentially does not allow density fluctuations with wavelengths which are larger than the unit cell size. These constraints are considered to be the origin of the vdW loop in molecular simulations.

According to the theory of spinodal decomposition [6], only the density fluctuations with wavelengths larger than a certain critical value (l_c) can grow. If the cell size is smaller than l_c, the system has no chance to separate into vapor and liquid phases, even in the spinodal region, so that the simulation system will remain in a uniform single phase. If the cell size is significantly larger than l_c, the characteristic size of the separating phase (domain) will grow until it becomes comparable with the unit cell size. The phase separation will then be stopped by finite size effects before a macroscopic phase separation is achieved, and it is expected that the vdW like loop remains and the magnitude of the loop should depend on the unit cell size.

A question arises here: does the vdW loop completely vanish in an infinitely large scale molecular simulation? In simulation studies, the vdW loop was first observed in the pioneering work of Alder and Wainwright [7] for the liquid-solid phase transition in a hard-disk (two-dimensional hard-core) system. Nowadays, it is generally believed that the magnitude of the vdW loop will become weaker with increasing system size, and will completely vanish in an infinitely large scale simulation in which surface effects are negligible. Although this behavior for the vdW loop has been predicted by a theoretical analysis based on thermodynamics [8], it has never been confirmed directly by a molecular simulation. Recently, our group has tried to answer the question by performing a Monte Carlo simulation for a 4 000-particle system [9], but could not clearly confirm the tendency of the vdW loop vanishing with an increase in system size. The purpose of the present work is to confirm this behavior directly through a molecular simulation. In this study, I have performed a large scale molecular dynamics (MD) simulations for a 55 296-particle system, in which the system separates into vapor and liquid phases semi-macroscopically, so that we can observe the growth of the domain size. By investigating the behavior of the vdW loop in terms of the average domain size and extrapolating the data to the limit of infinitely large domain size, we can answer this question.

II. Methodology

The LJ potential model, which has been used widely in simulation studies, is regarded

as a good model for simple fluids such as the noble gases. The potential energy between two LJ particles is given by

$$U(r) = 4\epsilon \left[\left(\frac{\sigma}{r}\right)^{12} - \left(\frac{\sigma}{r}\right)^{6} \right], \tag{2}$$

where r is the pair separation, σ and ϵ are the LJ parameters. Based on simulation studies, it has been shown that the LJ model can predict three phases: gas, liquid and solid. Many simulation studies have been undertaken to determine the PVT relation for the LJ fluid [2, 3, 4, 5]. In simulation studies, particle-particle interaction is taken into account for separation distances shorter than an appropriate cutoff radius r_c. Since the LJ model has infinitely long range interaction, contributions to the thermodynamic properties of particle-particle interaction beyond the cutoff radius are generally not negligible. Thus, we usually divide the thermodynamic properties into two parts, i.e., the short-range contribution ($r_{ij} < r_c$) and the long range correction (LRC) term. The pressure P is then given by

$$P = P_{Short} + P_{LRC}. \tag{3}$$

Using the virial theorem, the short range contribution is given by

$$P_{Short} = \rho k_B T - \frac{\rho}{3N} \left\langle \sum_{i}^{N} \sum_{j>i}^{r_{ij}<r_c} r_{ij} \frac{dU(r_{ij})}{dr_{ij}} \right\rangle, \tag{4}$$

and the LRC is given by

$$P_{LRC} = -\frac{2\pi}{3}\rho^2 \int_{r_c}^{\infty} r^3 \frac{dU(r)}{dr} g(r) dr, \tag{5}$$

where ρ ($= \frac{N}{V}$) is the number density, and k_B is the Boltzmann constant. The integration in Eq. (5) is usually performed by assuming that the radial distribution function, $g(r)$, converges to 1 for $r \geq r_c$. This assumption is almost correct in the one-phase region of the phase diagram except for the region very close to the critical point. However, as has already been shown in the simulation studies of spinodal decomposition [10, 11], $g(r)$ has a long-range tail in the vapor-liquid coexistence region, because the separating phases form growing patterns with correlation lengths which are much larger than a typical particle-particle distance. For that reason, it is difficult to calculate accurately the LRC term in a simulation run in such regions.

In this work, I use the cutoff LJ potential [12], instead of Eq. (2), which is given by

$$\begin{aligned} U(r) &= 4\epsilon \left\{ \left[\left(\frac{\sigma}{r}\right)^{12} - \left(\frac{\sigma}{r}\right)^{6} \right] \right. \\ &\quad + \left[6\left(\frac{\sigma}{r_c}\right)^{12} - 3\left(\frac{\sigma}{r_c}\right)^{6} \right] \left(\frac{r}{r_c}\right)^{2} \\ &\quad \left. - \left[7\left(\frac{\sigma}{r_c}\right)^{12} - 4\left(\frac{\sigma}{r_c}\right)^{6} \right] \right\} \end{aligned} \tag{6}$$

for $r < r_c$, and $U(r) = 0$ for $r \geq r_c$. It should be noted that Eq. (6) includes no linear term of r for better computational efficiency; this avoids having to take the square root of r. The cutoff radius $r_c = 2.5\sigma$ is adopted in this study. By using the present potential model, we do not have to take into account the LRC term, because it ensures that both the potential energy and the force go smoothly (without discontinuity at $r = r_c$) to zero for $r \leq r_c$. A comparison of the cutoff LJ potential and the original LJ potential is shown in Fig. 1. The thermodynamic properties of the cutoff LJ fluid is no more same as the original LJ fluid [13, 14]. However, since the cutoff LJ fluid also shows a large vdW loop when a unit cell size is small, as is shown later, the difference between the two models is not important for the present purpose.

I have carried out MD simulations for the system composed of 256 cutoff LJ particles at several densities to calculate the PV isotherm. The thermodynamic properties such as the pressure and internal energy are monitored by averaging over 10 000 steps after equilibrium. Fig. 2 shows the P-ρ isotherm at $T^* = 0.7$, where the asterisk denotes a reduced quantity in terms of the LJ parameters: $P^* = P\frac{\sigma^3}{\epsilon}$, $\rho^* = \rho\sigma^3$ and $T^* = T\frac{k_B}{\epsilon}$. Since the 256-particle system is not large enough to lead to a macroscopic phase separation, the vdW loop is inevitably observed, as is shown in Fig. 2. I then performed the following two simulations with a much larger system composed of 55 296 ($= 256 \times 6^3$) particles.

Simulation A. First, a 256-particle system was equilibrated at $T^* = 0.7$ and $\rho^* = 0.4$. Then, the 216 ($= 6^3$) identical 256-particle unit cells were merged into one large unit cell, as is shown in Fig. 3 (a). New initial velocities were given to each particle following the Boltzmann distribution. The MD simulation was performed at $T^* = 0.7$ and $\rho^* = 0.4$ up to $t = 100\tau$, where $\tau = \sqrt{\frac{m\sigma^2}{\epsilon}}$, corresponding to 2.1 ps for an argon-like fluid.

Simulation B. The same as with simulation A, but $\rho^* = 0.6$ was used instead of $\rho^* = 0.4$. The MD simulation was performed at $T^* = 0.7$ and $\rho^* = 0.6$ up to $t = 50\tau$.

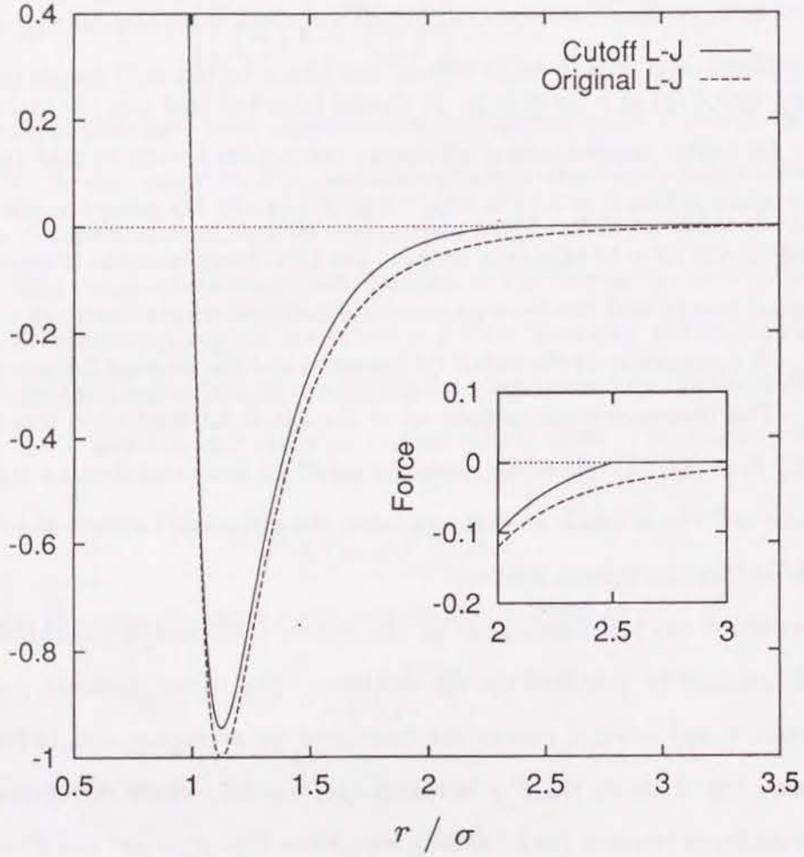

Fig. 1. Comparison of the cutoff LJ potential with the original LJ potential ($U(r)$). The insert shows comparison of force ($-\frac{dU(r)}{dr}$).

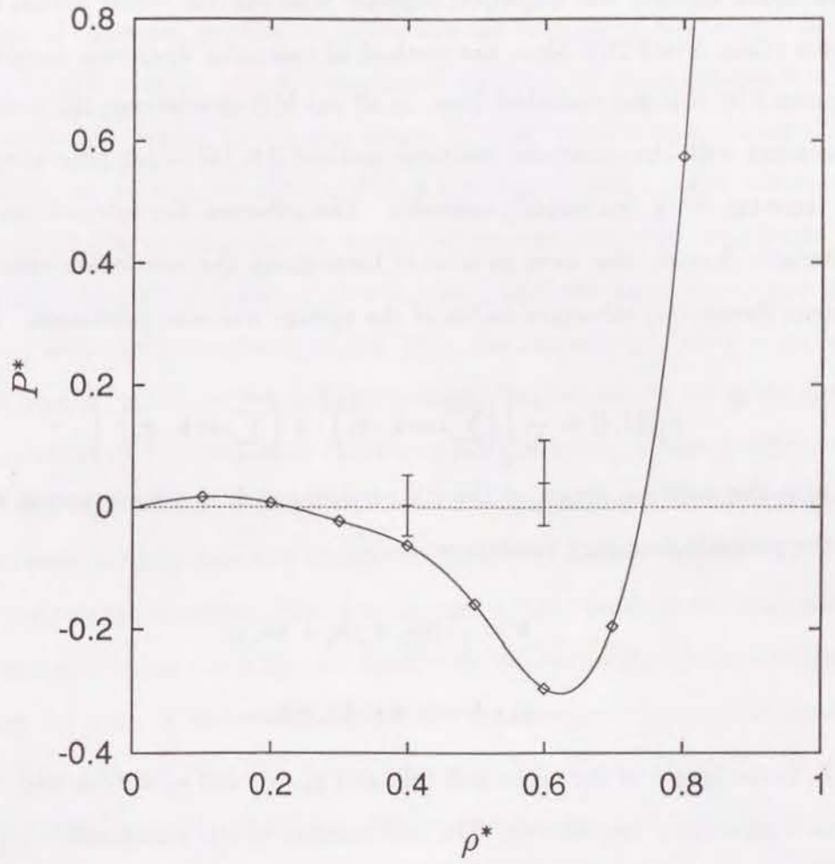

Fig. 2. P-ρ isotherm for the cutoff LJ model at $T^* = 0.7$. The simulation results for 256-particle system are shown ($\diamond$). The solid line is drawn to guide the eye. The extrapolated values (for the limit of $k_1 = 0$) using the simulation results for the 55 296-particle system are also shown ($+$). Error bars indicate the statistical errors of the present simulations.

The periodic boundary conditions were used as usual. I used the leapfrog algorithm for numerical integrations of Newton's equations of motion with a timestep of 0.01τ. The cell index method was employed together with the list vector option of the vector processor (Cray Y-MP2E). Since the method of molecular dynamics simulation is quite well known [15], it is not described here. In all our MD simulations, the temperature was kept constant with the constraint isotherm method [15, 16] which generates a trajectory in the constant-NVT (canonical) ensemble. The pressure, the internal energy, and the characteristic domain size were monitored throughout the simulation runs. The time-dependent (temporal) structure factor of the system was also calculated. This is given by

$$S(|\mathbf{k}|,t) = \frac{1}{N}\left[\left(\sum_{i=1}^{N}\cos\mathbf{k}\cdot\mathbf{r}_i\right)^2 + \left(\sum_{i=1}^{N}\sin\mathbf{k}\cdot\mathbf{r}_i\right)^2\right], \tag{7}$$

where $\mathbf{r}_i$ is the position vector of the ith particle and $\mathbf{k}$ is a wave vector which should follow the periodic boundary conditions, i.e.,

$$\mathbf{k} = \frac{2\pi}{L_c}(i\mathbf{e}_x + j\mathbf{e}_y + k\mathbf{e}_z), \tag{8}$$

$$i,j,k = 0,\pm1,\pm2,\pm3,..., \tag{9}$$

where L_c is the length of the cubic unit cell, and $\mathbf{e}_x$, $\mathbf{e}_y$, and $\mathbf{e}_z$ are the unit vector in the x, y, and z directions, respectively. The first moment of the wavenumber $k_1(t)$ is defined by

$$k_1(t) = \frac{\int_0^{k_{cut}} k\tilde{S}(k,t)dk}{\int_0^{k_{cut}} \tilde{S}(k,t)dk}, \tag{10}$$

which measures a characteristic wavenumber of the system. Here k_{cut} is an appropriate cutoff wave number; and $k_{cut} = \frac{\pi}{\sigma}$ is adopted in this work. $\tilde{S}(k,t)$ is the 'macroscopic' structure factor defined by

$$\tilde{S}(k,t) = S(k,t) - S^{eq}(k), \tag{11}$$

where $S^{eq}(k)$ denotes the equilibrium structure factor for a fully segregated macroscopic two phase system obtained by quenching to a state across the coexistence curve and waiting for the system to reach a new equilibrium. The first moment of the wavenumber $k_1(t)$ is proportional to the inverse of the characteristic domain size, i.e., $l(t) = \frac{2\pi}{k_1(t)}$.

III. Results and Discussions

A sequence of temporal particle configurations for simulation A is shown in Fig. 3. The unit cell length is 51.7σ, which corresponds to 176Å for an argon-like fluid. The 256-particle unit cells, which have a side length of 8.6σ, are shown by small blocks in Fig. 3 (a). One can see in parts (a–d) of Fig. 3 that the merged system, which initially ($t = 0\tau$) has an almost uniform density, begins to separate into vapor and liquid phases immediately after the start of the simulation ($t \simeq 20\tau$), and the characteristic size of liquid domains grows with simulation time. At $t = 100\tau$, the domain size becomes comparable with the cell length. Since particle configurations for simulation B are quite similar to those for simulation A, I do not show them here. In this study, I have performed three independent MD runs both for simulation A and B using different initial configurations, and averaged over all three data sets to improve statistical accuracies [17].

In order to study the dynamics of the domain growth more in detail, the time evolutions of the first moment of the wave number $k_1(t)$ were plotted in Fig. 4 for simulations A and B in a log-log scale. A decrease of $k_1(t)$ with time represents a growth of the average domain size. One can see from Fig. 4 that the power law growth ($k_1(t) \propto t^{-a}$) exists in the late time region ($k_1 < 0.5$), and the growth exponent a seems to converge to $\frac{1}{2}$ both in simulations A and B. Similar power law growth has been observed already in simulation studies of spinodal decompositions in which an instantaneous quenching of a system from a one-phase region into a two phase coexistence region was made [10, 11].

Temporal internal energies and pressures obtained from simulations A and B are shown in Figs. 5 and 6, respectively. One can see from Fig. 5 that the systems go toward new equilibrium states which have lower internal energies than the equilibrium states for the 256-particle system after removing the boundaries between the small unit cells. In Fig. 6, the initial pressures at $t = 0\tau$ correspond to the values on the vdW loop in Fig. 2 at $\rho^* = 0.4$ and 0.6, respectively. Except for the early time stage in the simulation A, the temporal pressure, which was initially negative, increases with time. This indicates that the vdW loop observed for the 256-particle system tends to vanish in the large scale

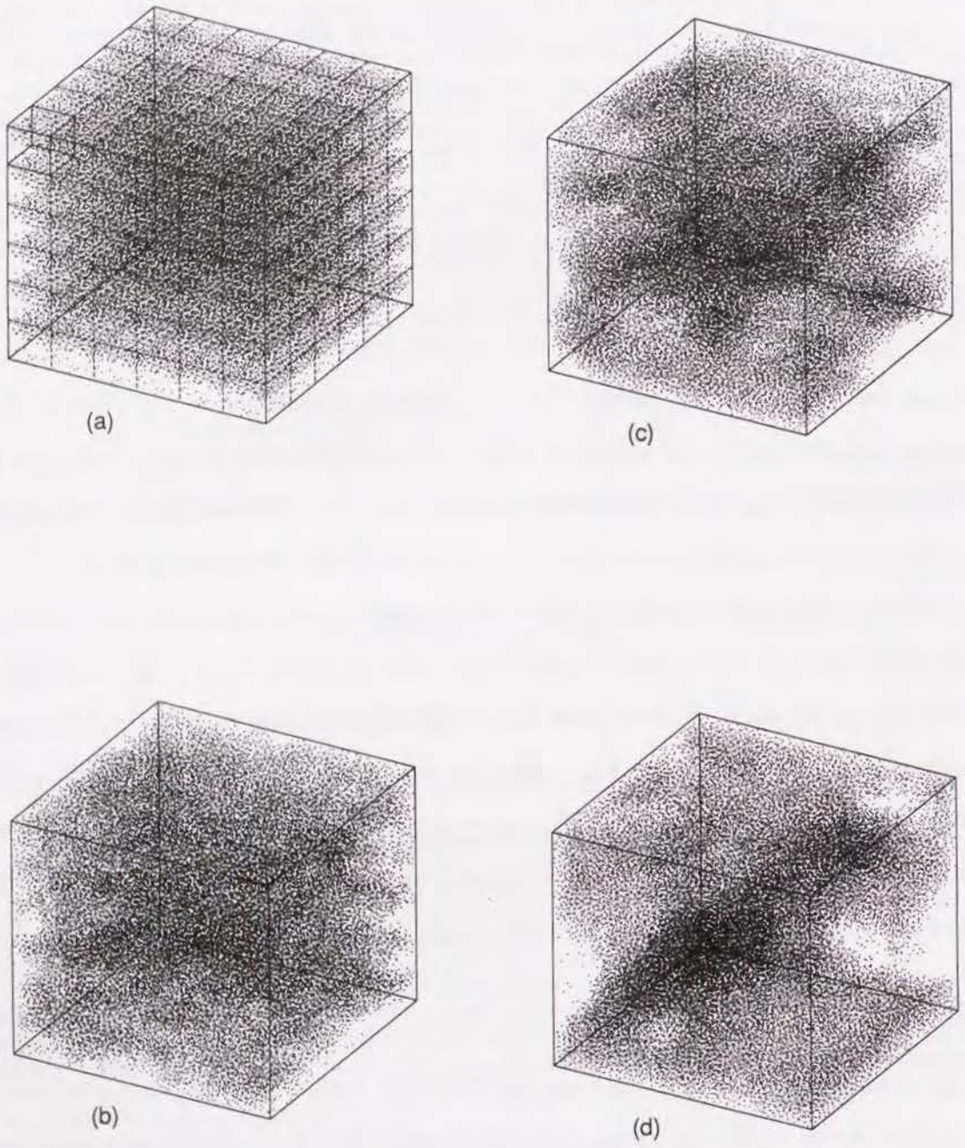

Fig. 3. Snapshots from Simulation A: (a) $t = 0\tau$, the 216 identical unit cells (small blocks) are merged into a large unit cubic cell, (b) $t = 20\tau$, (c) $t = 40\tau$, and (d) $t = 100\tau$.

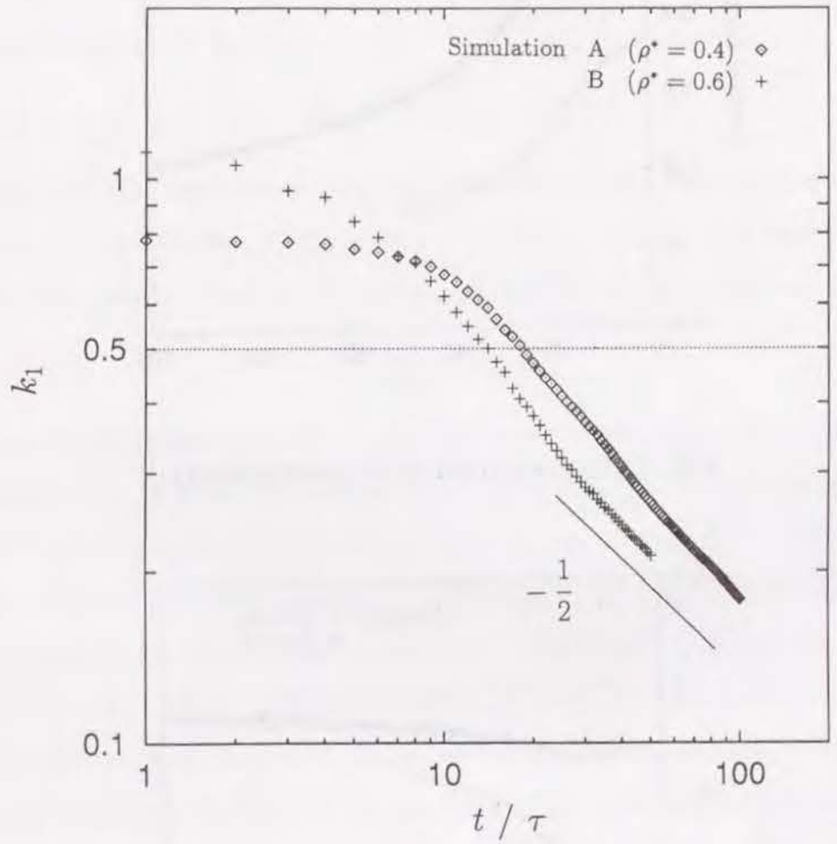

Fig. 4. The first moment of the wave number $k_1(t)$ versus simulation time.

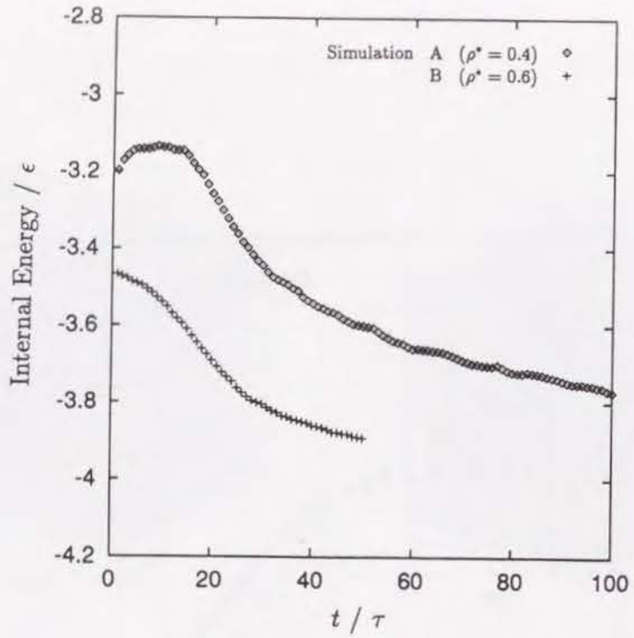

Fig. 5. Time evolution of the internal energy.

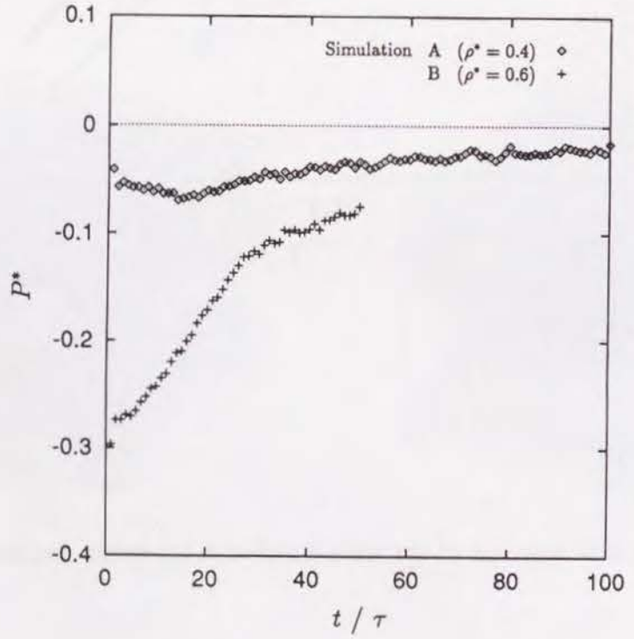

Fig. 6. Time evolution of the pressure.

simulation for the 55 296-particle system.

In Figs. 7 and 8, the temporal internal energies and pressures are plotted against k_1. Only the long time data, which exhibit power law growth behavior ($k_1 < 0.5$) as has already been discussed, are shown. From Fig. 7, the internal energy is found to decrease with time depending on k_1 as

$$U_{ex} \equiv U - U|_{k_1=0} \propto k_1. \tag{12}$$

Assuming that $\tilde{S}(k,t)$ satisfies the scaling hypothesis, i.e., the temporal domain patterns are statistically self similar, it follows that the relation $k_1 \propto \frac{1}{l(t)} \propto A$ holds, where A is the total surface area of the domain. Using this assumption, we can rewrite Eq. (12) as

$$U_{ex} \propto A. \tag{13}$$

This result is compatible with the conclusion which has been generally accepted [18] on the grounds that, in a long time stage in the domain growth, the excess energy of the system is mainly dominated by the domain wall energies. It is also obtained from Fig. 8 that the temporal pressures go toward an equilibrium value with the domain growth. Extrapolations of the pressure data of both at $\rho^* = 0.4$ and 0.6, indicated by the straight lines, seem to converge to the same value for the limit of $k_1 = 0$ within the statistical accuracy of the present data. This value is believable to be the equilibrium vapor pressure of the cutoff LJ fluid at $T^* = 0.7$ after macroscopic phase separation is achieved. These extrapolated values are also shown in Fig. 2. One finds that the vdW loop observed on the P-ρ isotherm calculated with the 256-particle system is considerably reduced for the 55 296-particle system with the extrapolation for the limit of $k_1 = 0$. From the present work, we can say that if a system is very large, a macroscopic phase separation ($k_1 \approx 0$) could be achieved, so that we can confirm that the vdW loop vanishes using MD simulation. It is, of course, a very hard task, but it will be possible not in the too distant future within the ordinary techniques of molecular simulation.

An alternative simulation technique, which is called the Gibbs ensemble Monte Carlo (GEMC) method, has been developed for studies of phase coexistence [19]. The GEMC avoids the interface problem by treating vapor and liquid phases in separate simulation systems. In this case, vapor and liquid phases form infinitely large uniform phases in

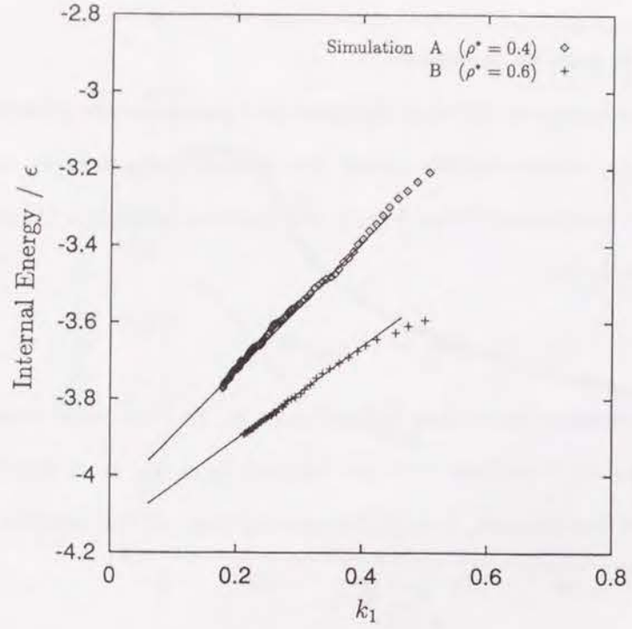

Fig. 7. The internal energy versus the first moment of the wave number $k_1(t)$. Only the data in the range of $k_1 < 0.5$ are shown. The strait lines are to guide the reader's eye.

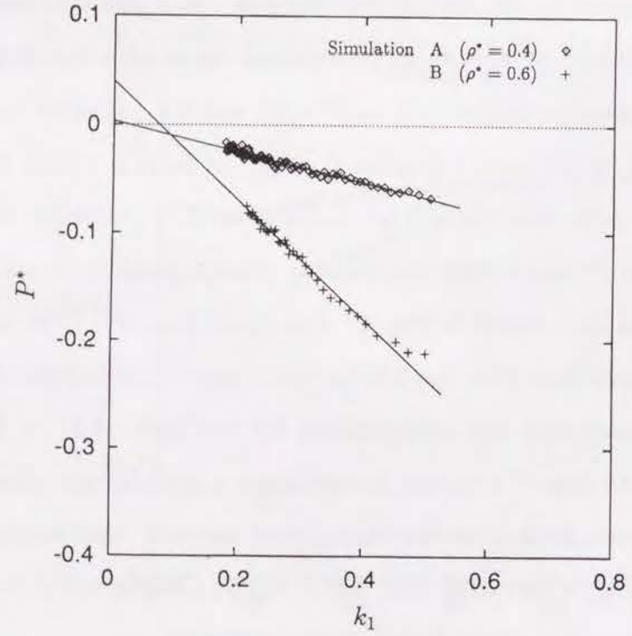

Fig. 8. The pressure versus the first moment of the wave number $k_1(t)$. Only the data in the range of $k_1 < 0.5$ are shown. The strait lines were determined by least square fittings of the data.

separate systems without an interface, and it has been shown that these two phases coexist under an equilibrium pressure of the vapor-liquid coexistence system. This is compatible with our present result. Another interesting scaling approach has been made by Rovere [20] for a two-dimensional LJ fluid near the critical point. He has performed finite-size scaling analysis using the density distribution functions and their moments.

IV. Concluding Remarks

I have carried out large scale MD simulations to confirm whether the vdW loop shows a tendency to vanish as expected. The present simulation result shows clearly that the depth of the vdW loop of the larger (55 296-particle) system becomes remarkably weaker than that of the smaller (256-particle) system. It is found that the vdW loop commonly observed in previous simulation studies are attributed to the additional constraint of the small size of unit cells and the use of the PBC.

I have also investigated the dependence of the depth of the vdW loop on the characteristic size of the density fluctuation (i.e. the average domain size). The depth of the loop was confirmed to decrease with the growth of the average domain size. The linear extrapolations of the k_1–P plots from the two simulation runs ($\rho^* = 0.4$ and 0.6) for the limit of $k_1 = 0$ give rise to nearly the same pressure value within the statistical accuracy of the present simulation. This corresponds to an equilibrium vapor pressure of the cutoff LJ fluid at $T^* = 0.7$.

References

[1] J. D. van der Waals, *Doctoral Dissertation* (Leiden, 1873).

[2] J. P. Hansen and L. Verlet, Phys. Rev. **184**, 151 (1969).

[3] J. J. Nicolas, K. E. Gubbins, W. B. Streett, and D. J. Tildesley, Mol. Phys. **37**, 1429 (1979).

[4] J. K. Johnson, J. A. Zollweg, and K. E. Gubbins, Mol. Phys. **78**, 591 (1993).

[5] Y. Choi, T. Ree, and F. H. Ree, J. Chem. Phys. **99**, 9917 (1993).

[6] J. D. Gunton, M. San Miguel, and P. S. Sahni, in *Phase Transitions and Critical Phenomena*, Vol. 8, edited by C. Domb and J. L. Lebowitz, (Academic, New York, 1983).

[7] B. J. Alder and T. E. Wainwright, Phys. Rev. **127**, 359 (1962).

[8] J. E. Mayer and W. W. Wood, J. Chem. Phys. **42**, 4268 (1965).

[9] A. Kido, O. Kitao, and K. Nakanishi, Chem. Phys. Lett. **199**, 403 (1992).

[10] S. W. Koch, R. C. Desai, and F. F. Abraham, Phys. Rev. A **27**, 2152 (1983); R. C. Desai, S. W. Koch, and F. F. Abraham, Physica **118**A, 136 (1983).

[11] R. Yamamoto and K. Nakanishi, Phys. Rev. B **49**, 14958 (1994).

[12] S. D. Stoddard and J. Ford, Phys. Rev. A **8**, 1504 (1973).

[13] B. Smit, J. Chem. Phys. **96**, 8639 (1992).

[14] M. J. P. Nijmeijer, A. F. Bakker, C. Bruin, and J. H. Sikkenk, J. Chem. Phys. **89**, 3789 (1988).

[15] M. P. Allen and D. J. Tildesley, *Computer Simulation of Liquids* (Clarendon, Oxford, 1987).

[16] W. G. Hoover, A. J. C. Ladd, and B. Moran, Phys. Rev. Lett. **48**, 1818 (1982); D. J. Evans, J. Chem. Phys. **78**, 3297 (1983); D. Brown and J. H. R .Clarke, Mol. Phys. **51**, 1243 (1984).

[17] P. Ossadnik, M. F. Gyure, and H. E. Stanley, Phys. Rev. Lett. **72**, 2498 (1994).

[18] K. Binder and D. Stauffer, Phys. Rev. Lett. **33**, 1006 (1974); K. Binder, Phys. Rev. B **15**, 4425 (1977).

[19] A. Z. Panagiotopoulos, Mol. Phys. **61**, 813 (1987).

[20] M. Rovere, J. Phys. Cond. Matter **5**, B193 (1993).

Chapter 4.

Can the "van der Waals loop" vanish?: Effect of surface free energy

Abstract

In Chapter 3, I have shown that the "van der Waals loop" of the equation of states, an artifact appeared in computer simulations for small size systems, can be removed by enlarging the system size. In this chapter I argue that large system-size simulation is required only when the surface free energy of domain is large in the course of the phase separation, which usually occurs when the system is quenched deeply into two-phase region. For a shallow quench, however, the "loop" effect is not serious because of the small surface free energy of domains. I also show that such a shallow quench can be also achieved effectively by reducing the attractive part of intermolecular potential while retaining the repulsive part of the potential at the same system temperature.

I. Introduction

It is well known that the van der Waals (vdW) equation of states [1],

$$P = RT\left(\frac{V}{N} - b\right)^{-1} - a\frac{N^2}{V^2}, \tag{1}$$

gives rise to the "van der Waals loop" inside the two-phase region of PV phase diagram where a vapor-liquid phase separation or nucleation is expected to occur. Such an unphysical loop feature stems from the mean-field assumption underlying the vdW equation of states. Interestingly, such a van der Waals like loop also appears in both typical molecular dynamics and Monte Carlo computer simulations for a small system, even though no mean-field like assumption is made in the simulation. It has been suggested that the apparent "loop" is owing to the finite-size effect in the simulation. Indeed, in the previous two articles [2, 3] we have reported that the "loop" behavior can be removed when a large-size system is employed in the computer simulation. To this extent, it may be more sensible to call the "van der Waals loop" appeared in the computer simulation the "small-size loop", as suggested by Allen and Tildesley [4], even though the Maxwell equal-area construction can still be applied onto this small-size loop to derive a realistic phase equilibrium.

In this chapter, the underlying physical reasons behind the small-size loop are explored a step further. It is shown that the surface free energy cost in the course of the domain formations during phase separation plays a central role for the explanation of the apparent small-size loop in the computer simulation. Therefore, one should expect that the loop effect should be reduced in a phase-coexisting state where the surface free energy (or surface tension) is relatively small , and for which small system size simulation may be sufficient for the calculation of an accurate equation of states. I demonstrate this point by using two different simulations with a modified Lennard-Jones model. Finally, a figure is given. This figure is useful for choosing a sensible, if not the minimum, system size for a computer simulation in order to accomplish a reasonably accurate equation of states without large loop effects.

II. Models

Our molecular dynamics study is based on the well-known Lennard-Jones (LJ) potential model

$$U(r) = 4\epsilon\left[\left(\frac{\sigma}{r}\right)^{12} - \left(\frac{\sigma}{r}\right)^{6}\right], \tag{2}$$

which has been extensively used in simulation studies [5, 6, 7, 8]. Here r is the inter-particle separation, σ and ϵ are the LJ parameters. It is also known that in the computer simulation of a full LJ system, particle-particle interaction is only taken into account within a cutoff distance r_c, beyond which the thermodynamic properties are determined by assuming the pair correlation function is unity. Therefore, the full thermodynamic quantities from simulation involve two parts: a short range part ($r_{ij} < r_c$) and a long range correction (LRC) term. For example, the pressure is determined from

$$P = P_{Short} + P_{LRC}, \tag{3}$$

where the short range part is given by using the virial theorem

$$P_{Short} = \rho k_B T - \frac{\rho}{3N}\left\langle \sum_{i}^{N} \sum_{j>i}^{r_{ij}<r_c} r_{ij}\frac{dU(r_{ij})}{dr_{ij}} \right\rangle, \tag{4}$$

while the LRC part is given approximately by

$$P_{LRC} = -\frac{2\pi}{3}\rho^2 \int_{r_c}^{\infty} r^3 \frac{dU(r)}{dr} dr. \tag{5}$$

Here ρ $(= \frac{N}{V})$ is the number density, and k_B is the Boltzmann constant.

In this study, since we are only interested in reducing the loop effect, I use a modified LJ potential for a simplicity (to avoid the difficulty in calculating the long-range correction term P_{LRC} for a non-uniform system) [9, 10, 11]. In the first simulation of this study, I use the same potential as that used in Ref. 3, that is

$$\begin{aligned} U(r) \;=\; & 4\epsilon\left\{\left[\left(\frac{\sigma}{r}\right)^{12} - \left(\frac{\sigma}{r}\right)^{6}\right]\right. \\ & + \left[6\left(\frac{\sigma}{r_c}\right)^{12} - 3\left(\frac{\sigma}{r_c}\right)^{6}\right]\left(\frac{r}{r_c}\right)^{2} \\ & \left. - \left[7\left(\frac{\sigma}{r_c}\right)^{12} - 4\left(\frac{\sigma}{r_c}\right)^{6}\right]\right\} \end{aligned} \tag{6}$$

for $r < r_c$, and $U(r) = 0$ for $r \geq r_c$. No linear term of r is included to avoid the square root calculation, and r_c is taken as 2.5 σ. This modified LJ potential ensures both the potential energy and the force go smoothly to zero at $r = r_c$.

I added a free parameter C in front of the attractive term of the modified LJ potential to control the strength of the attraction, namely,

$$\begin{aligned} U(r,C) \;=\; & 4\epsilon\left\{\left[\left(\frac{\sigma}{r}\right)^{12} - C\left(\frac{\sigma}{r}\right)^{6}\right]\right. \\ & + \left[6\left(\frac{\sigma}{r_c}\right)^{12} - 3C\left(\frac{\sigma}{r_c}\right)^{6}\right]\left(\frac{r}{r_c}\right)^{2} \\ & \left. - \left[7\left(\frac{\sigma}{r_c}\right)^{12} - 4C\left(\frac{\sigma}{r_c}\right)^{6}\right]\right\} \end{aligned} \tag{7}$$

Values between 0 and 1 is taken for the parameter C . The former case, $U(r, C = 0)$, represents the potential model of a soft-sphere system while the latter, $U(r, C = 1)$, recovers the modified LJ potential of Eq. (6). We can study systems between these two limiting cases by varying the parameter C.

III. Results

I have carried out constant temperature molecular dynamics (MD) simulations for a system composed of 256 modified LJ particles at several densities and temperatures. The $P\rho$ equations of states are then derived at each temperature. A leapfrog algorithm is used for numerical integration of the Newton's equations of motion with a time step of 0.01τ. The periodic boundary conditions are used as usual. In each MD simulation, the temperature is kept constant by using a constraint isotherm method [4, 12] so that thermodynamic averages are taken in a constant-NVT (canonical) ensemble. The pressure, the internal energy, and the characteristic domain size is monitored throughout the simulation runs. The pressure and internal energy are obtained by averaging over 10 000 steps after the equilibration.

The static structure factor of the system,

$$S(|\mathbf{k}|) = \frac{1}{N}\left\langle \left(\sum_{i=1}^{N} \cos \mathbf{k}\cdot\mathbf{r}_i\right)^2 + \left(\sum_{i=1}^{N} \sin \mathbf{k}\cdot\mathbf{r}_i\right)^2 \right\rangle, \tag{8}$$

is also calculated, where the average $< ... >$ is taken over simulation time, $\mathbf{r}_i$ is the position vector of the ith particle, and $\mathbf{k}$ is a wave vector which follows the periodic boundary conditions,

$$\mathbf{k} = \frac{2\pi}{L_c}(i\mathbf{e}_x + j\mathbf{e}_y + k\mathbf{e}_z), \tag{9}$$

$$i, j, k = 0, \pm 1, \pm 2, \pm 3, ..., \frac{L_c}{\sigma}; (i^2 + j^2 + k^2 \neq 0), \tag{10}$$

where L_c is the length of the cubic unit cell, and $\mathbf{e}_x$, $\mathbf{e}_y$, and $\mathbf{e}_z$ are the unit vector in x, y, and z directions. As in Ref. 3, the first moment of the wavenumber k_1 is obtained by

$$k_1 = \frac{\int_0^{k_{cut}} k\tilde{S}(k)dk}{\int_0^{k_{cut}} \tilde{S}(k)dk}, \tag{11}$$

which measures a characteristic wavenumber of the system. Here $k_{cut}(= \frac{\pi}{\sigma})$ is an appropriate cutoff wavenumber and $\tilde{S}(k)$ is the "macroscopic" structure factor defined by

$$\tilde{S}(k) = S(k) - S^{eq}(k, T^*), \tag{12}$$

where $S^{eq}(k, T^*)$ denotes the equilibrium structure factor for a fully segregated macroscopic two phase system at temperature T^* obtained by quenching a system to a state on the coexistence curve and waiting for the system to reach an equilibrium. Note that the first moment of the wavenumber k_1 is inversely proportional to the characteristic domain size l, i.e., $l = \frac{2\pi}{k_1}$.

(A) First Simulation:

The modified LJ potential of Eq. (6) is used. Fig. 1 shows the $P\rho$ isotherms at both $T^* = 0.7$ and 0.9. Here the asterisk denotes a reduced quantity in terms of the LJ parameters: $P^* = P\frac{\sigma^3}{\epsilon}$, $\rho^* = \rho\sigma^3$, and $T^* = T\frac{k_B}{\epsilon}$. One can see from Fig. 1 that a larger loop is observed at lower temperature $T^* = 0.7$ while the loop becomes much shallower at relatively higher temperature $T^* = 0.9$. Both calculations are carried out using a 256-particle system size. In Ref. 3, we have shown that a system size as large as 55 296-particle has to be used in order to remove the loop at $T^* = 0.7$ in the MD simulation. On the other hand, a 256-particle size seems to give a well behaved equation of states at $T^* = 0.9$ although small loop behavior still presents. This residual loop behavior is expected to be removed with a somewhat larger size than 256, but 55 296 may not be needed. In any

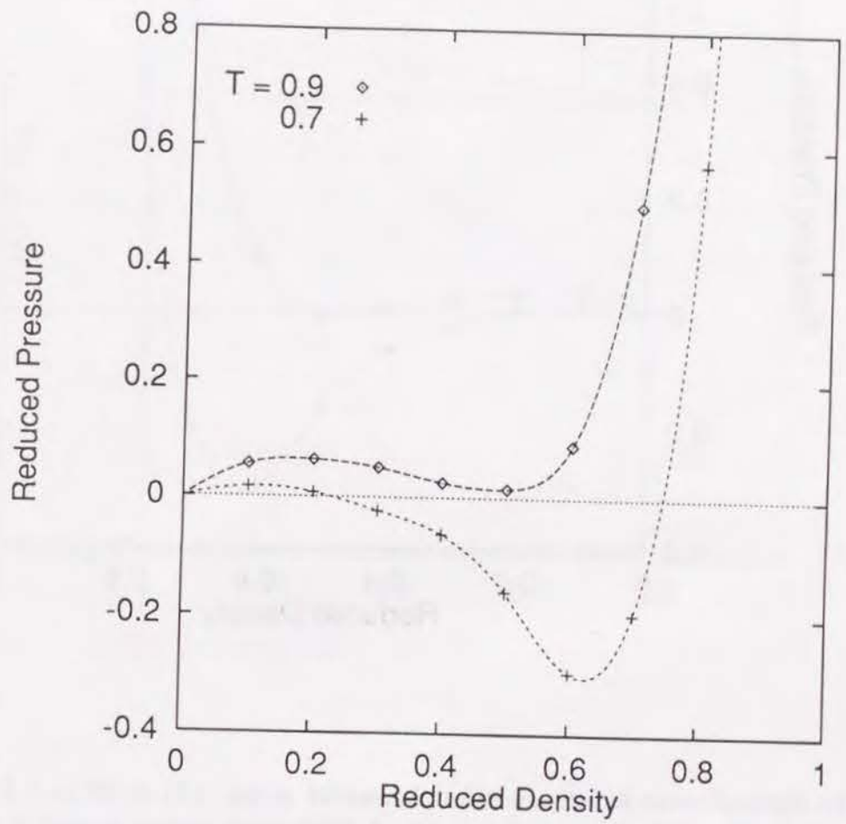

Fig. 1. Pρ isotherms for the modified LJ model of Eq. (6) at $T^* = 0.7$ (+) and $T^* = 0.9$ ($\diamond$). MD calculation is made for a 256-particle system. The lines are to guide the eye.

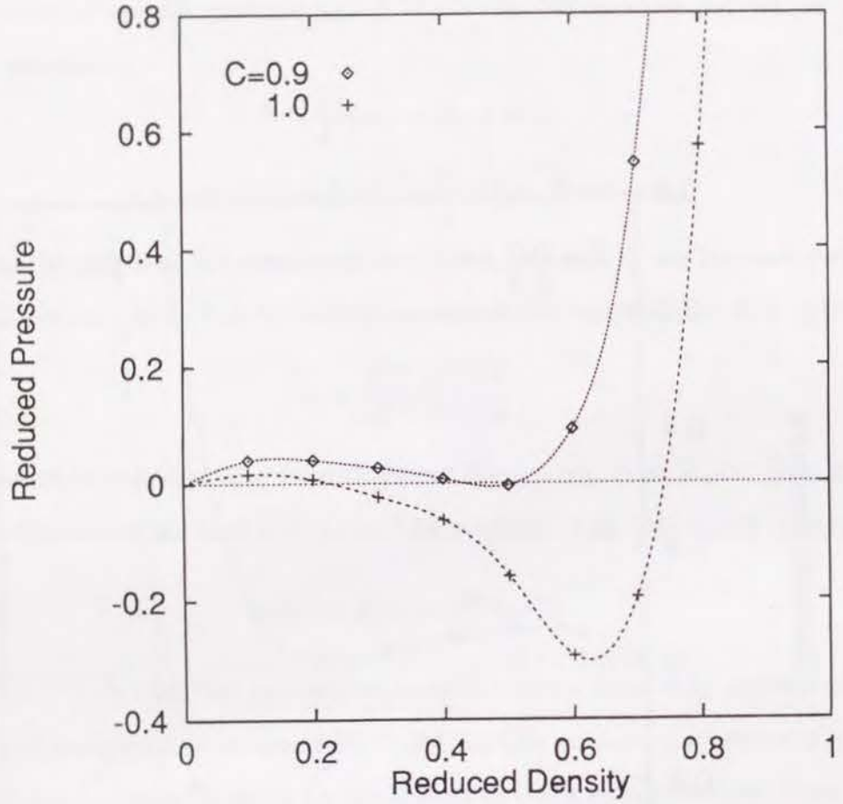

Fig. 2. Pρ isotherms for the modified LJ model of Eq. (7) at $T^* = 0.7$. $\diamond$ is the calculation for $C = 0.9$ while + is for $C = 1$. A 256-particle system is used in both cases. The lines are to guide the eye.

case, the error due to the small-size loop to the equation of states is much smaller at $T^* = 0.9$ than that at $T^* = 0.7$.

(B) Second Simulation:

The modified LJ potential of Eq. (7) is used. Temperature is fixed at $T^* = 0.7$. Results are shown in Fig. 2. The first calculation is for $C = 1$, the same as simulation (A), that is, for the modified LJ model system. The second calculation is for $C = 0.9$, which leads to a smaller attractive inter-particle potential than that of $C = 1$. Clearly, as is shown in Fig. 2, the system with the smaller attractive potential exhibits a smaller

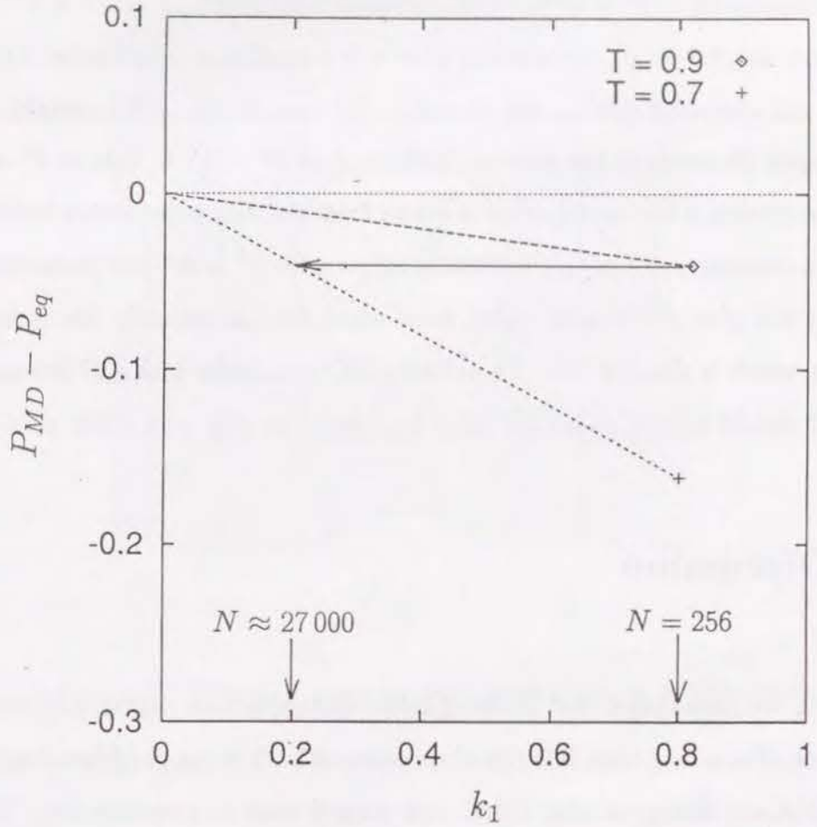

Fig. 3. Depth of the loop in terms of the pressure difference $P_{MD} - P_{eq}$ versus the first moment of the wavenumber k_1 at $\rho^* = 0.5$. Here the modified LJ model of Eq. (6) is used. Simulation is made at temperature $T^* = 0.7$ (+) and $T^* = 0.9$ ($\diamond$), respectively.

loop than the system with the larger attractive potential.

As we know that a system with a smaller attractive part of potential will have a lower critical point for the vapor-liquid transition. In case (B), both calculations are made at the same system temperature $T^* = 0.7$. Thus, reducing the C value in Eq. (7) is effectively similar to have a shallower temperature quench in case (A), which gives a smaller loop.

In Fig. 3, the pressure difference between P_{MD} (calculated from a 256-particle system with the modified LJ potential of Eq. (6)) with P_{eq} (determined from the Maxwell equal-area construction) is plotted against k_1 which measures the average domain size as well

as the system size ($k_1 \propto L_c^{-1} \propto N^{-\frac{1}{3}}$). Clearly, larger pressure difference is obtained at the lower temperature ($T^* = 0.7$), which indicates a greater loop at $T^* = 0.7$ in Fig. 1. This figure is helpful for us, by starting from a few small-size simulations, to identify a larger but not oversized system size to reduce the loop depth. For example, to reduce the loop depth (in terms of the pressure difference) of $T^* = 0.7$ to that of $T^* = 0.9$ with 256-particle system, a horizontal arrow is drawn from the data point shown by diamond in Fig. 3. The crossing point of this horizontal arrow with $T^* = 0.7$ line (from 256-particle simulation) will give rise to a k_1 value, from which we can estimate the corresponding system size, which is about 27 000. Therefore, a MD simulation with a 27 000-particle size at $T^* = 0.7$ should exhibit about the same loop depth as that with a 256-particle size at $T^* = 0.9$.

IV. Discussion

In Ref. 3, we have shown that in the spinodal decomposition region, a typical particle configuration after a long-time MD run is composed of both domains of liquid and bubbles. Simulations A and B suggest that a shallower quench leads to a smaller loop. Combining these two facts, I present an explanation of the apparent vdW loop in a small system-size simulation. I simply demonstrate that the depth of the vdW loop depends on both the surface tension of the domain as well as the average domain size. Let us assume that the vapor-like and liquid-like phases coexist after a long-time MD run. If the average density ρ of the system is high, a liquid-like phase dominates the system and bubbles exist in a continuous liquid phase as is shown in Fig. 4. Assuming the Laplace equation can be applied here (in a qualitative sense since the vapor-like phase is not a spheric bubble), then we can write

$$P_g - P_l = \frac{2\gamma}{R}, \tag{13}$$

where P_g is the pressure in the vapor phase, P_l is the pressure in the liquid phase, γ is the surface tension, and R is the radius of a bubble. Assuming also P_g (after a long MD run) is not far from P_{eq} so that one can expand P_g in the Gibbs-Thomson equation with

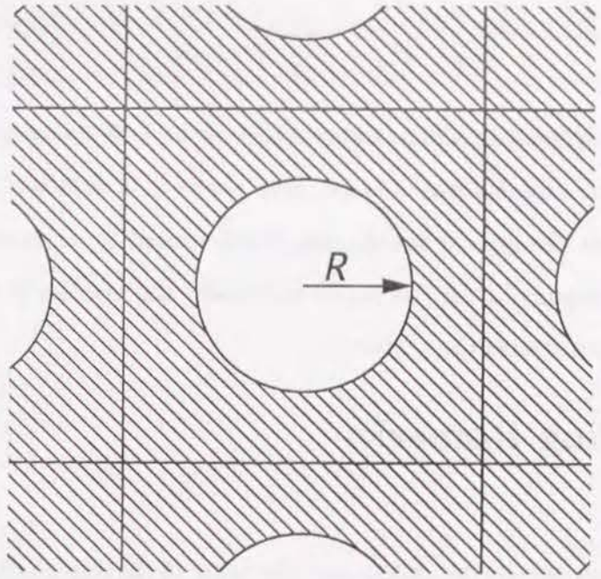

Fig. 4. A schematic picture of a vapor-liquid coexistence at a high average density.

respect to P_{eq}. That gives

$$P_g \approx P_{eq}\left(1 - a\frac{2\gamma}{R}\right), \tag{14}$$

where P_{eq} is an equilibrium pressure with planner interface, and $a = 1/k_B T(\rho_l - \rho_g)$ is a constant.

Substituting Eq. (14) into Eq. (13) gives

$$P_l \approx P_{eq}\left(1 - a\frac{2\gamma}{R}\right) - \frac{2\gamma}{R}. \tag{15}$$

The pressure P_{MD} obtained from a MD simulation is averaged over all particles in the system. Thus, P_{MD} is given, at least qualitatively, by

$$P_{MD} = \frac{N_g}{N}P_g + \frac{N_l}{N}P_l \tag{16}$$

$$= P_{eq} - \left(aP_{eq} + \frac{N_l}{N}\right)\frac{2\gamma}{R}, \tag{17}$$

where N is a total number of particles in the system, N_g and N_l are numbers of particles in vapor and liquid phases, respectively,. Eq. (17) indicates the depth of the vdW loop

at large ρ is negative and depends on both γ and k_1 as follows

$$P_{MD} - P_{eq} \propto -\frac{2\gamma}{R} \propto -2\gamma k_1. \tag{18}$$

Eq. (18) provides an explanation for the larger ρ part of the loop where negative pressures show up. Eq. (18) also explains why a larger loop shows in a simulation with a smaller system. This is because the typical bubble size, characterized by R, is smaller in a small size system. Similar argument can be made to explain the smaller ρ part of the loop where a vapor phase dominates the system.

V. Concluding Remarks

Chapters 3 and 4 are devoted to understand the cause of the unrealistic "van der Waals loop" occurred in a small-size computer simulation for the study of subcritical equations of states. In Chapter 3, we have shown that the apparent loop behavior is truly a finite size effect that can be removed by using a larger system size in a computer simulation. In this study, I demonstrate that an important physical reason behind the small-size loop effect is due to the domain surface free energy during the phase separation. With the same system size, it is found that the larger of the surface free energy, the greater the loop exhibits. This is shown through two MD simulation studies using a modified LJ model.

I have also investigated the dependence of the depth of a small-size loop on the characteristic domain size. Of course, the small-size loop can be always removed using an extremely large system size, but oversizing is very inefficient in the computational study. It is noted that Fig. 3 is obtained from small system-size simulations. In this respect, Fig. 3 is particularly useful for us to identify an appropriate system size, that is, a size large enough for reducing the loop but not oversized for the sake of saving computing time.

As is mentioned by the referee, the attractive potential is not necessarily in most of the real system. However, what I would like to say in this work is that it is possible to estimate an appropriate system size to remove effectively the strange loop. A fluid system which has a strong attractive potential (comparing to the system temperature) will require very

large system size to reduce the van der Waals loop in molecular simulation. It should be noted that this condition is satisfied even for a fluid with weak attractive interaction if the system temperature is very low. A fluid with weak attractive potential however requires a system not as large as the system required in the former condition.

References

[1] J. D. van der Waals, *Doctoral Dissertation* (Leiden, 1873).

[2] A. Kido, O. Kitao, and K. Nakanishi, Chem. Phys. Lett. **199**, 403 (1992).

[3] R. Yamamoto, O. Kitao, and K. Nakanishi, submitted for publication.

[4] M. P. Allen and D. J. Tildesley, *Computer Simulation of Liquids* (Oxford University, Oxford, 1987).

[5] J. P. Hansen and L. Verlet, Phys. Rev. **184**, 151 (1969).

[6] J. J. Nicolas, K. E. Gubbins, W. B. Streett, and D. J. Tildesley, Mol. Phys. **37**, 1429 (1979).

[7] J. K. Johnson, J. A. Zollweg, and K. E. Gubbins, Mol. Phys. **78**, 591 (1993).

[8] Y. Choi, T. Ree, and F. H. Ree, J. Chem. Phys. **99**, 9917 (1993).

[9] S. D. Stoddard, and J. Ford, Phys. Rev. A **8**, 1504 (1973).

[10] B. Smit, J. Chem. Phys. **96**, 8639 (1992).

[11] M. J. P. Nijmeijer, A. F. Bakker, C. Bruin, and J. H. Sikkenk, J. Chem. Phys. **89**, 3789 (1988).

[12] W. G. Hoover, A. J. C. Ladd, and B. Moran, Phys. Rev. Lett. **48**, 1818 (1982); D. J. Evans, J. Chem. Phys., **78**, 3297 (1983); D. Brown and J. H. R. Clarke, Mol. Phys. **51**, 1243 (1984).

Chapter 5.

Computer simulation of vapor-liquid phase separation in two- and three-dimensional fluids: Growth law of domain size

Abstract

The late-time growth law of the vapor-liquid phase separation in two- and three-dimensional one-component fluids has been investigated by molecular dynamics simulations in which instantaneous quenching of fluid composed of 50 000 (2D) or 78 732 (3D) Lennard-Jones particles into the corresponding two phase (spinodal) region has been performed. The power law growth of the characteristic length scale, i.e., $l(t) \sim t^a$ is observed in both the 2D and 3D systems in the late stage. All molecular dynamics simulations which I have carried out, except for the cases in which the scaling regime has not been reached in simulation time, confirm that the asymptotic growth exponent is $\frac{1}{2}$ in both two- and three-dimensions. It is also found that thermal noise has no effect on the growth exponent but gives rise to a substantial delay of the transition time to the asymptotic regime. This work provides temporal domain patterns associated with the phase separation processes suggesting that the domain structures are sensitive to the temperature of the system.

I. Introduction

The dynamical aspects of phase separations are not very well understood. Many experimental, theoretical, and numerical approaches have been applied to this problem [1]. In experimental studies, metal alloys and binary fluid mixtures in the vicinity of the critical point have been extensively investigated by x-ray and neutron small-angle scattering experiments; the time scales of the phase separations are comparable to the experimental time scales in such systems. These studies related to the spinodal decomposition have been reviewed in Refs. 1 and 2.

Lifshitz and Slyozov have theoretically analyzed the dynamics of aggregation of solute from supersaturated dilute solutions using a scaling concept [3]. They found that the late-time behavior of the growth law of the solute domain scales as $l(t) \sim t^{\frac{1}{3}}$, where $l(t)$ is the characteristic length of the domain size. This relation is known as the Lifshitz–Slyozov rule and agrees well with x-ray scattering experiments on spinodal decomposition.

Numerical studies have also been done for phase separation problems by Monte Carlo (MC) simulations for kinetic Ising models. Two types of kinetic Ising models are studied. One is the Glauber model in which the order parameter is not conserved, and the other is the Kawasaki model in which the order parameter is conserved. The former model is considered to be a good model for magnets, and the latter is good for metal alloys. The MC studies for these models are summarized in Refs. 1 and 4. It has been found that both the Glauber and the Kawasaki models show power law growth of domain size as $l(t) \sim t^a$, and the growth exponent a is found to be $\frac{1}{2}$ for the Glauber model and $\frac{1}{3}$ for the Kawasaki model. The growth law for the Kawasaki model agrees with the Lifshitz-Slyozov rule.

A different type of numerical studies has been applied to phase separation problems based on either of the following two phenomenological equations, i.e., the time-dependent Ginzburg-Landau (TDGL) equation which is the case for nonconserved order parameter,

$$\frac{\partial \psi(\mathbf{r},t)}{\partial t} = -L\frac{\delta H[\psi(\mathbf{r},t)]}{\delta \psi(\mathbf{r},t)}, \tag{1}$$

or the Cahn-Hilliard-Cook (CHC) equation which is the case for conserved order parameter,

$$\frac{\partial \psi(r,t)}{\partial t} = L\nabla^2\frac{\delta H[\psi(\mathbf{r},t)]}{\delta \psi(\mathbf{r},t)}, \tag{2}$$

where $\psi(\mathbf{r},t)$ is the order parameter of the system at point $\mathbf{r}$ and at time t, L is a phenomenological parameter, and $H[\psi(\mathbf{r},t)]$ is the coarse-grained free-energy functional given by

$$H[\psi(\mathbf{r},t)] = \int d\mathbf{r}\left[\frac{1}{2}(\nabla\psi)^2 - \frac{\tau}{2}\psi^2 + \frac{g}{4}\psi^4\right], \tag{3}$$

with temperature-dependent phenomenological parameters τ and g which are positive. The late-time growth behavior of phase separations has been discussed by solving these equations numerically. Oono and Puri have proposed an efficient computational method to solve TDGL and CHC equations using discrete space and time [6]. This numerical method is called the cell dynamical system (CDS). Using the CDS, it is found that the average domain size $l(t)$ shows a power law growth as $l(t) \sim t^a$ in the late stage, and the exponent a is found to be $\frac{1}{2}$ for the TDGL equation and $\frac{1}{3}$ for the CHC equation, respectively. These results coincide with the Monte Carlo results for the Glauber and the Kawasaki models. Thus, it is believable that the growth exponent is $\frac{1}{2}$ for the case of nonconserved order parameter and $\frac{1}{3}$ for the case of conserved order parameter.

Recent progress of computers makes it possible to study phase separation phenomena by molecular dynamics (MD) simulation. The advantage of MD simulation is that both static and dynamic correlations and hydrodynamic effects are all taken into consideration. The hydrodynamic effects are known to be important in the late stages of the phase separation dynamics of fluid systems such as fluid binary mixtures and polymer melts [7, 8, 9, 10, 11, 12]. Velasco and Toxvaerd [13] have carried out MD simulations for two-dimensional binary fluid mixtures and found that the growth exponent is $\frac{1}{2}$ in the early stage, and that a crossover to a higher exponent takes place in the late stage. Ma *et al.* [14] have also performed MD simulations for three-dimensional binary fluid mixtures and found that the growth exponent is 0.55. Both MD results have shown that the growth exponent is clearly larger than $\frac{1}{3}$, which is predicted by the MC simulation or the CHC equation which ignores the hydrodynamic effects.

In the case of a one-component fluid, the characteristic time scale relevant to the vapor-liquid phase separation is too short to observe experimentally. Koch *et al.* [15]

have studied the dynamics of vapor-liquid phase separation in a two-dimensional one-component fluid by MD simulations using a 5041-particle system. They have found that the characteristic length scale of the system grows in proportion to $t^{\frac{1}{2}}$ for the isothermal simulation and in proportion to $t^{\frac{1}{3}}$ for the adiabatic simulation. They have analyzed their simulation results by a similar way to Lifshitz and Slyozov and concluded that the growth exponent of $\frac{1}{2}$ obtained by their isothermal simulations is independent of the system dimensionality [15, 16].

In this study, I investigate more accurately the dynamics of vapor-liquid phase separation in two- and three-dimensional fluids via MD simulations with a 50 000-particle system for two dimensions and with a 78 732-particle system for three dimensions. The main purpose of the present work is to examine the analysis of Koch *et al.* on the isothermal phase separation, which stated that the growth exponent is $\frac{1}{2}$ and independent of the system dimensionality. First, their isothermal simulation results on a two-dimensional fluid are checked by adopting a much larger system size. Then I study the growth law dynamics in a three-dimensional fluid by MD simulation. If I can show that the growth exponents are $\frac{1}{2}$ in both two- and three-dimensions, it strongly suggests that their analysis is correct. In the adiabatic condition (the exponent is $\frac{1}{3}$ in Koch *et al.*'s simulation), the separation dynamics is supposed to be more complicated than the isothermal case. Since the system temperature increases with time because of the latent heat, the free-energy functional has a time dependency; it corresponds to the case in Eq. (3) that the parameters τ and g are not constant during the separation process. In this study, only the isothermal case is treated.

II. Simulation Methodology

In order to investigate the late-time growth behavior of phase separations by computer simulations, we have to use a quite large system because the characteristic length scale, i.e., the average size of the domains, easily becomes comparable to the system size as the separation grows. In this work, I use a 50 000-particle system for a two-dimensional fluid and a 78 732-particle system for a three-dimensional fluid. Because of the finite system

Table I. Critical and triple point constants for two- and three- dimensional Lennard-Jones fluids.

Dimension	T_c^*	ρ_c^*	T_t^*	Source	Method
2	0.56	0.325	0.41	Ref.17(a)	Theory[a]
	0.533	0.335	0.415	Ref.17(a)	MC
			0.40	Ref.17(b)	MC
3	1.36	0.36	0.68	Ref.18(a)	MC
	1.35	0.35		Ref.18(b)	MD
	1.313	0.310	0.69	Ref.18(c)	MD, MC

[a] Perturbation theory and cell theory.

size, simulations are stopped when the characteristic length scale $l(t)$ breaks the condition of $l(t) < \frac{L_c}{4}$ for the two-dimensional system and of $l(t) < \frac{L_c}{2}$ for the three-dimensional system, where L_c is the length of the simulation cell. For both two- and three-dimensional systems, each particle interacts through the Lennard-Jones (L-J) potential within the cutoff radius $r_{cut} = 2.7\sigma$,

$$\phi(r) = 4\epsilon\left[\left(\frac{\sigma}{r}\right)^{12} - \left(\frac{\sigma}{r}\right)^{6}\right]. \tag{4}$$

The periodic boundary conditions are used as usual. The leapfrog algorithm is used to integrate Newton's equations of motion with a time step of 0.01τ, where τ $(= \sqrt{\frac{m\sigma^2}{\epsilon}})$ is the unit time of the L-J fluid, which is equal to 2.1 ps for an argon-like fluid. The cell index method is employed together with the list vector to save the computation time on a vector processor (Cray Y-MP2E). Since the numerical method for molecular dynamics simulation is available in the literature [17], I do not repeat it.

The phase diagrams of the two- and three-dimensional L-J fluids are presented in Refs. 18 and 19. Table I summarizes the critical point and the triple point constants for these model fluids. Our MD simulations are carried out by the instantaneous quenching of homogeneous systems, which are initially equilibrated at the supercritical (one phase) region, into an unstable (two phase) region. I have performed four experiments (A–D) for the two-dimensional (2D) fluid and four experiments (E–H) for the three-dimensional (3D) fluid under the following conditions, so that we can investigate the effects of the system dimensionality and the thermal noises on the phase separation dynamics.

A. 2D fluid ($T_c^* \approx 0.56$)

Exp. A. The system is initially equilibrated at the density $\rho^* = 0.325$ and the temperature $T^* = 0.8$, corresponding to the one phase region in the phase diagram of the two-dimensional L-J fluid. Then, the system is quenched into $T^* = 0.41$ (the triple point temperature) by the instantaneous velocity scaling of all particles, while the density remains unchanged.

Exp. B. The same as Exp. A, but the system is quenched into $T^* = 0.45$.

Exp. C. The same as Exp. A, but the system is quenched into $T^* = 0.48$.

Exp. D. The same as Exp. A, but the system is quenched into $T^* = 0.50$.

B. 3D fluid ($T_c^* \approx 1.35$)

Exp. E. The system is initially equilibrated at the density $\rho^* = 0.35$ and the temperature $T^* = 1.8$, corresponding to the one phase region in the phase diagram of the three-dimensional L-J fluid. Then, the system is quenched into $T^* = 0.7$ (just above the triple point temperature), while the density remains unchanged.

Exp. F. The same as Exp. E, but the system is quenched into $T^* = 1.0$.

Exp. G. The same as Exp. E, but the system is quenched into $T^* = 1.05$.

Exp. H. The same as Exp. E, but the system is quenched into $T^* = 1.1$.

In all the above simulations, the temperature is kept constant during each simulation run by the constraint isotherm method [17, 20], which generates a trajectory on the constant-NVT (canonical) ensemble. In Ref. 13 one can find a discussion on a comparison of some isotherm methods for the phase separation dynamics of binary liquid mixture. It seems that the growth dynamics is not sensitive to the choice of the isotherm method. The phase separation begins immediately after the quenching by the mechanism of spinodal decomposition. Since we are interested only in the late-time growth behavior of the vapor-liquid phase separation, I did not analyze the data in the early stage of the separation process. The time-dependent (temporal) structure factor of the system is calculated

throughout the simulation runs by

$$S(k = |\mathbf{k}|, t) = \frac{1}{N}\left[\left(\sum_{i=1}^{N} \cos \mathbf{k} \cdot \mathbf{r}_i\right)^2 + \left(\sum_{i=1}^{N} \sin \mathbf{k} \cdot \mathbf{r}_i\right)^2\right], \tag{5}$$

where N is the total number of particles, $\mathbf{r}_i$ is the position vector of the ith particle, and $\mathbf{k}$ is a wave vector:

(2D)

$$\frac{L_c}{2\pi}\mathbf{k} = (1,0), (0,1), (1,1), (1,-1), (0,2), \ldots \ ,$$

(3D)

$$\frac{L_c}{2\pi}\mathbf{k} = (1,0,0), (0,1,0), (0,0,1), (1,1,0), \ldots \ .$$

The first moment of the wave number $k_1(t)$ was evaluated by

$$k_1(t) = \frac{\int_0^{k_{\rm cut}} k\tilde{S}(k,t)dk}{\int_0^{k_{\rm cut}} \tilde{S}(k,t)dk}, \tag{6}$$

which measures a characteristic wave number of the system. Here $k_{\rm cut}$ is an appropriate cutoff wave number, and $k_{\rm cut} = \frac{\pi}{\sigma}$ is adopted in this work. $\tilde{S}(k,t)$ is the "macroscopic" structure factor defined by

$$\tilde{S}(k,t) = S(k,t) - S^{\rm eq}(k), \tag{7}$$

where $S^{\rm eq}(k)$ denotes the equilibrium structure factor for a fully segregated macroscopic two phase system. The equilibrium structure factor $S^{\rm eq}(k)$ was obtained by quenching to the point across the coexistence curve and waiting for the system to reach an equilibrium. The first moment of the wave number $k_1(t)$ is regarded as a length proportional to the inverse of the characteristic length scale, i.e., $l(t) = \frac{2\pi}{k_1(t)}$.

III. Results and Discussion

A. two-dimensional fluid

Temporal sequences of atomic configurations after the quench for the experiments A, B, C, and D are shown in Figs. 1, 2, 3, and 4, respectively. One can see that the phase separation begins immediately after the quench and the domain size increase with simulation time in all the experiments. However, there is a notable difference between

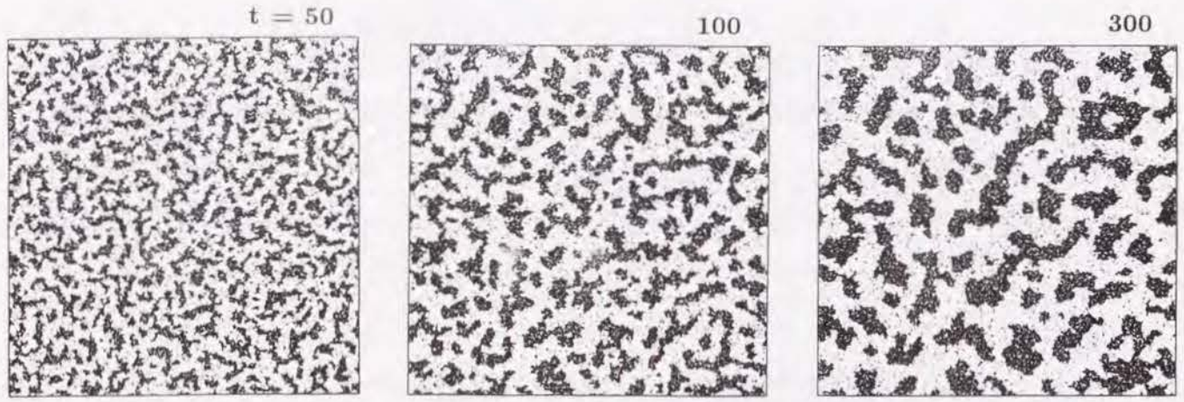

Fig. 1. Snapshots of the simulation experiment A ($T^* = 0.41$). The labels refer to simulation time in units of τ.

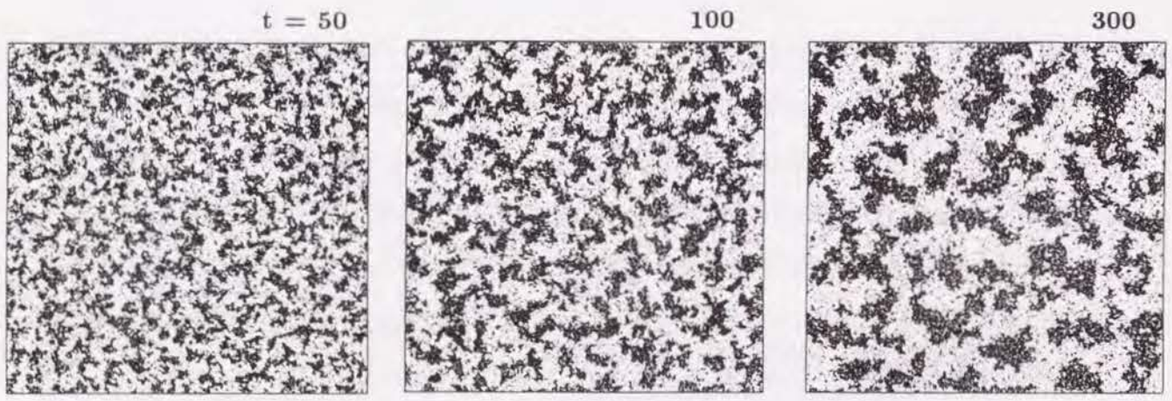

Fig. 2. Snapshots of the simulation experiment B ($T^* = 0.45$). The labels refer to simulation time in units of τ.

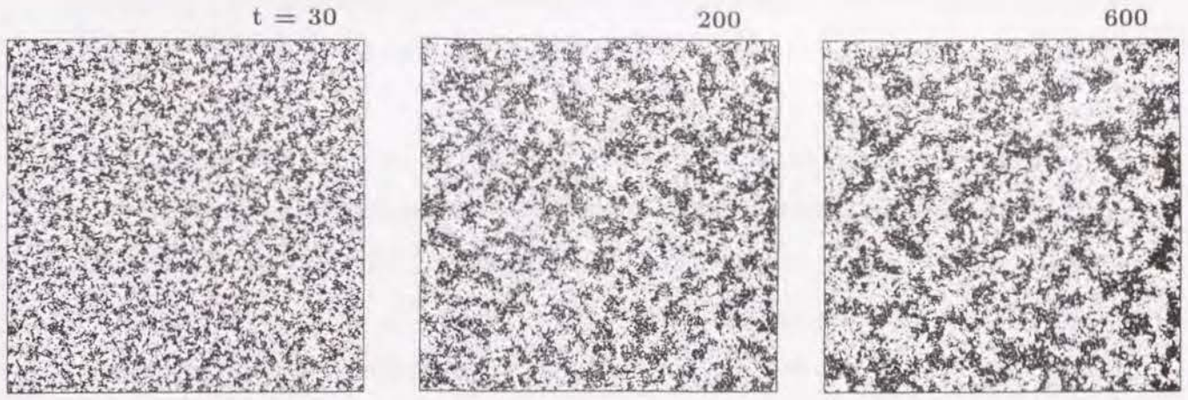

Fig. 3. Snapshots of the simulation experiment C ($T^* = 0.48$). The labels refer to simulation time in units of τ.

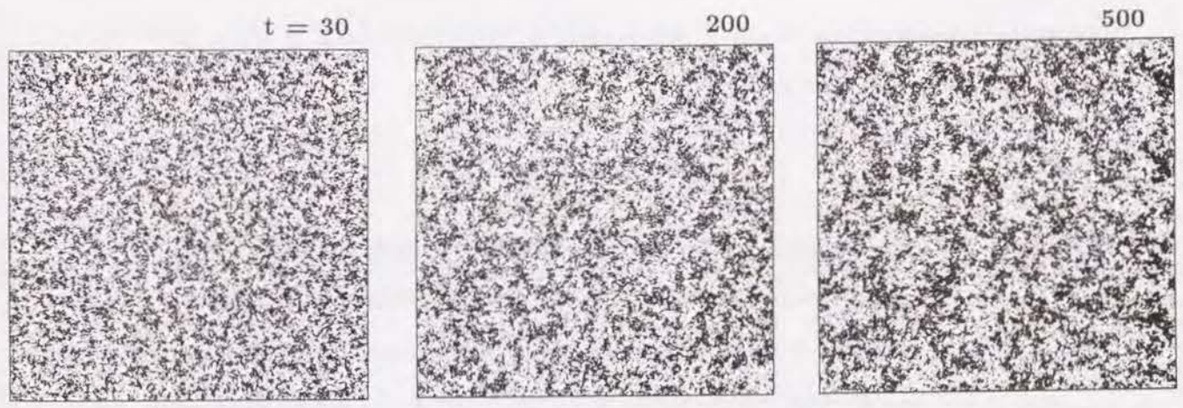

Fig. 4. Snapshots of the simulation experiment D ($T^* = 0.50$). The labels refer to simulation time in units of τ.

domain structures. It is observed that the roughness of the vapor-liquid interface increases with increasing annealing temperature of the system. This is attributed to the following effects: the surface tension decreases, and the thermal noise increases with increasing temperature.

The time evolution of the structure factor for the experiment A is shown in Fig. 5 as a typical example. One can observe that the peak position shifts to a smaller k value and the peak height increases with simulation time. This shift of the peak position indicates the growth of the domain size according to $l(t) \sim \frac{1}{k(t)}$. In Fig. 6, I have plotted the first moment of the wave number $k_1(t)$ for each experiment against the simulation time in log-log scale. The growth exponent is given by the negative of the slope. It is confirmed that power law growth clearly exists in the late-time region ($k_1 < 0.28$ in Fig. 6), and the asymptotic growth exponent is found to converge to $\frac{1}{2}$ for both the experiments A ($T^* = 0.41$) and B ($T^* = 0.45$). For the experiments C ($T^* = 0.48$) and D ($T^* = 0.50$), the asymptotic growth regime has not yet been reached. As is shown later, this is also confirmed by our scaling analysis. Table II summarizes the simulation results on the growth exponents for the two-dimensional fluid.

The scaling hypothesis for $\tilde{S}(k,t)$ are tested. The scaling hypothesis has been established by experiments on metal alloys and by simulations for the Ising model in an asymptotic growth regime as follows:

$$F(x) = (k_1)^d \tilde{S}(k,t), \tag{8}$$

where d is the dimensionality of the system and $F(x)$ is a time-independent universal structure function. The scaled structure factor $(k_1)^2\tilde{S}(k,t)$ obtained from the experiments A, B, C, and D at different times is shown in Figs. 7, 8, 9, and 10, respectively. For the experiments A and B, the data points can be seen to lie on a smooth master curve. Thus, we can conclude that an asymptotic growth (scaling) regime has been reached for these two experiments A and B. However, for the experiments C and D, we see that no asymptotic growth regime has yet been obtained within our simulation time.

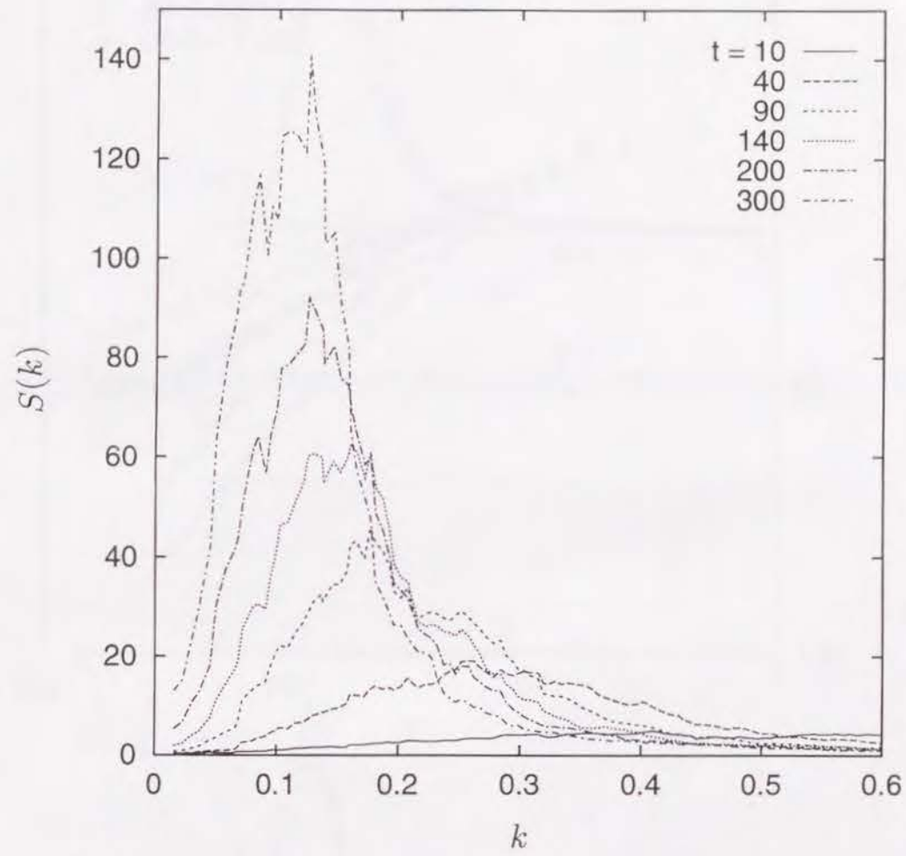

Fig. 5. Time evolution of the structure factor for the experiment A.

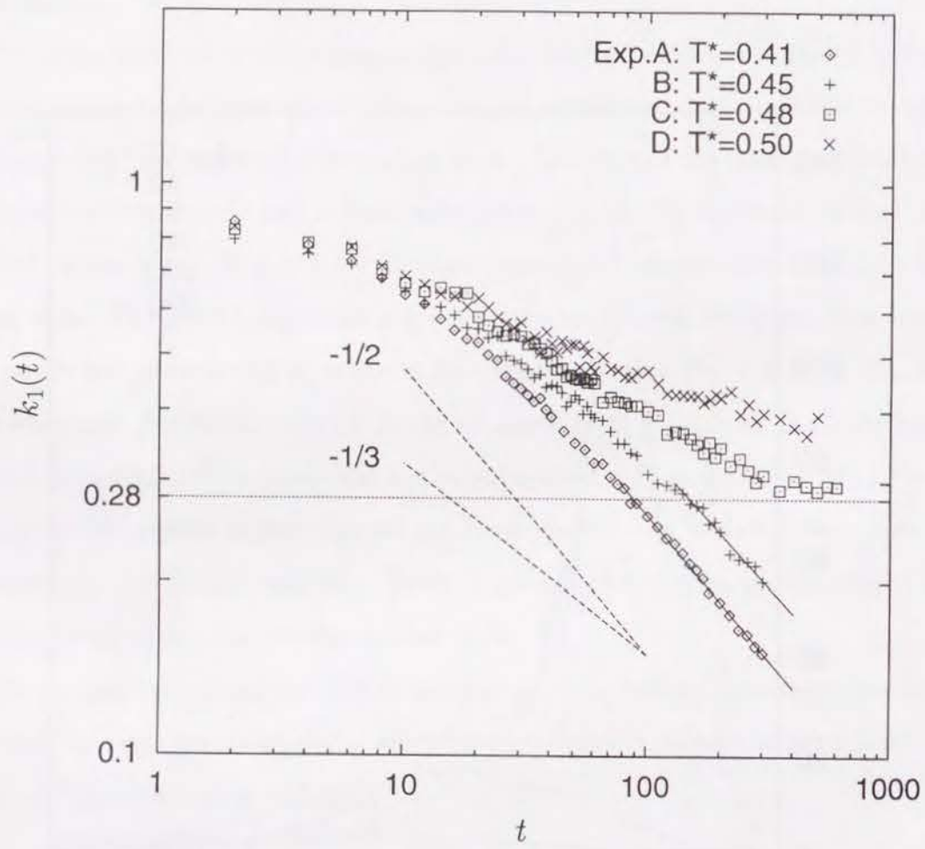

Fig. 6. First moment of the wave number $k_1(t)$ versus simulation time for the experiments A–D. The growth exponents converge to $-\frac{1}{2}$ at late stages ($k_1 < 0.28$) in experiments A and B. The solid lines show the least square fitting results using data for $k_1 < 0.28$. The dashed lines show the slopes of $-\frac{1}{2}$ and $-\frac{1}{3}$ for comparison.

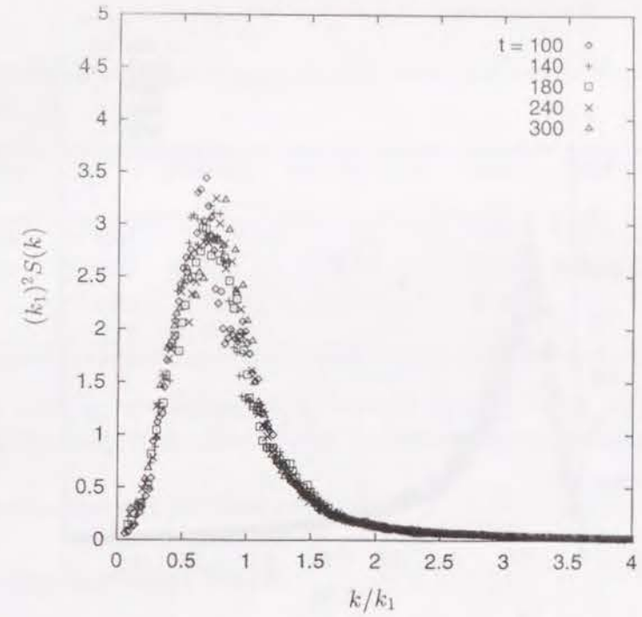

Fig. 7. Plots of the scaled structure factor for the experiment A.

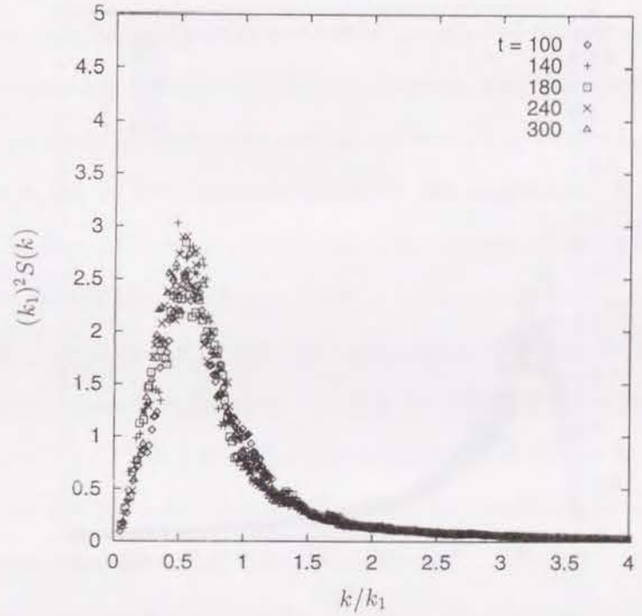

Fig. 8. Plots of the scaled structure factor for the experiment B.

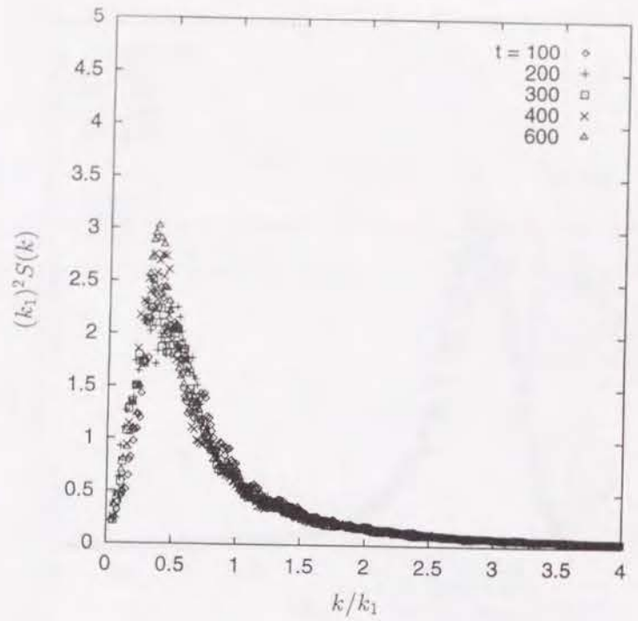

Fig. 9. Plots of the scaled structure factor for the experiment C.

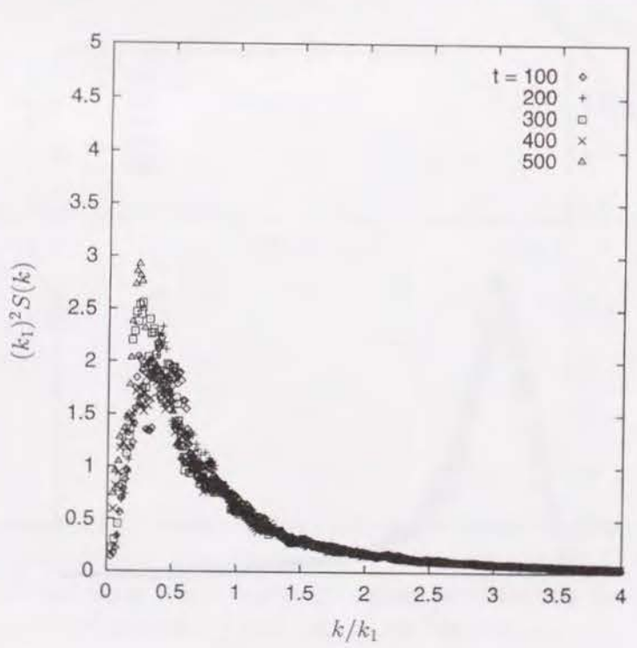

Fig. 10. Plots of the scaled structure factor for the experiment D.

Table II. Summary of simulation runs for the phase separation experiments for a two-dimensional fluid.

Exp.	N	Density ρ^*	Temperature T^*	Time τ	Exponent[a]
A	50 000	0.325	0.41	300	0.499 ±0.008
B	50 000	0.325	0.45	300	0.467 ±0.030
C	50 000	0.325	0.48	600	[b]
D	50 000	0.325	0.50	500	[b]

[a] Evaluated by least square fitting using data for $k_1 < 0.28$. ± on the listed exponent values shows the accuracy of the data fitting. It does not mean the accuracy of the present simulations.
[b] Asymptotic regime has not yet been reached.

B. three-dimensional fluid

Temporal sequences of atomic configurations after the quench for the experiments E and G are shown in Figs. 11 and 12, respectively. As in the case of the two-dimensional fluid, phase separation begins immediately after the start of the quench. The domain size increases with simulation time in all the experiments, and the roughness of the vapor-liquid interface seems to increase with increasing annealing temperature.

The time evolution of the structure factor for the experiment E is shown in Fig. 13 as an example. In Fig. 14, I have plotted the first moment of the wave number $k_1(t)$ for each experiment against the simulation time in log-log scale. As in the two-dimensional fluid, power law growth exists in the late-time region ($k_1 < 0.45$ in Fig. 14), and the asymptotic growth exponent is found to converge to $\frac{1}{2}$ for the experiments E ($T^* = 0.70$), F ($T^* = 1.00$), and G ($T^* = 1.05$). For the experiment H ($T^* = 1.10$), the asymptotic growth regime has not yet been reached. Table III summarizes the simulation results on the growth exponent for the three-dimensional fluid.

The test of the scaling hypothesis for $\tilde{S}(k,t)$ of the three-dimensional fluid has also been made. The scaled structure factors $(k_1)^3\tilde{S}(k,t)$ obtained from the experiments E, F, G, and H are shown in Figs. 15, 16, 17, and 18, respectively. The data points seem to deviate from each other for the experiments G and H, but almost lie on a smooth master curve for the experiments E and F. Thus, we can conclude that the scaling regime

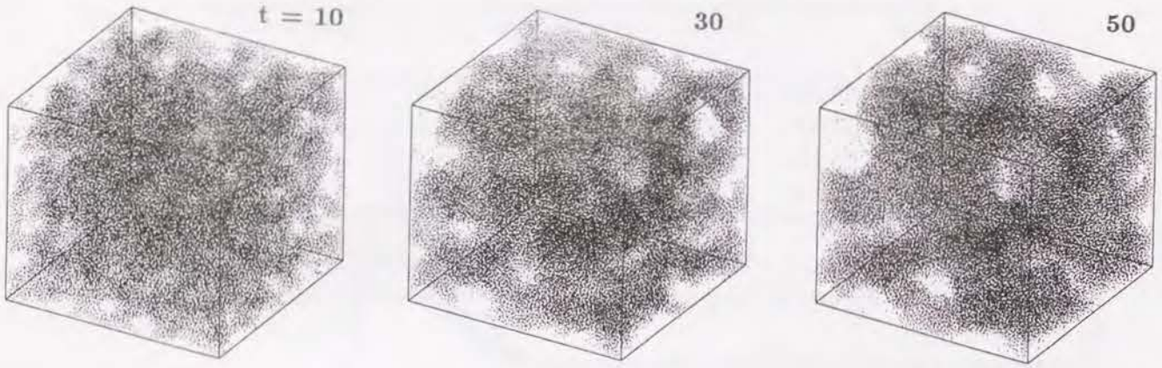

Fig. 11. Snapshots of the simulation experiment E ($T^* = 0.70$). The labels refer to simulation time in units of τ.

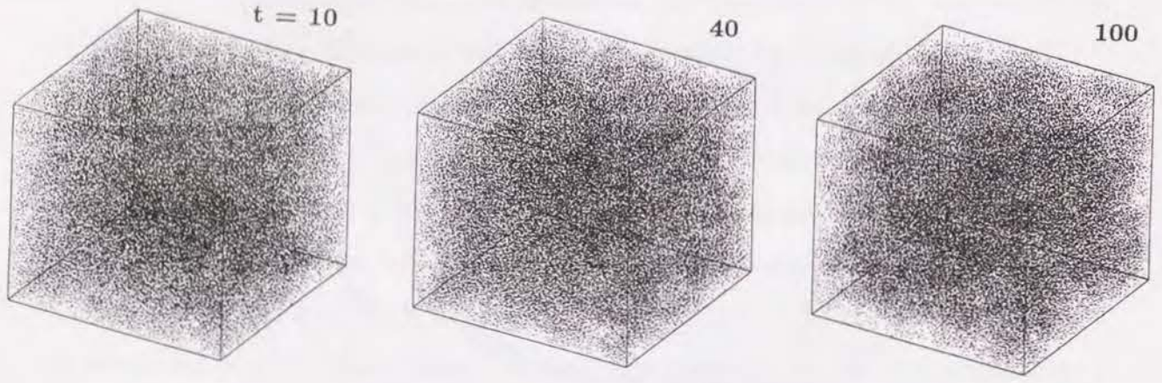

Fig. 12. Snapshots of the simulation experiment G ($T^* = 1.05$). The labels refer to simulation time in units of τ.

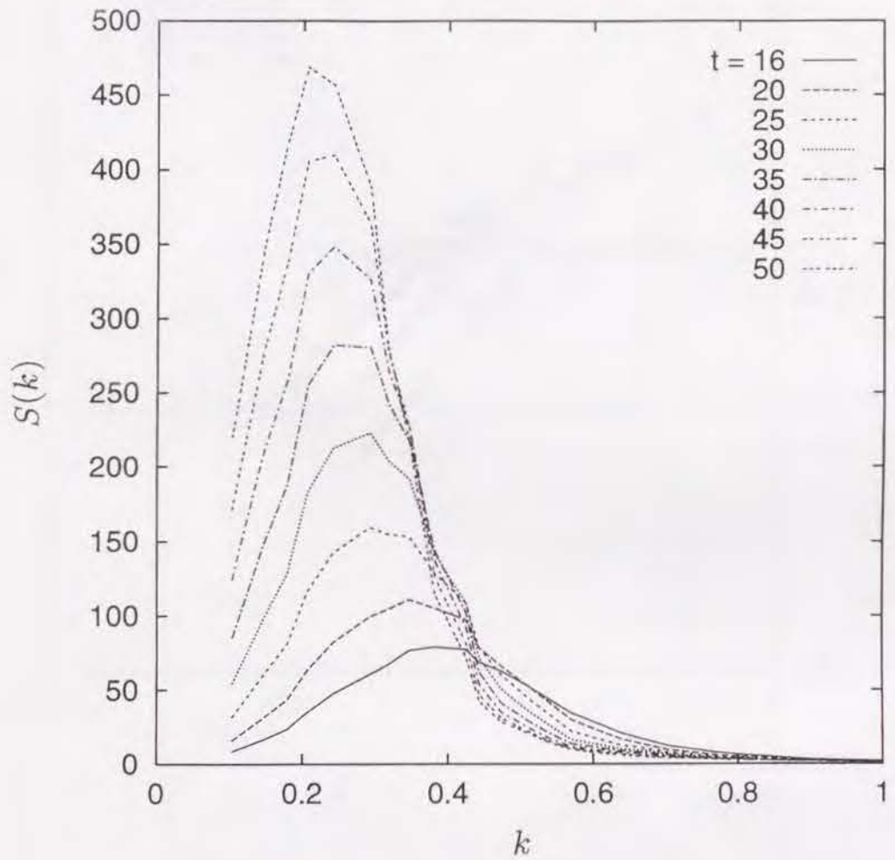

Fig. 13. Time evolution of the structure factor for the experiment E.

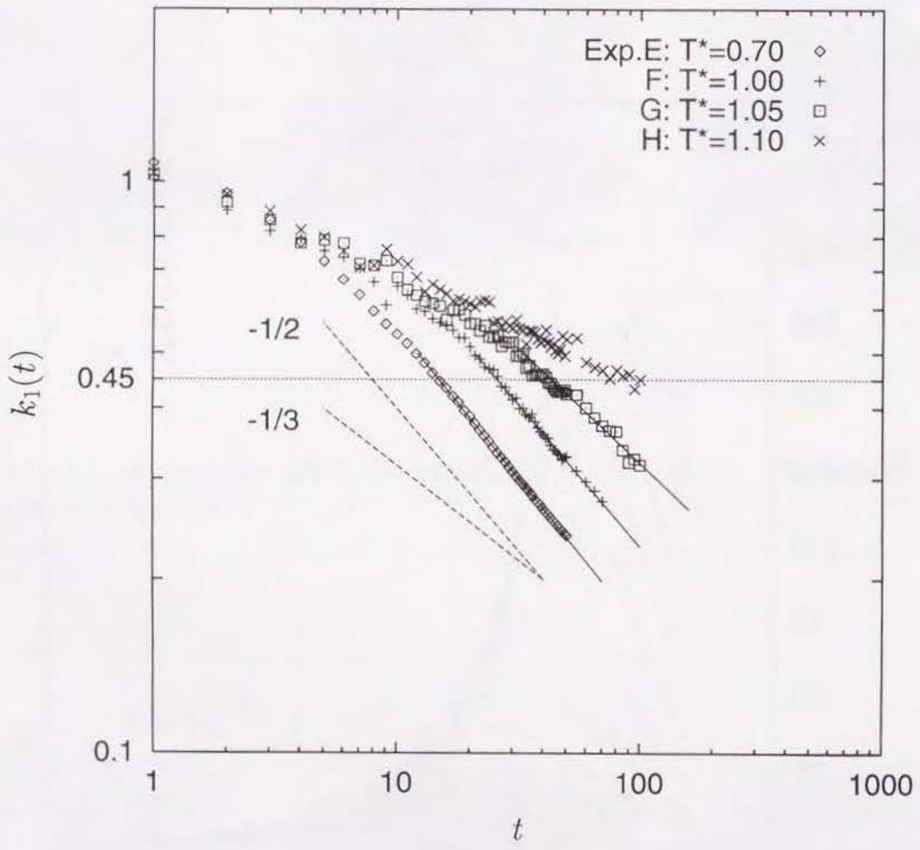

Fig. 14. First moment of the wave number $k_1(t)$ versus simulation time for the experiments E–H. The growth exponents converge to $-\frac{1}{2}$ at late stages ($k_1 < 0.45$) in experiments E, F, and G. The solid lines show the least square fitting results using data for $k_1 < 0.45$. The dashed lines show the slopes of $-\frac{1}{2}$ and $-\frac{1}{3}$ for a comparison.

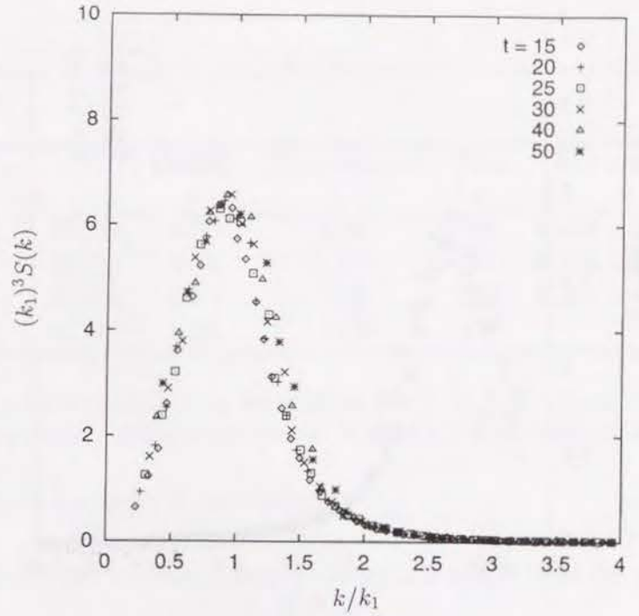

Fig. 15. Plots of the scaled structure factor for the experiment E.

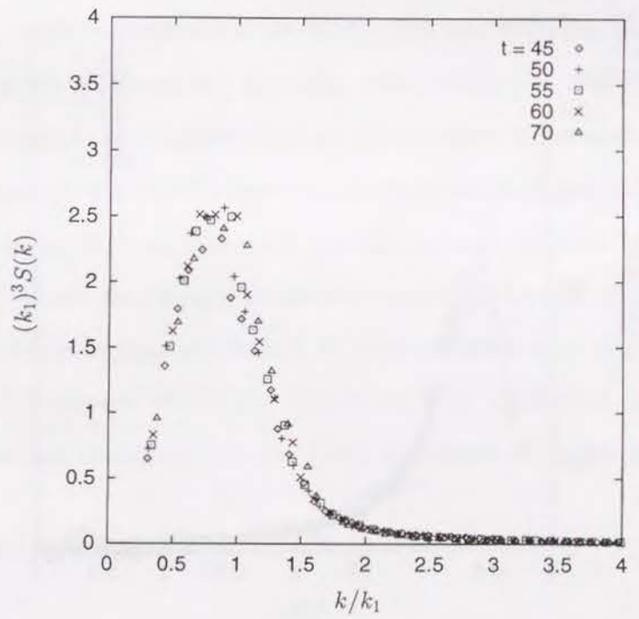

Fig. 16. Plots of the scaled structure factor for the experiment F.

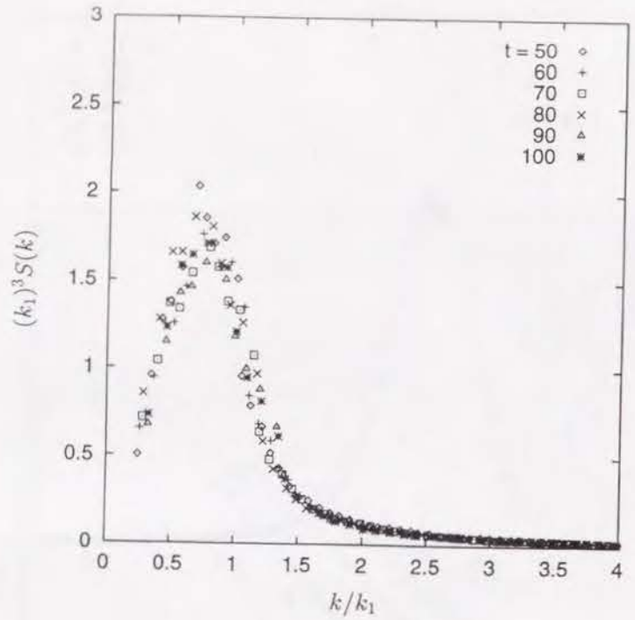

Fig. 17. Plots of the scaled structure factor for the experiment G.

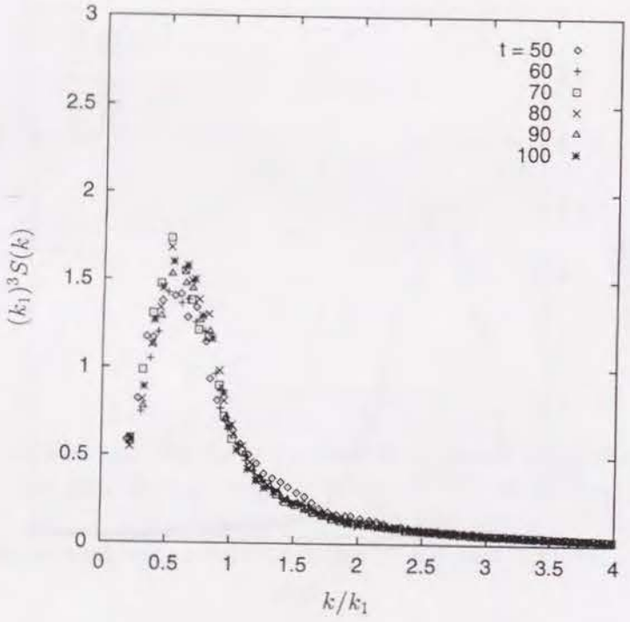

Fig. 18. Plots of the scaled structure factor for the experiment H.

Table III. Summary of simulation runs for the phase separation experiments for a three-dimensional fluid.

Exp.	N	Density ρ^*	Temperature T^*	Time τ	Exponent[a]
E	78 732	0.35	0.70	50	0.529 $\pm$0.002
F	78 732	0.35	1.00	70	0.502 $\pm$0.008
G	78 732	0.35	1.05	100	0.404 $\pm$0.025
H	78 732	0.35	1.10	100	[b]

[a] Evaluated by least square fitting using data for $k_1 < 0.45$. $\pm$ on the listed exponent values shows the accuracy of the data fitting. It does not mean the accuracy of the present simulations.
[b] Asymptotic regime has not yet been reached.

has been reached at least for these two experiments E and F, and the asymptotic growth exponent is $\frac{1}{2}$ for the three-dimensional fluid as well.

The results of the present MD simulations for two- and three-dimensional fluids strongly suggest that the asymptotic growth exponent for the vapor-liquid phase separation is $\frac{1}{2}$ in both two- and three-dimensions. This coincides with the simulation result of Koch *et al.* on a two-dimensional fluid [15, 16] and also supports their analysis, which stated that the growth exponent is $\frac{1}{2}$ and independent of system dimensionality. It is also confirmed that thermal noise has no effect on the asymptotic exponent, but gives rise to a substantial delay of the transition time till the asymptotic regime is reached. A similar result has been obtained from numerical simulation with the CHC equation including thermal noise [5]. These results seem to be consistent with the phenomenon called critical slowing down. I suppose that the failure of some simulations at high temperatures to converge to the $\frac{1}{2}$ exponent within the simulation time is affected by this effect. The analysis of the domain structures is particularly of interest. It is discussed in Chapter 6.

IV. Concluding Remarks

I have studied the asymptotic growth law of the vapor-liquid phase separation for the two- and three-dimensional one-component Lennard-Jones fluids by MD simulations, using a 50 000-particle system for two-dimensional fluids and a 78 732-particle system for

three-dimensional fluids. MD simulations have been carried out by instantaneous quenching of a homogeneous system, which has been equilibrated at supercritical temperature, into the two phase region. The phase separation begins immediately after the quench of the homogeneous system, and the time-dependent (temporal) structure factor $S(k,t)$ has been calculated throughout the simulation runs. The characteristic length scale has been found to grow as $l(t) \sim t^a$ in the late-time (scaling) regime, which corresponds to $k_1 < 0.28$ for the two-dimensional fluid and $k_1 < 0.45$ for the three-dimensional fluid in this work, and the asymptotic growth exponent was found to be $\frac{1}{2}$ in common with two and three dimensions. This strongly suggest that Koch *et al.*'s analysis is correct. Thermal noise was found to have no effect on the asymptotic exponent, but to give rise to a substantial delay of the transition time to the asymptotic regime.

It is observed that the roughness of the vapor-liquid interface increases with increasing annealing temperature in both two- and three-dimensional fluids. This is attributed to the following two effects: the surface tension decreases, and thermal noise increases with increasing system temperature. The atomic configurations obtained by the MD simulations indicate that the domain structure is notably sensitive to the system temperature. In fact, the domain structures of the two-dimensional L-J fluid have been reported to suggest a fractal nature at $T^* = 0.45$ (Langevin dynamics simulation) [21] or at $T^* \approx 0.5$ (constant-NVE MD simulation) [22]. Analysis of the domain structures for the present simulations is reported in Chapter 6.

References

[1] J. D. Gunton, M. San Miguel, and P. S. Sahni, in *Phase Transitions and Critical Phenomena*, edited by C. Domb and J. L. Lebowitz (Academic, New York, 1983), Vol. 8.

[2] V. Gerold and G. Kostorz, J. Appl. Crystallogr. **11** 376 (1978).

[3] I. M. Lifshitz and V. V. Slyozov, J. Phys. Chem. Solids **19**, 35 (1961).

[4] A. Sadiq and K. Binder, J. Stat. Phys. **35**, 517 (1984).

[5] T. M. Rogers, K. R. Elder, and R. C. Desai, Phys. Rev. B **37**, 9638 (1988).

[6] Y. Oono and S. Puri, Phys. Rev. A **38**, 434 (1988); **38**, 1542 (1988).

[7] N. C. Wong and C. Knobler, J. Chem. Phys. **69**, 725 (1976).

[8] E. D. Siggia, Phys. Rev. A **20**, 595 (1979).

[9] T. Koga and K. Kawasaki, Phys. Rev. A **44**, R817 (1991).

[10] S. Puri and B. Dünweg, Phys. Rev. A **45**, R6977 (1992).

[11] J. E. Farrell and O. T. Valls, Phys. Rev. B **40**, 7027 (1989).

[12] J. E. Farrell and O. T. Valls, Phys. Rev. B **42**, 2353 (1990).

[13] E. Velasco and S. Toxvaerd, Phys. Rev. Lett. **71**, 388 (1993).

[14] W-J. Ma, A. Maritan, J. R. Banavar, and J. Koplik, Phys. Rev. A **45**, R5347 (1992).

[15] S. W. Koch, R. C. Desai, and F. F. Abraham, Phys. Rev. A **27**, 2152 (1983).

[16] R. C. Desai, S. W. Koch, and F. F. Abraham, Physica A **118**, 136 (1983).

[17] M. P. Allen and D. J. Tildesley, *Computer Simulation of Liquids*, (Clarendon, Oxford 1987).

[18] (a) J. A. Barker, D. Henderson, and F. F. Abraham, Physica A **106**, 226 (1981); (b) J. M. Phillips, L. W. Bruch, and R. D. Murphy, J. Chem. Phys. **75**, 5097 (1981).

[19] (a) J. P. Hansen and L. Verlet, Phys. Rev. **184**, 151 (1969); (b) J. J. Nicolas, K. E. Gubbins, W. B. Street, and D. J. Tildesley, Mol. Phys. **37**, 1429 (1979); (c) J. K. Johnson, J. A. Zollweg, and K. E. Gubbins, *ibid.* **78**, 591 (1993); (d) Y. Choi, T. Ree, and F. H. Ree, J. Chem. Phys. **99**, 9917 (1993).

[20] W. G. Hoover, A. J. C. Ladd, and B. Moran, Phys. Rev. Lett. **48**, 1818 (1982); D. J. Evans, J. Chem. Phys. **78**, 3297 (1983); D. Brown and J. H. R. Clarke, Mol. Phys. **51**, 1243 (1984).

[21] M. Schöbinger, S. W. Koch, and F. F. Abraham, J. Stat. Phys. **42**, 1071 (1986).

[22] R. C. Desai and A. R. Denton, in *On Growth and Form*, edited by H. E. Stanley, and N. Ostrowsky (Martinus Nijhoff, The Hague 1986).

Chapter 6.

Computer simulation of vapor-liquid phase separation in two- and three-dimensional fluids: Domain structure

Abstract

Fluids undergoing phase separation exhibit complicated domain patterns. In this study molecular-dynamics simulations are performed for two- and three-dimensional Lennard-Jones fluids in order to investigate the relationship between statistical properties of domain structure and system temperature. The asymptotic form factor of each pattern is obtained using scaling and its temperature dependence studied. In particular the asymptotic tail of the form factor is analyzed. This tail is related to the domain-wall structure. At low system temperatures, the form factor satisfies Porod's law; its asymptotic tail decreases as $S(k) \sim k^{-(D+1)}$ where D is the system dimensionality. However, it is found that the decay of the asymptotic tail becomes slower than that of the Porod tail at higher temperatures in both the two- and three-dimensional systems. This indicates that the dimension of the domain wall is fractal and increases with increasing system temperature.

I. Introduction

Phase separation is a typical subject of pattern formation far from equilibrium. The important characteristics of phase separation are the random nature of the domain pattern and its growth [1]. While there are few purely theoretical treatments for such a nonequilibrium process, many computational studies have been made. In particular, the growth law of the domain size has been extensively investigated by means of computer simulations in the spinodal region where the uniform phase is unstable. Phase separations can generally be put into two categories: those of a conserved order parameter and those of a nonconserved order parameter. In vapor-liquid phase separation, the order parameter is the local density of the fluid. Since the total density of the system is conserved, this process belongs to the case of a conserved order parameter. In the study of the dynamics of phase separation for a conserved order parameter, the following two models have been widely employed in numerical studies. One is the Kawasaki model [2] which is a conserved-order-parameter version of the kinetic Ising model; the Hamiltonian is given by

$$\mathcal{H} = -J\sum_{i,j} S_i S_j - H\sum_i S_i, \tag{1}$$

where J is the interaction parameter, $\sum_{i,j}$ is usually taken only over nearest-neighbor pairs, $S_i = \pm 1$, and H is an external field. This model reduces to the lattice gas model with the definition $S_i \equiv 1 - 2c_i$ in which $c_i = 1$ if the site is occupied and $c_i = 0$ if the site is unoccupied. The other model is given by the Cahn-Hilliard-Cook (CHC) equation [3] based on a phenomenological Ginzburg-Landau theory. The CHC equation corresponds to a conserved-order-parameter version of the time-dependent Ginzburg-Landau equation which is given by

$$\frac{\partial\psi(\mathbf{r},t)}{\partial t} = L\nabla^2\frac{\delta H[\psi(\mathbf{r},t)]}{\delta\psi(\mathbf{r},t)} + \sigma(\mathbf{r},t), \tag{2}$$

where $\psi(\mathbf{r},t)$ is the order parameter of the system at point $\mathbf{r}$ and time t, L is a phenomenological parameter, and $\sigma(\mathbf{r},t)$ is Gaussian white noise. $H[\psi(\mathbf{r},t)]$ is the coarse-grained free-energy functional given by

$$H[\psi(\mathbf{r},t)] = \int d\mathbf{r}\left[\frac{1}{2}(\nabla\psi)^2 - \frac{\tau}{2}\psi^2 + \frac{g}{4}\psi^4\right], \tag{3}$$

with temperature-dependent positive phenomenological parameters τ and g. Computer simulations using these models provide evolutions of the domain patterns during phase separation, showing there exists an apparent scaling property in the course of evolution [1, 4, 5]. In a late-time stage of the phase separation, the temporal patterns are statistically equivalent to each other if they are scaled by the proper time-dependent characteristic length.

A weak point in these numerical studies is that the relation between the models and real fluids is unclear. On the other hand, molecular-dynamics (MD) simulations enable us to study phase separation for more realistic fluids such as Lennard-Jones (LJ) fluids [6, 7, 8, 9]. Another advantage of MD simulations is that static and dynamic correlations as well as hydrodynamic effects are taken into consideration. An important finding from MD simulations is that the domain pattern undergoing phase separation shows a fractal nature under certain conditions. Schöbinger *et al.* [10] have performed a constant-temperature Langevin dynamics simulation for the two-dimensional LJ fluid at a reduced temperature $T^* = 0.45$. They found that the capacity dimension of the domain (liquid clusters) is 1.8, being significantly smaller than the Euclidean dimension of 2. Desai and Denton [11] have performed a constant-NVE MD simulation for the two-dimensional LJ fluid at a reduced temperature $T^* \approx 0.5$ and found that the domain has a fractal dimension of 1.7. Such fractal behavior is also predicted analytically by Klein [12] using scaling in an early stage of the spinodal decomposition.

Previously I have carried out MD simulations for two- and three-dimensional LJ fluids undergoing spinodal decomposition and found that the structure of the domain pattern clearly shows a temperature dependence [9]. In particular, I have observed that the domain-wall (vapor-liquid interface) structure is greatly affected by the system temperature. The snapshots of atomic configurations for both two- and three-dimensional fluids suggest that the domain wall seems to be smooth at low temperatures, while it becomes rough at higher temperatures. In the present study, I investigate the relationship between statistical properties of the domain structure and the system temperature by means of MD simulations. The asymptotic form factor of the domain pattern undergoing spinodal decomposition is determined for various temperatures using scaling and its temperature

Table I. Simulation conditions for two- and three-dimensional systems.

Run	Dimension	N	Before quenching		After quenching		Time (τ)
			ρ^*	T^*	ρ^*	T^*	
Sim. A	2	50 000	0.325	0.80	0.325	0.35	220
Sim. B[a]	2	50 000	0.325	0.80	0.325	0.41	300
Sim. C[b]	2	50 000	0.325	0.80	0.325	0.45	300
Sim. D[c]	3	78 732	0.350	1.80	0.350	0.70	50
Sim. E	3	78 732	0.350	1.80	0.350	0.80	70
Sim. F	3	78 732	0.350	1.80	0.350	0.90	100

[a] This corresponds to the simulation experiment A in Ref. 9.
[b] This corresponds to the simulation experiment B in Ref. 9.
[c] This corresponds to the simulation experiment E in Ref. 9.

dependence is studied. In particular, I analyze the asymptotic tail of the form factor in the large-wave-number limit to determine the domain-wall structure.

II. Simulation Methodology

Since the characteristic length scale of the domain pattern can become comparable to the system size as the pattern grows, a reasonably large system is required to eliminate finite-size effects at late times in the phase separation. I have used a 50 000-particle system for a two-dimensional fluid and a 78 732-particle system for a three-dimensional fluid. In both two- and three-dimensional fluids, each particle interacts through the LJ potential with a cutoff length of $r_{cut} = 2.7\sigma$. The leapfrog algorithm is used with an integration time step of 0.01τ, where τ is the unit time of the LJ fluid. The present MD simulations were carried out by instantaneous quenching of homogeneous systems which are initially equilibrated at the supercritical (one phase) region, into an unstable (two phase) region. Quenching was done by scaling of the velocity of all particles while the density remains unchanged. After the quenching, the system was annealed at a constant temperature by the constraint isotherm method [13, 14]. Details of the present simulation are found in Refs. 9 and 13.

Three simulation runs (A–C) for the two-dimensional LJ fluid (critical temperature $T_c^* \approx 0.56$), and three runs (D–F) for the three-dimensional LJ fluid (critical temperature $T_c^* \approx 1.35$) are performed. The simulation conditions are summarized in Table I. Temporal structure factors were monitored during the simulation runs, which are given by

$$S(|\mathbf{k}|,t) = \frac{1}{N}\left[\left(\sum_{i=1}^{N}\cos\mathbf{k}\cdot\mathbf{r}_i(t)\right)^2 + \left(\sum_{i=1}^{N}\sin\mathbf{k}\cdot\mathbf{r}_i(t)\right)^2\right], \tag{4}$$

where $\mathbf{r}_i(t)$ is the position vector of the ith particle at time t and $\mathbf{k}$ is a wave-vector which follows the periodic boundary conditions

$$\mathbf{k} = \frac{2\pi}{L_c}(i\mathbf{e}_x + j\mathbf{e}_y), \tag{5}$$

$$i,j = 0,\pm1,\pm2,\pm3,..., \tag{6}$$

for the two-dimensional system, and

$$\mathbf{k} = \frac{2\pi}{L_c}(i\mathbf{e}_x + j\mathbf{e}_y + k\mathbf{e}_z), \tag{7}$$

$$i,j,k = 0,\pm1,\pm2,\pm3,..., \tag{8}$$

for the three-dimensional system. L_c is the length of the unit cell, and $\mathbf{e}_x$, $\mathbf{e}_y$, and $\mathbf{e}_z$ are the unit vectors in the x, y, and z directions. The raw structure factor $S(k,t)$ obtained directly from the MD simulations can be divided into two parts: a macroscopic part which determines the domain pattern and a microscopic part which represents a short-ranged particle-particle correlation. In this study we are only interested in the macroscopic part, that is, the form factor of the domain pattern. To eliminate the microscopic part of the raw structure factor, $\tilde{S}(k,t)$ is defined by:

$$\tilde{S}(k,t) \equiv S(k,t) - S^{eq}(k,T^*), \tag{9}$$

where $S^{eq}(k,T^*)$ denotes the equilibrium structure factor for a fully segregated macroscopic two-phase system at a temperature T^*. I have determined $S^{eq}(k,T^*)$ by quenching a smaller simulation system to the temperature T^* on the coexistence curve and waiting for the system to reach an equilibrium. Thus, $\tilde{S}(k,t)$ stands for the form factor of the pattern [15].

To determine the asymptotic form factor of the domain patterns, scaling was used as usual. It is widely known from experimental and numerical studies [1, 4, 5] that temporal form factors of the pattern undergoing phase separation satisfy a following scaling law at a late-time stage:

$$F(x) = (k_1)^D \tilde{S}(k,t), \tag{10}$$

where $F(x)$ is a time-independent master form factor, D is the dimensionality of the system, and x is the reduced wave-number defined as $\frac{k}{k_1}$. The first moment of the wave number k_1 is defined by

$$k_1 \equiv \frac{\int_0^{k_{cut}} k\tilde{S}(k,t)dk}{\int_0^{k_{cut}} \tilde{S}(k,t)dk}, \tag{11}$$

where k_{cut} is an appropriate cutoff wave number, for which I employed $k_{cut} = \frac{\pi}{\sigma}$ in this work. The characteristic length scale of the pattern is measured by k_1, which is inversely proportional to the characteristic length.

III. Results

A. Two-dimensional fluid

Snapshots from the simulation experiments for the two-dimensional fluid are shown in Fig. 1(a) for simulation A at $t = 220\tau$, (b) for simulation B at $t = 300\tau$, and (c) for simulation C at $t = 300\tau$, where τ is the unit time of the LJ fluid. As is already mentioned in Chapter 5 of the present study [9], one can see from Fig. 1 that the domain pattern clearly exhibits a temperature dependence. The domain wall looks smooth in Fig. 1(a), while the domain wall becomes clearly rough with increasing temperature as is shown in Figs. 1(b) and 1(c). Increasing temperature causes decreasing surface tension and increasing thermal noise on the surface. I suppose that this causes the surface roughening. To study the change in domain patterns quantitatively, I determine the asymptotic form factor of the pattern at each temperature. In Figs. 2(a), 3(a), and 4(a), the scaled form factor $(k_1)^2\tilde{S}(k,t)$ is plotted as a function of reduced wave number $\frac{k}{k_1}$. These scaled form factors for different simulation times lie for the most part on a single master curve. This means that the domain patterns obtained from the present simulations satisfy the scaling properties from which we can obtain the time-independent master form factor. By

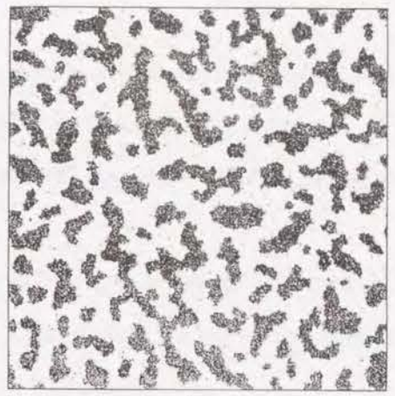

(a)

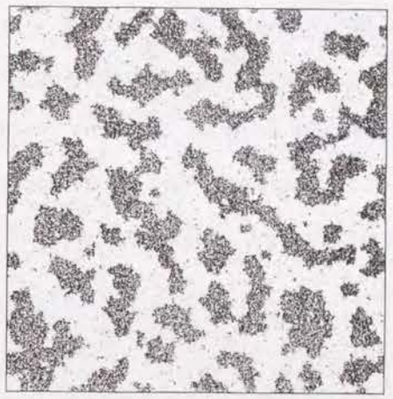

(b)

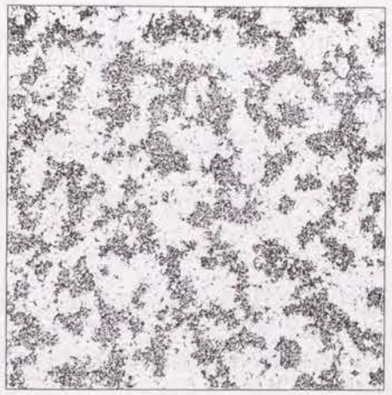

(c)

Fig. 1. Snapshots obtained from MD simulations for the two-dimensional fluid. (a) simulation A ($T^* = 0.35$ and $t = 220\tau$), (b) simulation B ($T^* = 0.41$ and $t = 300\tau$), (c) simulation C ($T^* = 0.45$ and $t = 300\tau$).

comparing the master form factor for different temperatures, the following temperature dependences are observed: (1) The peak position of the form factor shifts slightly to a smaller wave number with increasing temperature, and (2) the peak height decreases with increasing temperature.

The asymptotic tail of the form factor is related to the domain-wall structure. It is widely known that the master form factor follows Porod's law [16] in the large-wave-number limit,

$$F(x) \sim x^{-(D+1)}. \tag{12}$$

Numerical, experimental, and theoretical studies support this law [17, 18, 19].

It can be shown that the master form factor with smooth domain walls satisfies Porod's law. It has been shown by Bale and Schmidt [21] that Porod's law can be extended to the case of a rough interface. They have derived the asymptotic tail behavior of the form factor for a system with a fractal domain wall as follows:

$$F(x) \sim x^{-(2D-F_s)}, \tag{13}$$

where F_s is the fractal dimension of the domain wall and follows the inequality $D-1 \leq F_s \leq D$. Equation (13) indicates that the decay of the asymptotic tail of the master form factor for a fractal domain wall is slower than that of the Porod tail. If the domain has a smooth interface, that is, if $F_s = D-1$, then Eq. (13) reduces to Porod's law. The derivation of Eq. (13) and detailed explanations of the asymptotic behavior of the form factor are found in Ref. 22. Bale and Schmidt have applied Eq. (13) to the scattering data of a lignite coal and found that the fractal dimension of the boundary surface of the pores is 2.56 ± 0.03.

In Figs. 2(b), 3(b), and 4(b), the scaled form factor for the LJ system is plotted as a function of reduced wave number using a log-log scale. According to Eq. (13), the asymptotic tail in the large-wave-number limit follows a straight line with a slope equal to $-(2D - F_s)$. Deviations from the straight lines are observed in the large-wave-number region ($x \approx 10$); this is attributed to a misalignment of the microscopic part from the temporal structure factor $S(k,t)$ with $S^{eq}(k,T^*)$ in Eq. (9). It turns out that the asymptotic tail satisfies well Porod's law at low temperatures, whereas significant

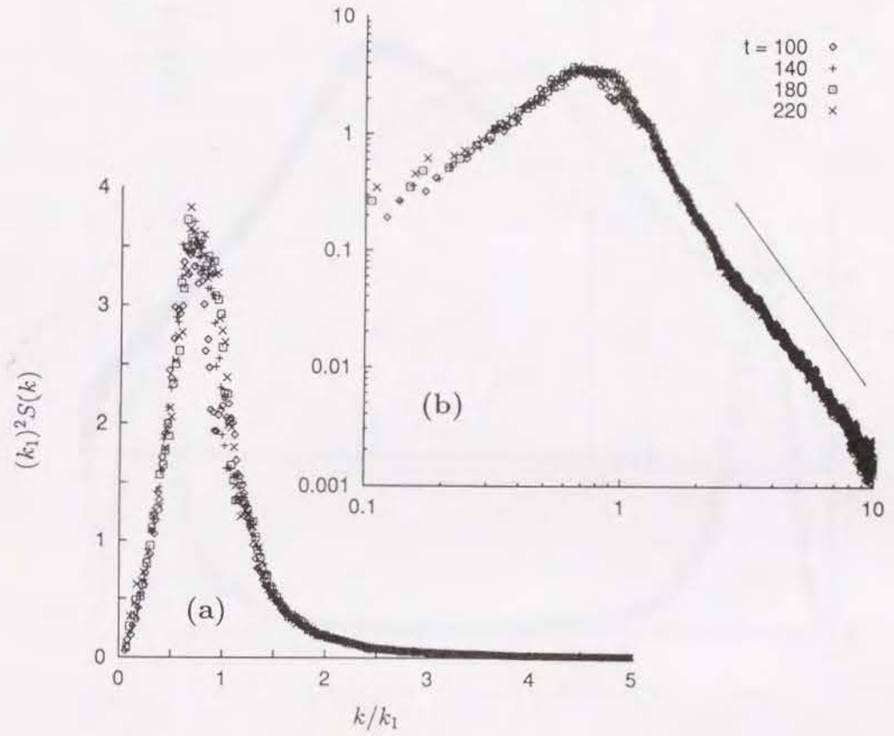

Fig. 2. Scaled form factors at different simulation times for simulation A (2D, $T^* = 0.35$). (a) normal plot, (b) log-log plot. The solid line shows the slope of the Porod tail (-3) for a comparison.

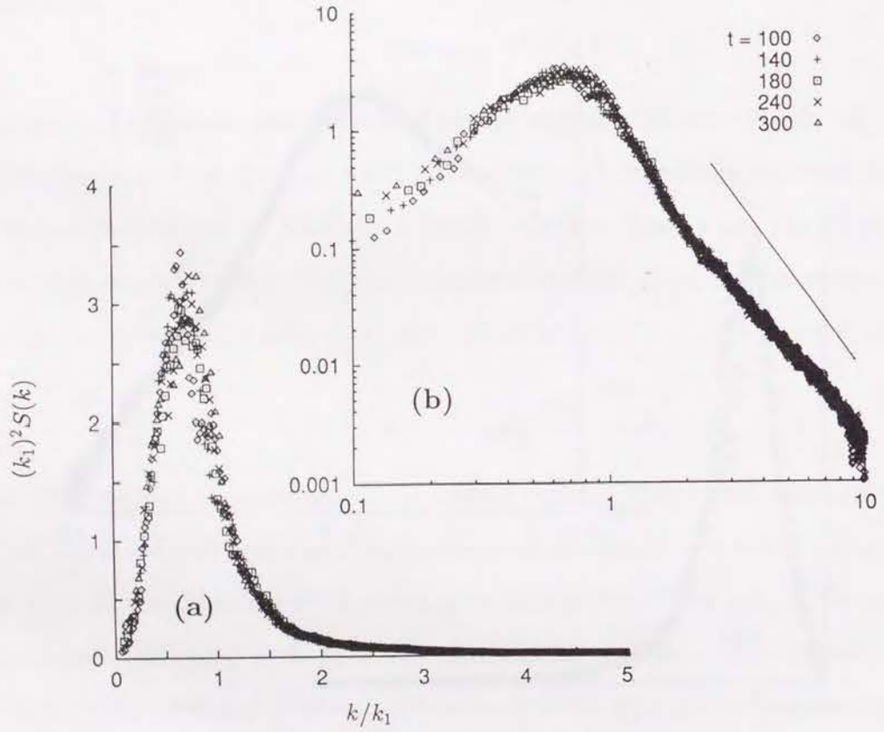

Fig. 3. Scaled form factors at different simulation times for simulation B (2D, $T^* = 0.41$). (a) normal plot, (b) log-log plot. The solid line shows the slope of the Porod tail (-3) for a comparison.

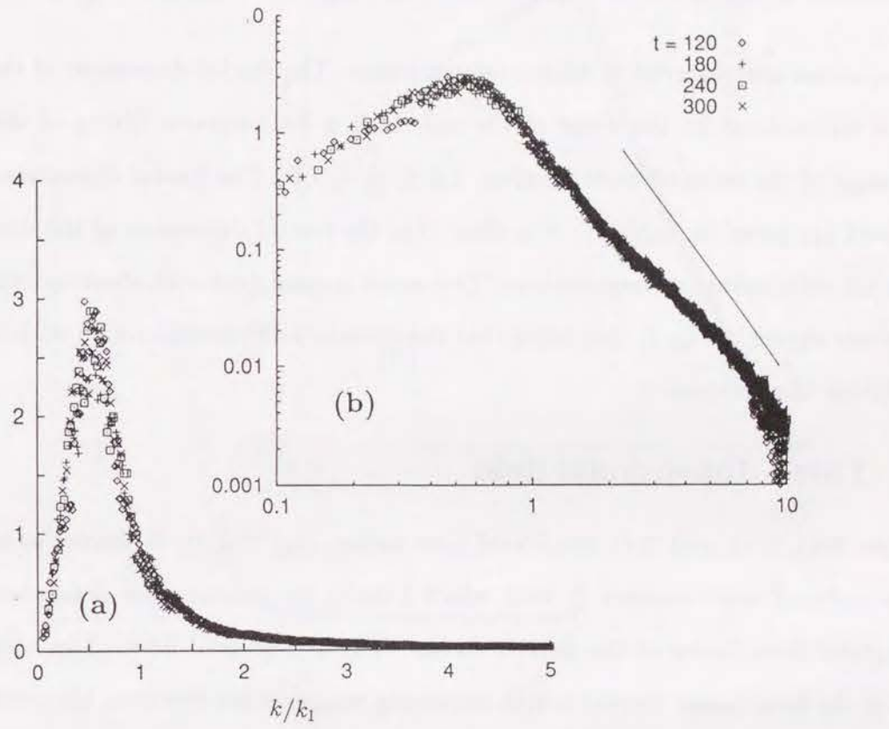

Fig. 4. Scaled form factors at different simulation times for simulation C (2D, $T^* = 0.45$). (a) normal plot, (b) log-log plot. The solid line shows the slope of the Porod tail (-3) for a comparison.

Table II. Simulation results of the fractal dimension of the domain wall for the two-dimensional system.

Run	T^*	Slope	$\sigma_S{}^a$	F_s
Sim. A	0.35	-2.7^b	0.064	1.3
Sim. B	0.41	-2.4^b	0.080	1.6
Sim. C	0.45	-2.2^b	0.080	1.8

[a] Standard deviation according to the present data fitting.
[b] Evaluated by least-squares fitting of the data within the range $3.0 \leq \frac{k}{k_1} \leq 7.0$.

discrepancies are observed at higher temperatures. The fractal dimension of the domain wall is determined by the slope of the tail using a least-squares fitting of the data in the range of the reduced wave number, $3.0 \leq \frac{k}{k_1} \leq 7.0$. The fractal dimensions F_s thus obtained are listed in Table II. It is clear that the fractal dimension of the domain wall increases with increasing temperature. This result is consistent with observations from the snapshots shown in Fig. 1, indicating that the domain wall becomes rough with increasing simulation temperature.

B. Three-dimensional fluid

In Figs. 5(a), 6(a), and 7(a), the scaled form factor, $(k_1)^3\tilde{S}(k,t)$, is plotted as a function of the reduced wave number $\frac{k}{k_1}$ with which I study the temperature dependence of the asymptotic form factor of the pattern in the three-dimensional fluid. The height of the peak in the form factor decreases with increasing temperature; however, the peak position remains unchanged.

The scaled form factor is plotted as a function of reduced wave number in Figs. 5(b), 6(b), and 7(b) using a log-log scale. As in the two-dimensional case, the asymptotic tail of the master form factor satisfies Porod's law at low temperatures, but large discrepancies are observed at higher temperatures. The fractal dimension of the domain wall is determined by the slope of the tail using a least-squares fitting. The fractal dimensions F_s of the domain wall thus obtained are listed in Table III. It is found that the fractal dimension of the domain wall increases with increasing temperature also in the three-dimensional fluid.

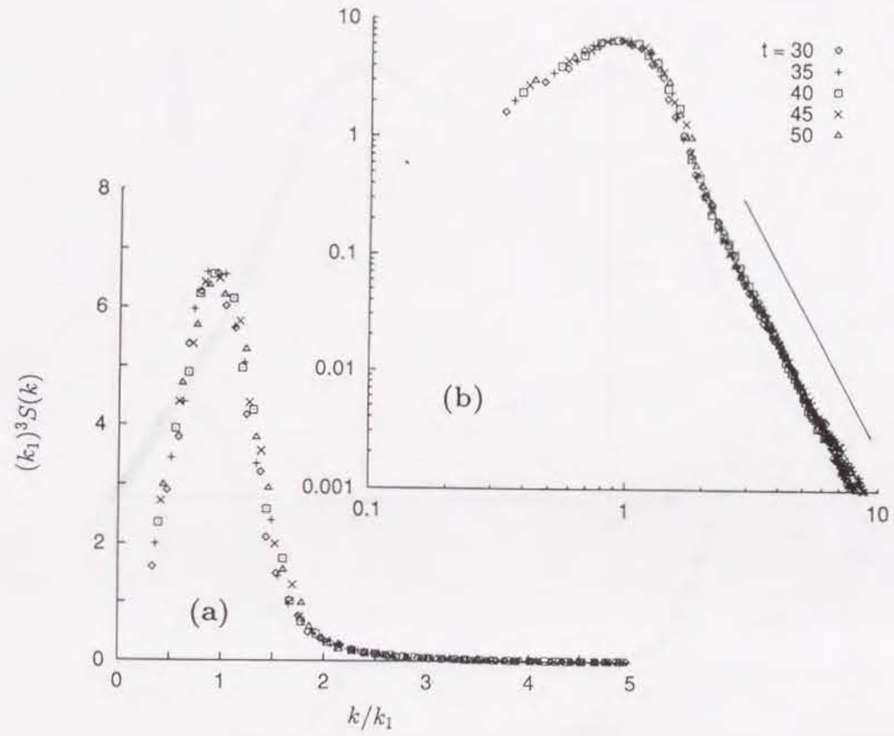

Fig. 5. Scaled form factors at different simulation times for simulation D (3D, $T^* = 0.70$). (a) normal plot, (b) log-log plot. The solid line shows the slope of the Porod tail (-4) for a comparison.

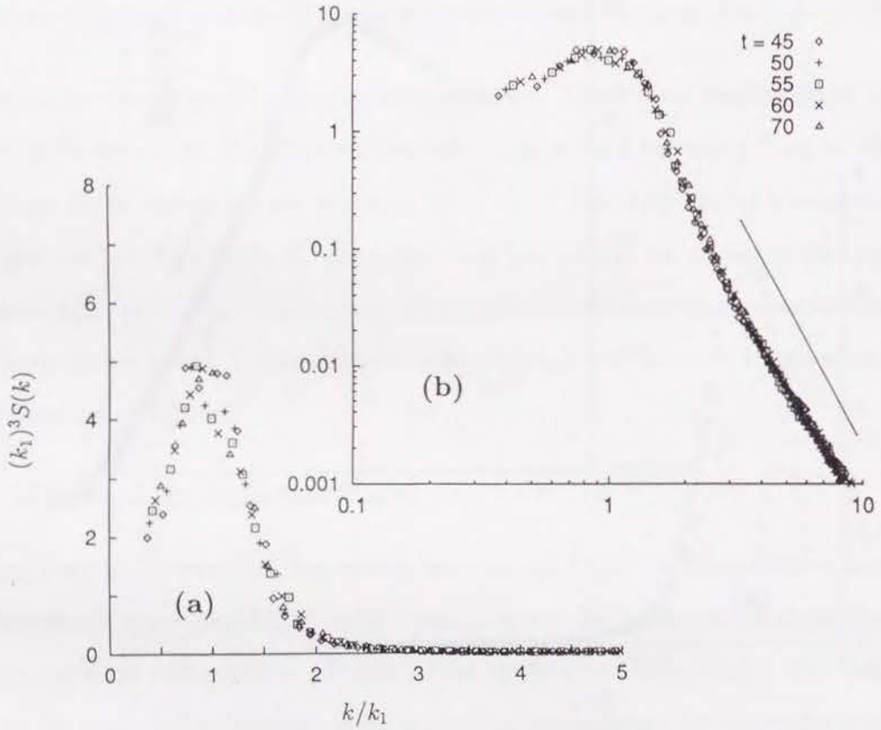

Fig. 6. Scaled form factors at different simulation times for simulation E (3D, $T^* = 0.80$). (a) normal plot, (b) log-log plot. The solid line shows the slope of the Porod tail (-4) for a comparison.

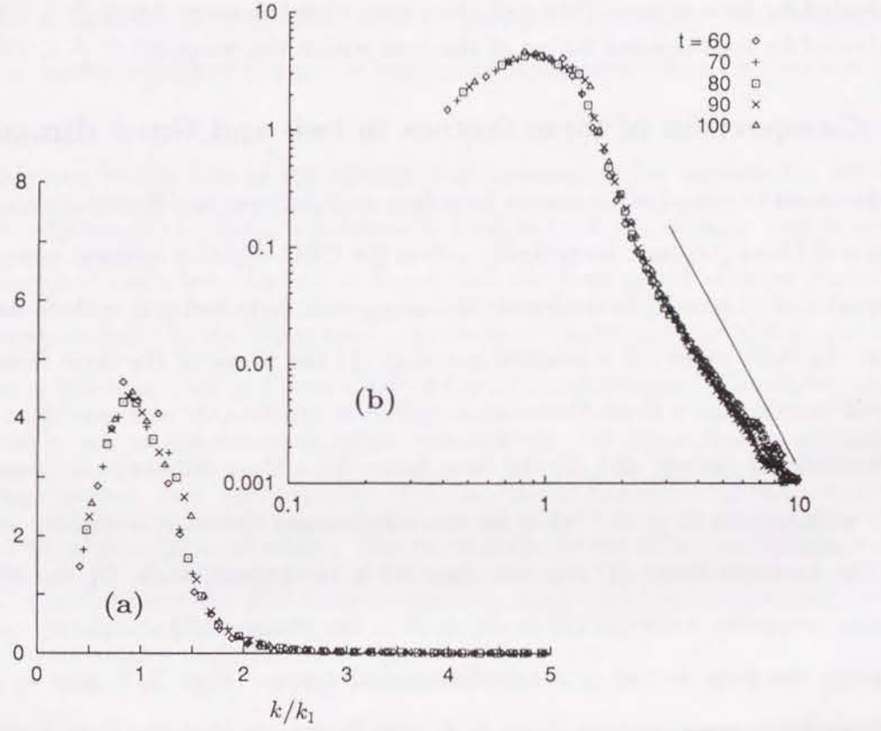

Fig. 7. Scaled form factors at different simulation times for simulation F (3D, $T^* = 0.90$). (a) normal plot, (b) log-log plot. The solid line shows the slope of the Porod tail (-4) for a comparison.

Table III. Simulation results of the fractal dimension of the domain wall for the three-dimensional system.

Run	T^*	Slope	σ_S[a]	F_s
Sim. D	0.70	-4.0[b]	0.072	2.0
Sim. E	0.80	-3.6[b]	0.082	2.4
Sim. F	0.90	-3.0[c]	0.109	3.0

[a] Standard deviation according to the present data fitting.
[b] Evaluated by least-squares fitting of the data within the range $3.0 \leq \frac{k}{k_1} \leq 7.0$.
[c] Evaluated by least-squares fitting of the data within the range $3.5 \leq \frac{k}{k_1} \leq 7.0$.

C. Comparison of form factors in two and three dimensions

It is of interest to compare the master form factors of patterns in different dimensions. Shinozaki and Oono [17] have numerically solved the CHC equation without noise using the cell dynamical system [5] to determine the asymptotic form factor in a three-dimensional system. In their paper, it is pointed out that (1) the shape of the form factor around the peak position for a three-dimensional system is significantly narrower than that for a two-dimensional system, and (2) the form factor for a three-dimensional system is symmetric with respect to $\frac{k}{k_1} = 1$ while for two-dimensional system it is slightly asymmetric [20]. The narrower shape (1) was not observed in the present work. On the other hand, a similar symmetry behavior (2) is obtained in the present MD simulation results. By comparing the form factors of a two-dimensional system (Figs. 2, 3, and 4) and those of a three-dimensional system (Figs. 5, 6, and 7), we see that the form factor for the two-dimensional system is slightly asymmetric.

IV. Concluding Remarks

MD simulations have been carried out for two- and three-dimensional LJ fluids in order to investigate the relationship between statistical properties of the domain structure and the system temperature during spinodal decomposition. I have determined the asymptotic form factor of the domain patterns in two- and three-dimensional fluids for various temperatures using scaling. I have obtained evidence that the form factor in the two-dimensional system is slightly asymmetric in contrast to the asymmetric behavior for the

three-dimensional system. It is observed that the peak position of the form factor shifts to a small wave number for the two-dimensional system and it enhances an asymmetric behavior of the form factor.

The snapshots of atomic configurations obtained from the MD simulations show that the domain patterns undergoing phase separation clearly have a temperature dependence. In both two- and three-dimensional systems, the domain wall seems to be smooth at low temperatures; however, it becomes rougher at higher temperatures. Decreasing surface tension and increasing thermal noise as temperature increases cause this surface roughening.

To study the roughening of the domain wall accurately, the asymptotic tail of the master form factor of the domain patterns is analyzed. If the domain wall is smooth, the tail follows Porod's law. Indeed, it found that the form factor satisfies Porod's law at low temperatures. On the other hand, the slope of the asymptotic tail in the log-log plot becomes less than that of Porod's law at higher temperatures. This shows that the domain wall is not as smooth as at lower temperatures but has a fractal dimension at higher temperatures. It is also observed that the fractal dimension of the domain wall increases with increasing temperature. This result is consistent with observations from the snapshots obtained from the MD simulations, indicating that the domain wall becomes rougher with increasing temperature.

References

[*] Present address: Division of Science of Materials, Graduate School of Science and Technology, Kobe University, Kobe 657, Japan.

[1] J. D. Gunton, M. San Miguel, and P. S. Sahni, in *Phase Transitions and Critical Phenomena*, edited by C. Domb and J. L. Lebowitz (Academic, New York, 1983), Vol. 8.

[2] K. Kawasaki, in *Phase Transitions and Critical Phenomena*, edited by C. Domb and M. S. Green (Academic, New York, 1972), Vol. 2.

[3] J. W. Cahn and J. E. Hilliard, J. Chem. Phys. **28**, 258 (1958); **31**, 688 (1959); H. E. Cook, Acta Metall. **18**, 297 (1970).

[4] A. Sadiq and K. Binder, J. Stat. Phys. **35**, 517 (1984).

[5] Y. Oono and S. Puri, Phys. Rev. A **38**, 434 (1988); **38**, 1542 (1988).

[6] S. W. Koch, R. C. Desai, and F. F. Abraham, Phys. Rev. A **27**, 2152 (1983).

[7] W-J. Ma, A. Maritan, J. R. Banavar, and J. Koplik, Phys. Rev. A **45**, R5347 (1992).

[8] E. Velasco and S. Toxvaerd, Phys. Rev. Lett. **71**, 388 (1993); P. Ossadnik, M. F. Gyure, and H. E. Stanley, *ibid.* **72**, 2498 (1994).

[9] R. Yamamoto and K. Nakanishi, Phys. Rev. B **49**, 14958 (1994).

[10] M. Schöbinger, S. W. Koch, and F. F. Abraham, J. Stat. Phys. **42**, 1071 (1986).

[11] R. C. Desai and A. R. Denton, in *On Growth and Form*, edited by H. E. Stanley and N. Ostrowsky (Martinus Nijhoff, The Hague, 1986).

[12] W. Klein, Phys. Rev. Lett. **65**, 1462 (1990).

[13] M. P. Allen and D. J. Tildesley, *Computer Simulation of Liquids* (Clarendon, Oxford, 1987).

[14] W. G. Hoover, A. J. C. Ladd, and B. Moran, Phys. Rev. Lett. **48**, 1818 (1982); D. J. Evans, J. Chem. Phys. **78**, 3297 (1983); D. Brown and J. H. R. Clarke, Mol. Phys. **51**, 1243 (1984).

[15] The subtraction of $S^{eq}(k, T^*)$ in Eq. (9) is only casually justified. However, since our system is composed of particles, $S(k,t)$ calculated directly from computer simulations has a peak around $k = \frac{2\pi}{\sigma}$, where σ, the size parameter of the LJ particle, presents a typical inter-particle distance in the liquid phase. In this study, we are interested in the asymptotic tail of the form factor; it is necessary to eliminate the peak around $k = \frac{2\pi}{\sigma}$ which is unimportant for domain patterns. I therefore simply subtracted $S^{eq}(k, T^*)$ from $S(k,t)$. One can find the same subtraction also in Ref. 1 on p.386. This simple subtraction is generally believed to work well for Ising systems as well as fluid systems at least as a first approximation.

[16] G. Porod, in *Small Angle X-ray Scattering*, edited by O. Glatter and O. Kratky (Academic Press, New York, 1982).

[17] A. Shinozaki and Y. Oono, Phys. Rev. Lett. **66**, 173 (1991).

[18] T. Ohta and H. Nozaki, in *Space-Time Organization in Macromolecular Fluids*, edited by F. Tanaka, M. Doi, and T. Ohta, Springer Series in Chemical Physics Vol. 51 (Springer-Verlag, Berlin, Heidelberg, 1989).

[19] K. Koga and K. Kawasaki, Physica A **196**, 389 (1993); K. Koga, K. Kawasaki, M. Takenaka, and T. Hashimoto, *ibid.* **198**, 473 (1993).

[20] M. Bahiana as discussed in A. Shinozaki and Y. Oono, Phys. Rev. Lett. **66**, 173 (1991).

[21] H. D. Bale and P. W. Schmidt, Phys. Rev. Lett. **53**, 596 (1984).

[22] H. Tomita, in *Formation, Dynamics and Statistics of Patterns*, edited by K. Kawasaki, M. Suzuki, and A. Onuki (World Scientific, Singapore, 1990), Vol. 1.

General Conclusion

This thesis consists of two parts. Part I (Chapters 1 and 2) describes studies on the thermodynamic properties of fluoro propane fluids by means of Monte Carlo simulation using realistic potential models, and Part II (Chapters 3 to 6) describes studies on phase equilibria and phase separation dynamics of the Lennard-Jones model fluids by means of molecular dynamics simulation.

In Chapter 1, *Ab initio* quantum-chemical calculations and subsequent preparation of intermolecular potential function were carried out for a pair of isomers, $CH_3CF_2CF_3$ (HFC-245cb, CB) and $CH_2FCF_2CHF_2$ (HFC-245ca, CA). The experimental data indicate that CB has smaller intermolecular attractive interaction than CA in contradiction with the fact that CB has a larger dipole moment than CA. The present *ab initio* calculations showed that the attractive interaction is mostly dominated by the electrostatic intermolecular interaction between H and F. It was also confirmed that the order in the magnitude of the attractive interaction for CB dimer and CA dimer is reverse to that of the dipole moment values. This difference in the attractive interaction can be the reason for the peculiar differences in thermodynamic properties between CB and CA. To understand the above contents more in detail, pair potential functions were constructed for CB and CA using an atom-atom interaction model. Our model explained the difference in the attractive interaction as follows: fractional charges on C atoms disturb the attractive interaction between H and F. This effect is more significant in CB pair than in CA pair because the absolute value of the fractional charge on each C atom is larger in CB than in CA. This makes CB dimer has a smaller intermolecular attraction than CA dimer.

The procedure which I adopted to construct the pair potential models for CB and CA is simple and transferable to other fluoro propanes in general. One can construct the pair

potential models and perform systematic molecular simulations by use of the procedure. In Chapter 2, I showed Monte Carlo simulation results which have been performed for propane and four fluoro propanes: HFC-245ca, HFC-245cb, HFC-236fa and C_3F_8 using the above procedure without any modifications (Model I). From the simulation results on the thermodynamic properties (U and P), it was found that Model I overestimates the intermolecular potential energies. I therefore modified Model I by introducing an empirical scaling factor into the potential function (Model II). Model II was found to reproduce successfully the thermodynamic properties of these fluids as well as the liquid structures of liquid propane. Liquid structures of an isomer pair of fluoro propanes, CA and CB, have also been investigated. It was confirmed that both CA and CB have almost an identical carbon-carbon pair distribution and the hydrogen-bond like interaction between H and F discussed in Chapter 1 really exists in the liquid state. I conclude that Model II is expected to be a reliable potential model for a series of fluoro propanes to perform systematic molecular simulations.

There is a serious problem when one investigates phase equilibrating phenomena by means of molecular simulation. A van der Waals like loop always appears in both typical molecular dynamics and Monte Carlo computer simulations for a small system. Chapters 3 and 4 concerned the underlying physical reasons behind the van der Waals like loop (small-size loop) by molecular dynamics simulations. In Chapter 3, I considered the relationship between average domain size of the system undergoing vapor-liquid phase separation and the magnitude of the small-size loop. I have carried out large scale MD simulations to confirm whether the small-size loop tends to vanish expectedly as the domain size increases. The present simulation clearly showed that the magnitude of the small-size loop becomes remarkably smaller as the domain glows. The dependence of the depth of the vdW loop on the average domain size has also been studied. The depth of the loop decreases lineally with the average domain size. The linear extrapolations of the k_1–P plots give equilibrium vapor pressures of the model fluid. In Chapter 4, I considered the relationship between the magnitude of surface free energy of the vapor-liquid interface and the magnitude of the small-size loop. I demonstrated that an important physical reason behind the small-size loop effect is due to the surface free energy of the domain

during the phase separation. It was found that with the same system size, the larger of the surface free energy, the greater the loop exhibits. It means that a fluid system which has a strong attractive pair potential (comparing to the system temperature) will require very large system size to reduce the van der Waals loop in molecular simulation. The small-size loop can be always removed using an extremely large system size as is shown in Chapter 3, but over-sizing is very inefficient in the computational study. I note that Fig. 3 in Chapter 4 is obtained from small system-size simulations. In this respect, this figure is particularly useful for us to identify an appropriate system size, that is, a size large enough for reducing the loop but not oversized for the sake of saving computing time.

Chapters 5 and 6 concerned studies of vapor-liquid phase separation by means of molecular dynamics simulation. The asymptotic growth law of the vapor-liquid phase separation for the two- and three-dimensional one-component Lennard-Jones fluids was discussed in Chapter 5. I have done molecular dynamics simulations using a 50 000-particle system for two-dimensional fluids and a 78 732-particle system for three-dimensional fluids. The phase separation began immediately after the quench of the homogeneous system, and the time-dependent (temporal) structure factor $S(k,t)$ was calculated throughout the simulation runs. The characteristic length scale was found to grow as $l(t) \sim t^a$ in the late-time (scaling) regime, which corresponds to $k_1 < 0.28$ for the two-dimensional fluid and $k_1 < 0.45$ for the three-dimensional fluid in this work, and the asymptotic growth exponent was found to be $\frac{1}{2}$ both in two and three dimensions. Thermal noise was found to have no effect on the asymptotic exponent, but to give rise to a substantial delay of the transition time to the asymptotic regime. In Chapter 6, the relationship between statistical properties of the domain structure during phase separation and the system temperature was discussed. The asymptotic form factor of the domain patterns in two- and three-dimensional fluids was determined for various temperatures using scaling. I obtained evidence that the form factor in the two-dimensional system is slightly asymmetric in contrast to the asymmetric behavior for the three-dimensional system. It was observed that the peak position of the form factor shifts to a small wave number for the two-dimensional system and it enhances an asymmetric behavior of the form factor. The snapshots of atomic configurations obtained from the MD simulations showed that the

domain patterns undergoing phase separation clearly have a temperature dependence. In both the two- and three-dimensional systems, the domain wall seems to be smooth at low temperatures; however, it becomes rougher at higher temperatures. Decreasing surface tension and increasing thermal noise as temperature increases cause this surface roughening. To study the roughening of the domain wall accurately, I analyzed the asymptotic tail of the master form factor of the domain patterns. If the domain wall is smooth, the tail follows Porod's law. Indeed, it was found that the form factor satisfies Porod's law only at low temperatures. On the other hand, the slope of the asymptotic tail in the log-log plot becomes less than that of Porod's law at higher temperatures. This shows that the domain wall is not as smooth as at lower temperatures but has a fractal dimension at higher temperatures. It was also observed that the fractal dimension of the domain wall increases with increasing temperature. This result is consistent with observations from the snapshots obtained from the MD simulations, indicating that the domain wall becomes rougher with increasing temperature.

Acknowledgments

The present study is a summary of my studies carried out at Division of Molecular Engineering, Graduate School of Engineering, Kyoto University from April 1992 to August 1994.

First of all, I wish to express special thanks to Professor Koichiro Nakanishi, who supervised the present work, for his helpful directions and encouragements. He provided me also an opportunity to study at Max-Planck-Institut für Chemie (MPIC), Mainz, Germany from October 1993 to March 1994. I acknowledge also Professor Karl Heinzinger for the collaboration and the Physical Chemistry Group of MPIC for their kind hospitality.

I would like to thank Professor Hiroshi Fujimoto, Professor Tsuyoshi Nakajima, Dr. Hideki Tanaka and Dr. Osamu Kitao for their supporting and directing the present work. I am grateful especially to Professor Hiroyuki Tomita for giving me very important suggestions to carry out the present work. I thank Professor Xiao Cheng Zeng for the collaboration and Miss Joanne Button for critical readings of the manuscript.

Sincere acknowledgments are expressed to Professor Akira Onuki, Professor Toyonori Munakata, and Professor Yasuaki Hiwatari for their helpful discussions and interest in my work. I would like to thank also Professor Yoji Kawamoto, Professor Hironobu Kubota, Professor Yoshiyuki Tanaka, and Dr. Shigenobu Matsuo for their continuous encouragements during my research life.

Finally, I express my sincere gratitude to my wife, Aki Hamada, for supporting and understanding me all the time.

List of Publications

Chapter 1. R. Yamamoto, O. Kitao, and K. Nakanishi, Intermolecular Interaction of Fluoro Propanes, *Mol. Simulation* **12**, 383–391 (1994).

Chapter 2. R. Yamamoto, O. Kitao, and K. Nakanishi, Monte Carlo Simulation of Fluoro Propane, *Fluid Phase Equilibria* **104**, 349–361 (1995).

Chapter 3. R. Yamamoto, O. Kitao, and K. Nakanishi, Can the van der Waals loop vanish?: Effect of domain size *Mol. Phys.* **84**, 757–768 (1995).

Chapter 4. R. Yamamoto, H. Tanaka, K. Nakanishi, and X.C. Zeng, Can the van der Waals loop vanish?: Effect of surface free energy *Chem. Phys. Lett.* **231**, 401–406 (1995).

Chapter 5. R. Yamamoto and K. Nakanishi, Computer simulation of vapor-liquid phase separation in two- and three-dimensional fluids: Growth law of domain size, *Phys. Rev. B* **49**, 14958–14966 (1994); R. Yamamoto and K. Nakanishi, Computer simulation of vapor-liquid phase separation, *Molec. Simulation*, in press.

Chapter 6. R. Yamamoto and K. Nakanishi, Computer simulation of vapor-liquid phase separation in two- and three-dimensional fluids. II. Domain structure, *Phys. Rev. B* **51**, 2715–2722 (1995).

Other publications not contained in this thesis

1. R. Yamamoto, S. Matsuo, and Y. Tanaka, Thermal Conductivity of Halogenated Ethanes, HFC-134a, HCFC-123 and HCFC-141b, *Int. J. Thermophys.* **14**, 79-90 (1993).

2. S. Matsuo, R. Yamamoto, Y. Tanaka, and H. Kubota, Viscosity of Mixtures of Fluoroalcohols and Water at High Pressures, *Int. J. Thermophys.* **14**, 835-849 (1993).

3. S. Matsuo, R. Yamamoto, H. Kubota, and Y. Tanaka, Volumetric Properties of Mixtures of Fluoroalcohols and Water at High Pressures, *Int. J. Thermophys.* **15**, 245-259 (1994).